

**DEVELOPMENT OF WATER-BASED ADHESIVES FOR ORIENTED
POLYPROPYLENE (OPP) LAMINATION**

Sarocha Ruanpan

A Dissertation Submitted in Partial Fulfilment of the Requirements
for the Degree of Doctor of Philosophy
The Petroleum and Petrochemical College, Chulalongkorn University
in Academic Partnership with
The University of Michigan, The University of Oklahoma,
and Case Western Reserve University

2017

บทคัดย่อและแฟ้มข้อมูลฉบับเต็มของวิทยานิพนธ์ตั้งแต่ปีการศึกษา 2554 ที่ให้บริการในคลังปัญญาจุฬาฯ (CUIR)
เป็นแฟ้มข้อมูลของนิสิตเจ้าของวิทยานิพนธ์ที่ส่งผ่านทางบัณฑิตวิทยาลัย

The abstract and full text of theses from the academic year 2011 in Chulalongkorn University Intellectual Repository (CUIR)
are the thesis authors' files submitted through the Graduate School.

Thesis Title: Development of Water-Based Adhesives for Oriented Polypropylene (OPP) Lamination
By: Sarocha Ruanpan
Program: Polymer Science
Thesis Advisors: Assoc. Prof. Hathaikarn Manuspiya
Prof. Mark D. Soucek

Accepted by The Petroleum and Petrochemical College, Chulalongkorn University, in partial fulfilment of the requirements for the Degree of Doctor of Philosophy.

..... College Dean
(Prof. Suwabun Chirachanchai)

Thesis Committee:

..... (Asst. Prof. Supa Wirasate) (Assoc. Prof. Hathaikarn Manuspiya)
..... (Prof. Mark D. Soucek) (Prof. Suwabun Chirachanchai)
..... (Assoc. Prof. Thanyalak Chaisuwan) (Asst. Prof. Stephan T. Dubas)

ABSTRACT

5482007063: Polymer Science Program

Sarocha Ruanpan: Development of Water-Based Adhesives for Oriented Polypropylene (OPP) Lamination

Thesis Advisors: Assoc. Prof. Hathaikarn Manuspiya, Prof. Mark D. Soucek 141 pp.

Keywords: Laminating adhesives/ Emulsion polymerization/ Porous clay heterostructure/ Core-shell morphology/ Peel strength

Eco-friendly laminating adhesive has been developed for flexible packaging industries due to urgent restriction of volatile organic compounds (VOCs) emissions from anthropogenic sources. The water-based polyurethane laminating adhesive was derived by a condensation polymerization of isophorone diisocyanate, polypropylene glycol and 2,2-bis(hydroxymethyl)propionic acid, while the water-based polyacrylate laminating adhesive was synthesized by an emulsion polymerization of 2-ethylhexyl acrylate, ethylene glycol methyl ether acrylate, styrene, 2-hydroxyethyl methacrylate and acrylic acid. The parameters influencing the adhesive's performance consisted of chemical composition, reinforcing fillers and manufacturing processes. Among those parameters, the fabrication of waterborne core-shell polyacrylate laminating adhesive through a two-stage seeded semi-batch emulsion polymerization was desirable with a rigid core having a glass transition temperature (T_g) of $-14.9\text{ }^{\circ}\text{C}$ encapsulated by a soft shell having T_g ranging from $-18.4\text{ }^{\circ}\text{C}$ to $-32.0\text{ }^{\circ}\text{C}$, depending on variables. The optimal formulation was accomplished using a core-to-shell ratio of 0.5 and 10 wt% of ethylene glycol methyl ether acrylate concentration in its shell, giving a bonded joint 180° peel strength 214.5 N/m with high cohesive strength and good adhesion to various substrates. This water-based laminating adhesive system has the possibility of replacing solventborne technology.

บทคัดย่อ

สโรชา เรือนแป้น : การพัฒนา กาวน้ำสำหรับกระบวนการลามิเนตฟิล์มพอลิโพรพิลีนที่ถูกดึงยืด (Development of Water-Based Adhesives for Oriented Polypropylene (OPP) Lamination) อ. ที่ปรึกษา : รศ. ดร. หทัยกานต์ มนัสปิยะ และ ศ. ดร. มาร์ค ดี ซูเซค 141 หน้า

กาวลามิเนตที่เป็นมิตรต่อสิ่งแวดล้อมได้รับการพัฒนาขึ้นสำหรับอุตสาหกรรมบรรจุภัณฑ์ชนิดอ่อนตัว เพื่อยับยั้งการปลดปล่อยสารระเหยอินทรีย์จากกิจกรรมของมนุษย์ กาวน้ำลามิเนตจากพอลิยูรีเทนได้จากการสังเคราะห์พอลิเมอร์แบบควบแน่นของไอโซโฟรอนไดไอโซไซยาเนต พอลิโพรพิลีนไกลคอล และกรด 2,2-บิสไฮดรอกซีเมทิลโพรพิโอนิก ขณะที่กาวน้ำลามิเนตจากพอลิอะคริเลตได้จากการสังเคราะห์พอลิเมอร์แบบอิมัลชันของ 2-เอทิลเฮกซิลอะคริเลต เอทิลีนไกลคอลเมทิลอีเทอร์อะคริเลต สไตรีน 2-ไฮดรอกซีเอทิลเมทาคริเลต และกรดอะคริลิก ในส่วนของตัวแปรที่มีอิทธิพลต่อประสิทธิภาพของกาวนั้นประกอบด้วย องค์ประกอบทางเคมี สารเสริมแรง และกระบวนการผลิต ในจำนวนตัวแปรทั้งหมด การผลิตกาวน้ำลามิเนตจากพอลิอะคริเลตชนิดแกนกลางและเปลือกหุ้ม ผ่านกระบวนการสังเคราะห์พอลิเมอร์แบบซีทีเอมในสองขั้นตอน จะให้ผลการศึกษาเป็นที่น่าพอใจมากที่สุด ด้วยแกนกลางแข็งที่มีอุณหภูมิการเปลี่ยนสถานะคล้ายแก้วที่ - 14.9 องศาเซลเซียสต่อหุ้มโดยเปลือกนิ่มที่มีอุณหภูมิการเปลี่ยนสถานะคล้ายแก้วระหว่าง - 18.4 ถึง - 32.0 องศาเซลเซียส ขึ้นกับตัวแปร สำหรับสูตรการสังเคราะห์ที่เหมาะสมที่สุดจะใช้อัตราส่วนระหว่างแกนกลางต่อเปลือกหุ้มที่ 0.5 และใช้ความเข้มข้นของเอทิลีนไกลคอลเมทิลอีเทอร์อะคริเลตในเปลือกหุ้มที่ร้อยละ 10 โดยน้ำหนัก ซึ่งจะให้ค่าความต้านทานการดึงลอกของรอยต่อระหว่างพื้นผิวยึดติด 214.5 นิวตันต่อเมตร ด้วยแรงเชื่อมแน่นที่สูงและการยึดติดที่ดีบนพื้นผิวหลายหลาก โดยระบบกาวน้ำลามิเนตที่ผลิตขึ้นนี้จะสามารถนำไปใช้แทนที่เทคโนโลยีตัวทำละลายได้

ACKNOWLEDGEMENTS

This dissertation would not have been accomplished without those who have made valuable contributions. The author is grateful for the scholarship and funding of the thesis provided by the Petroleum and Petrochemical College and the Research and Researcher for industries (RRi), Thailand Research Fund (TRF), Thailand: Grant number PHD56I0019.

The author would like to thank her supervisors, Assoc. Prof. Dr. Hathaikarn Manuspiya, for her enthusiastic guidance, constructive criticism, encouragement and precious time throughout the research; including in learning opportunities to acquire the knowledge, skills and experiences at the Petroleum and Petrochemical College, Chulalongkorn University, Thailand. Appreciation for valuable suggestion, chemical and technical supports during the academic years is extended to Nateethong Polymer Co., Ltd as the research collaboration.

The author is intensively obliged to Prof. Dr. Mark D. Soucek, who offered her an opportunity to pursue research with altering perspectives in the Department of Polymer Engineering at the University of Akron, Akron, Ohio, United States. His prompt advice, motivation, encouragement and scientific approach have enabled her to a very great extend to accomplish the research. The utilization of the experimental facilities at College of Polymer Science and Polymer Engineering National Polymer Innovation Center, the University of Akron, Akron, Ohio, United States is extremely appreciated.

Additionally, I would like to acknowledge Prof. Suwabun Chirachanchai, Assoc. Prof. Thanyalak Chaisuwan, Asst. Prof. Stephan T. Dubas and Asst. Prof. Supa Wirasate for being the thesis committees and giving valuable comments.

Million thanks toward the faculties, staffs and friends at the Petroleum and Petrochemical College, Chulalongkorn University, Thailand and the Department of Polymer Engineering, the University of Akron, Akron, Ohio, United States for giving her a hand, generous attitude and making worthy memories during her stay.

Eventually, her deepest gratitude is expressed to her beloved family for their overwhelming inspiration, understanding, patience and support throughout her study.

TABLE OF CONTENTS

	PAGE
Title Page	i
Abstract (in English)	iii
Abstract (in Thai)	iv
Acknowledgements	v
Table of Contents	vi
List of Tables	ix
List of Figures	xi
 CHAPTER	
I INTRODUCTION	1
 II LITERATURE REVIEW	 3
 III EXPERIMENTAL	 27
 IV SYNTHESIZED AMINO-FUNCTIONALIZED POROUS CLAY HETEROSTRUCTURE AS AN EFFECTIVE THICKENER IN WATERBORNE POLYURETHANE HYBRID ADHESIVES	 39
4.1 Abstract	39
4.2 Introduction	39
4.3 Experimental	41
4.4 Results and Discussion	47
4.5 Conclusions	62
4.6 Acknowledgements	63
4.7 References	63

CHAPTER		PAGE
V	IN-SITU EMULSION POLYMERIZATION OF WATER-BASED POLYACRYLATE LAMINATING ADHESIVES UTILIZING ULTRASONIC-DISPERSED NATURAL THICKENERS	68
	5.1 Abstract	68
	5.2 Introduction	68
	5.3 Experimental	70
	5.4 Results and Discussion	73
	5.5 Conclusions	80
	5.6 Acknowledgements	81
	5.7 References	81
VI	WATERBORNE ACRYLIC HYBRID ADHESIVES BASED ON A METHACRYLATE-FUNCTIONALIZED POROUS CLAY HETEROSTRUCTURE FOR POTENTIAL LAMINATION APPLICATION	84
	6.1 Abstract	84
	6.2 Introduction	84
	6.3 Experimental	86
	6.4 Results and Discussion	91
	6.5 Conclusions	106
	6.6 Acknowledgements	107
	6.7 References	107
VII	CORE-SHELL COPOLYACRYLATE NANOPARTICLES: SYNTHESIS AND APPLICATIONS IN ECO-FRIENDLY LAMINATING ADHESIVES	112
	7.1 Abstract	112
	7.2 Introduction	112

CHAPTER	PAGE
7.3 Experimental	114
7.4 Results and Discussion	119
7.5 Conclusions	126
7.6 Acknowledgements	126
7.7 References	127
VIII CONCLUSIONS AND RECOMMENDATIONS	130
REFERENCES	131
CURRICULUM VITAE	139

LIST OF TABLES

TABLE		PAGE
CHAPTER II		
2.1	Adhesive lamination process	7
CHAPTER IV		
4.1	Viscosity of WPU-x hybrid adhesives at temperature of 25 °C and shear rate of 85 s ⁻¹	53
4.2	The most characteristic ATR-FTIR bands of the WPU-x hybrid adhesives	54
4.3	The frequency (ν) and relative area (A) of the five spectral components in the C=O stretching region	55
4.4	Glass transition temperature (T_g), decomposition temperature (T_d) and weight loss of the WPU-x hybrid adhesives	59
CHAPTER V		
5.1	Specific surface area of natural thickeners	74
5.2	T_g values of water-based polyacrylate laminating adhesives incorporated with the natural thickeners	78
CHAPTER VI		
6.1	Physical characteristics of the WAC hybrid adhesives	96
6.2	The most characteristic FTIR bands of the WAC hybrid adhesives	99
6.3	The glass transition temperature (T_g), decomposition temperature (T_d), activation energy (E_a) and residue of the WAC hybrid adhesives	102

TABLE		PAGE
CHAPTER VII		
7.1	The CS polymerization recipes	117
7.2	Physical characteristics of the CS laminating adhesives	120
7.3	Contact angle and surface tension of the CS laminating adhesives	122
7.4	Experimental and theoretical T_g of the CS laminating adhesives	124

LIST OF FIGURES

FIGURE	PAGE
CHAPTER II	
2.1	3
2.2	5
2.3	5
2.4	9
2.5	10
2.6	11
2.7	14
2.8	14
2.9	16
2.10	17
2.11	19
2.12	23
2.13	25

FIGURE	PAGE
2.14 Typical XRD patterns and TEM micrographs of three distinct types of polymer/layered silicate nanocomposites.	26
CHAPTER IV	
4.1 The synthesis route of WPU-x hybrid adhesives.	43
4.2 TEM micrograph (25.0 kx magnification, scale bar = 100 nm) of APCH.	48
4.3 N ₂ /77K adsorption-desorption isotherm of APCH.	49
4.4 ATR-FTIR spectrum of APCH.	50
4.5 Representative FE-SEM images showing the surface morphology of the (a) APCH (20.0 kx magnification, scale bar = 2 μm), (b) WPU-0.0, (c) WPU-2.0 (500 x magnification, scale bar = 100 μm) and (d) a silicon mapping of WPU-2.0.	51
4.6 The variation of viscosity as a function of shear rate for WPU-x hybrid adhesives. Arrows show the measurements corresponding to increased and decreased shear rate.	52
4.7 ATR-FTIR spectra of the WPU-x hybrid adhesives.	55
4.8 Partially enlarged details of the WPU-x hybrid adhesives in the C=O stretching vibration of WPU-x with APCH contents of (a) 0, (b) 0.5, (c) 1.0, (d) 2.0 and (e) 3.0 wt%.	56
4.9 XRD patterns of WPU-x hybrid adhesives with different APCH contents.	57
4.10 DSC thermograms of WPU-x hybrid adhesives with different APCH contents. Thermograms were taken from the second heating scan.	58
4.11 TG curves of WPU-x hybrid adhesives with different APCH contents.	60

FIGURE		PAGE
4.12	The 180° peel strength of the WPU-x hybrid adhesives with different APCH contents.	61
CHAPTER V		
5.1	ATR-FTIR spectra of the natural thickeners.	73
5.2	N ₂ /77K adsorption-desorption isotherms of natural thickeners.	74
5.3	Brookfield viscosity of water-based polyacrylate laminating adhesives incorporated with the natural thickeners.	76
5.4	The particle diameter of water-based polyacrylate laminating adhesives incorporated with the natural thickeners.	76
5.5	The surface tension of the water-based polyacrylate laminating adhesives incorporated with the natural thickeners.	77
5.6	T _g plot of water-based polyacrylate laminating adhesives incorporated with the natural thickeners.	78
5.7	Average 180° peel strength of the water-based polyacrylate laminating adhesives incorporated with the natural thickeners.	79
CHAPTER VI		
6.1	Schematic description of grafting-to approach for WAC hybrid adhesive.	88
6.2	ATR-FTIR spectra of PCH and MPCH.	92
6.3	N ₂ /77K adsorption-desorption isotherms of (a) PCH and (b) MPCH.	93
6.4	DLS curves of WAC hybrid adhesives. Curves shown are representative of those seen from five samples.	97

FIGURE	PAGE
6.5 FE-SEM micrographs of (a) MPCH (10.0 kx magnification, scale bar = 5 μm), (b) 0.0MPCH, (c) 2.0MPCH (2.0 kx magnification, scale bar = 20 μm) and (d) EDX analysis showing the silicon mapping of 2.0MPCH.	98
6.6 (a) full range (b) enlarged wavenumber range of 1000-1500 cm^{-1} FTIR spectra of the WAC hybrid adhesives with different MPCH contents.	100
6.7 DSC thermograms of the WAC hybrid adhesives with different MPCH contents. Thermograms shown are taken from the second heating scan.	9 101
6.8 (a) TG (b) DTG thermograms of WAC hybrid adhesives with different MPCH contents.	103
6.9 Plot of $\ln[\ln(W_0/W_T)]$ versus θ for thermal degradation of WAC hybrid adhesives under a N_2 atmosphere at a heating rate of 10 $^\circ\text{C}/\text{min}$.	104
6.10 Average 180 $^\circ$ peel strength of the WAC hybrid adhesives with different MPCH contents. Data are shown as the average derived from ten measurements.	105

CHAPTER VII

7.1 The DLS curves of the CS laminating adhesives. The curves shown are representative of those seen from five samples.	121
7.2 DSC thermograms of the CS laminating adhesives. Thermograms shown are taken from the second heating scan.	123
7.3 Average 180 $^\circ$ peel strength of the CS laminating adhesives. Data are shown as average derived from ten measurements.	125

FIGURE	PAGE
7.4 Representative TEM micrograph of CS0.5E10 (25.0 kx magnification, scale bar = 200 nm).	125

CHAPTER I

INTRODUCTION

Laminating adhesives are extensively used as a binder in the manufacture of industrial flexible packaging, including bottle/box labels, dried-food packages, snack packages and non-foil condiment packages. The solventborne laminating adhesives derived by petroleum-based solvents, such as isopropanol, toluene (Anders and Lee, 2015), triethanolamine (Aung *et al.*, 2014) and ethyl acetate (Corcione *et al.*, 2008; Zhang *et al.*, 2011), are the conventional adhesives yielding high bond strength, high viscosity and fast-curing time. However, as motivated by the Thailand's centralized Environmental Protection Agency, the volatile organic compounds (VOC) emissions from anthropogenic sources are in urgent need of restriction as they are hazardous air pollutants (Corcoran, 2008). To overcome this drawback, the water-based laminating adhesive is produced by an emulsion polymerization process using deionized water as a diluent (Voss, 2002; Seyed *et al.*, 2005). On an environmental point, the water-based adhesives could be considered as a non-VOC adhesive, and offer significant potential cost savings. However, they have been reported to have a loss of adhesion, low viscosity and slow-curing time, resulting in a catastrophic failure of the bonded joints (Packham, 1992).

Theoretically, the cohesive strength is an attraction of adhesive particles via chemical bonding, crosslinking and intermolecular interaction; and solely holds the adhesive mass together, whereas the adhesion is a force located on a boundary layer between substrate and adhesive itself (Lee, 1991; Baldan, 2004). Consequently, the water-based laminating adhesive performance has been improved by the combination of cohesive strength and adhesion to substrates, resulting in a bonding effectiveness. This study focuses on two kinds of polymeric matrix, polyurethane and polyacrylate. The water-based polyurethane adhesives were formulated by an exothermic reaction between isophorone diisocyanate, polypropylene glycol and 2,2-bis(hydroxymethyl) propionic acid. The influence of the anionic group concentrations and also isocyanate-hydroxyl ratio on the laminating adhesive performance was investigated. Meanwhile, the water-based polyacrylate adhesives were formulated by emulsion polymerization processes of 2-ethylhexyl acrylate, ethylene glycol methyl ether acrylate, styrene, 2-

hydroxyethyl methacrylate and acrylic acid. The variables, including the influence of surfactant types, initiator types, monomer compositions, natural thickeners/reinforcing fillers and wetting agent types, on the water-based laminating adhesive performance were intensively studied.

Additionally, reinforcing fillers, such as clay minerals (Diaconu *et al.*, 2008; Kuan *et al.*, 2005), nanosilica (Lin *et al.*, 2008) and calcium carbonate (Gumfekar *et al.*, 2011), have been used to facilitate the cohesive strength via an organic-inorganic hybrid structure. Recently, a porous clay heterostructure (PCH) has attracted much attention as a relatively new class of mesoporous materials. Instead of clay minerals, PCH is frequently used as an inorganic reinforcing filler due to its high surface area ($\sim 500\text{-}1000\text{ m}^2/\text{g}$), which could be modified by an organosilane precursor to enhance a compatibility between phases. PCH was modified by 3-aminopropyltriethoxysilane and 3-(trimethoxysily) propyl methacrylate to acquire an amino-functionalized PCH (APCH) and a methacrylate-functionalized PCH (MPCH), respectively. The water-based polyurethane hybrid laminating adhesive reinforced with APCH and the water-based polyacrylate hybrid laminating adhesive reinforced with MPCH were evaluated as a natural thickener.

The manufacturing process is another parameter influencing the laminating adhesive performance. The standard core-shell copolyacrylate laminating adhesives were formulated by two-stage seeded semi-batch emulsion polymerization. A rigid core surrounded by a soft shell was preferable to simultaneously achieve the cohesive strength and adhesion to substrates. The series of water-based laminating adhesives were determined using the morphological, structural, physical, thermal and adhesion properties, in terms of 180° peel strength measurement of a paper/untreated oriented polypropylene (OPP) laminated joint, and reported the optimal formula.

CHAPTER II LITERATURE REVIEW

2.1 Oriented Polypropylene (OPP) Lamination

Lamination is an attractive technology combining performance and quality. Generally, it is the technique of manufacturing different materials in multiple layers as an illustration (Figure 2.1) to achieve unique properties of a composite, including high strength, stability, durability, thermal resistance and visual appearance (Carter, 1993). Due to the wide range of raw materials, e.g. plastic film, paper, non-woven, aluminum foil, reinforcement web etc., a high bond strength between layers is critical to success. Each laminated layer is usually permanently assembled by heat, pressure, welding, or adhesives.

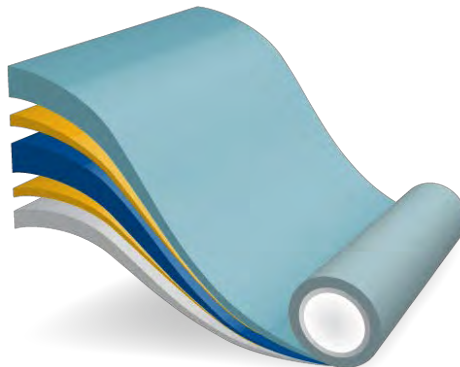


Figure 2.1 The internal structure of the laminated material.

Laminated materials have been extensively used in a variety of applications, especially in the flexible packaging industries. The packaging is the technology of enclosing or protecting products for distribution, storage, sale and use. The Paper-based packaging is normally used as a traditional package due to its non-uniformed shape, ease of print and low cost (Twede, 2005). On the other hand, the limitation of paper is less durable against an environment (very low heat and moisture resistance) led to a defect in both packages and products. In order to meet the requirements, the end-products with multi-functional properties are employed as a laminating paper

packaging. A plastic film, thin synthetic resin layer, is further used to overcome this drawback. The most common plastic films are polypropylene (PP), polyester (PET), low density polyethylene (LDPE) and oriented polypropylene (OPP). In this case, OPP provides various advantages such as low cost, ease of process, high gloss levels and soft products, generating a greater potential for the finished materials to scuff or scratch. Therefore, OPP is interesting among those plastic films to prolong the shelf-life of the printed paper packaging via lamination process. OPP lamination is able to prevent creased, faded, water damaged, stained and smudged occurring with paper-based packaging. Its applications involve in the cereal box, juice pack, book cover, and poster resulting in a hybrid laminate (Petrie, 2005).

2.2 Lamination Processes

The performance of laminated structures are frequently dependent upon the types of polymeric material, adhesive, and surface treatment combined to deliver the intended packaging efficiency. The multiple performance criteria such as mechanical properties, moisture or gas barrier property, sealability, printability and cost will be integrated to both flexible and rigid packages via the lamination processes (Wolf, 2010). The manufacture of laminated films is a relatively simple continuous process of effective coating and bonding. Laminating adhesive is preferred when the adhesive itself can provide additional functionality to the final products. There are different lamination processes depending upon the type of materials in which the optimization of them could yield substantial benefits to the production. In specific, laminating machinery can be classified into two categories according to how the adhesive is applied and then converted from liquid to solid (Petrie, 2005; Wolf, 2010; Singha, 2012). The generic diagrams of typical production lines in both dry and wet lamination are exhibited in Figure 2.2 - 2.3, respectively.

2.2.1 Dry Lamination Process

Dry lamination is a process in which the latex adhesives (dissolved in either solvent or water) is applied to the first substrate and evaporated in the drying oven before the lamination. The adhesive coated substrate in slightly tacky stage is

joined with another layer, afterwards. The instantaneous bonding with the high bond strength between layers is generally achieved during a high temperature and pressure nip. The dry lamination can be applied to a broader range of products, such as film-to-film and film-to-foil.

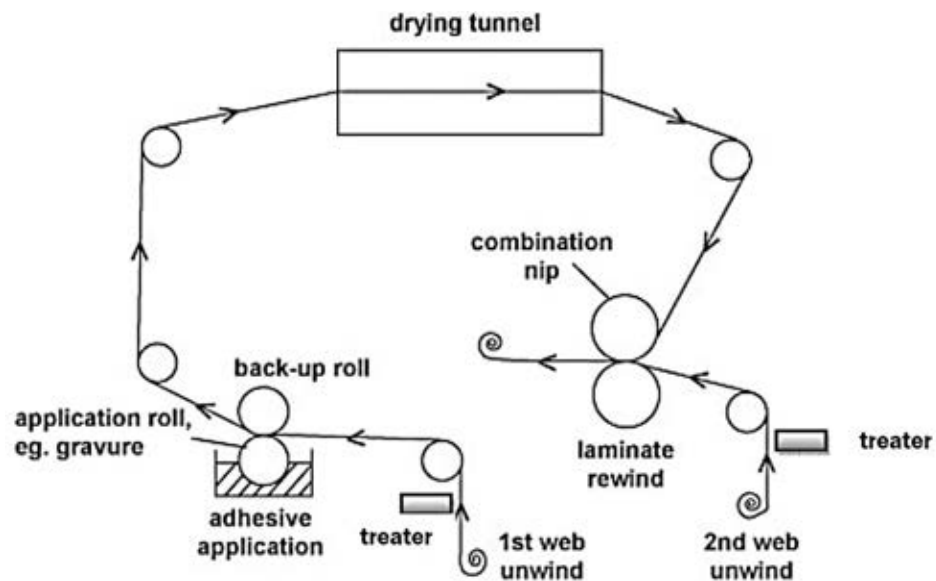


Figure 2.2 Typical dry lamination process configurations (Wolf, 2010).

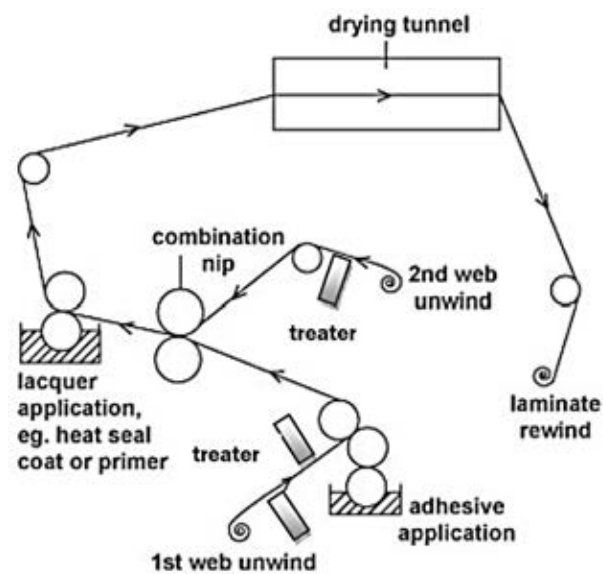


Figure 2.3 Typical wet lamination process configurations (Wolf, 2010).

2.2.2 Wet Lamination Process

In case of wet lamination process, the adhesive is applied to the first substrate by roller coating and then immediately nipped with another substrate. The resulting laminate is dried through the heating oven in order to remove any solvent and build up the bond strength. There are various types of adhesives used in wet lamination, for example waterborne natural products (starch or dextrin), waterborne synthetic latexes (polyvinyl acetate, polyurethane, polyester, and acrylic copolymer), and solvent-based adhesives. Moreover, the wet lamination via waterborne or solvent based adhesives is confined to applications, where at least one substrate is a porous material (e.g., paper, cardboard, textiles, etc.) to facilitate drying. Once cured, the bond strength is generally high enough to cause failure or tearing of porous substrate. Most often, the waterborne synthetic latex adhesives are utilized for the wet bonding because of their high initial strength and fast drying characteristics.

With either dry or wet laminating, full bond strength usually occurred over 24 hours. The bond strength must be sufficient to hold both of the substrates together and resist relaxation until high bond strengths can be achieved. The sub-processes of dry and wet lamination processes can be categorized and are described in Table 2.1. The lamination technique has the advantages of high speeds, ability to apply various films, ability to apply thin skins, and excellent print registration. However, it serves the disadvantages to consume medium energy, spend high capital cost, and require adhesive to bond films. In fact, combining the distinct material (OPP and paper) can be created the potential for the phase separation and also the structural degradation due to their thermodynamically incompatibility. The key is to generate heterogeneous layers within the laminated joints.

2.3 Laminating Adhesives

The laminating adhesive is a heterogeneous layer used to hold two different substrates together and then resist a separation (Kinloch, 1987; Ebnesajjad, 2010). In particular, surface phenomena, such as wettability, adhesion and cohesion, play an exceptionally important role in creating adhesive joints. For evaluation the properties

of the laminating adhesive, it focuses on the followings (Rowland, 1998): complete wetting on the surfaces; adhesion to both substrates with high bond strength; faster lamination speed of OPP/printed paper; higher surface gloss and sealing tightly; non-debonding when laminated film was folded; good shelf-life stability.

There are a large number of traditional adhesives on the market. It is helpful to organize these adhesives in groups with the common characteristics of facilitate their understanding and use. The adhesives could be classified in a number of ways, although no one classification is universally recognized. It includes source, function, chemical composition, physical form, manufacturing and its application (Ebnesajjad, 2009). In lamination process, the laminating adhesives can be divided in two types depending on the manufacturing systems, solvent-based adhesive and water-based adhesive, which are the evaporative or diffusive adhesives. Solvent-based adhesives consist of synthetic rubber, natural rubber, reclaimed rubber, acrylic, phenolic, vinyl resin, urethane, and miscellaneous. On the other hand, water-based adhesives consist of natural rubber, synthetic rubber, polyacrylic, vinyl resin, urethane, and carboxylic-containing copolymer (Society of Manufacturing Engineers (SME), 1970).

2.3.1 Solvent-Based Laminating Adhesives

Solvent-based laminating adhesive is a traditional adhesive with high bond strength, high tackiness, high viscosity and fast-curing time. The solvent-based adhesive can be formulated by many types of polymers as mentioned above. One of the most popular solvent-based laminating adhesives is polyester. But, the utilization of petroleum-derived solvents such as toluene, xylene, or hexane in manufacturing is very expensive depending upon the crude oil price. Furthermore, it can be exposed potentially harmful chemicals due to significant levels of volatile organic compound (VOC) which are considered to be the undesirable environmental impacts (Lichman, 1990; Ebnesajjad, 2009). The speed of which the solvent evaporates is a significant benefit in most production operations. Due to the lack of emulsifiers and surfactants, the moisture resistance of solvent-based adhesive is generally superior to waterborne systems (Petrie, 2005). These materials provide excellent wettability and adhesion to other polymeric films and metal foils.

2.3.2 Water-Based Laminating Adhesives

Due to environmental regulations (EPA, 2015), water-based adhesive with no VOC, waste water and reduction of energy is now an interesting alternative to current solvent-based adhesives used in OPP laminations. Water-based adhesives use water as a carrier fluid with solid content 40 - 50%. The use of water eliminates the problems of flammability, emission, and toxicity associated with organic solvents (Ebnesajjad, 2009). The emulsion polymerization is a major industrial process for the production of water-based polymeric dispersions using common polymeric materials as indicated above (Lovell and El-Aasser, 1998). The main disadvantage of these adhesives is low viscosity, low bond strength, poor moisture resistance, poor thermal resistance, and longer drying time required before developing tack or strength (Voss, 2002; Archer, 1997). These occurring adhesives are more commonly employed for labeling and other packaging applications, especially in the acrylate copolymer and polyurethane laminating adhesives.

2.3.2.1 *Water-Based Polyurethane Laminating Adhesives*

Polyurethane is a synthetic polymer derived by condensation polymerization between a diisocyanate and a polyol to generate a urethane linkage as indicated in Figure 2.4. Water-based polyurethane adhesives have high performance properties with an excellent adhesion to a wide range of flexible products. Besides, They have been developed for standard laminating equipment and fast line speeds. Since polyurethane dispersions are primarily linear polymers, their performance can be greatly improved by an addition of crosslinking agents, for example epoxy silane, carbodiimides and epoxies. The drawbacks of polyurethane dispersion are relatively high cost, poor weatherability and poor solvent resistance (Malavašič *et al.*, 1992).

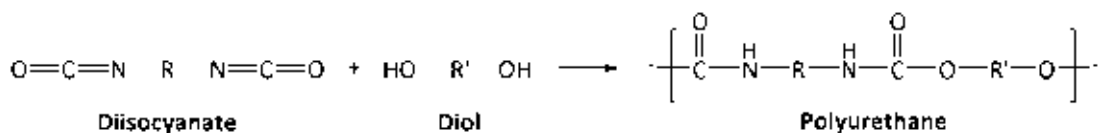


Figure 2.4 The synthesis route of polyurethane, where in the urethane groups –NH-(C=O)-O- link the molecular units.

2.3.2.2 Water-Based Polyacrylate Laminating Adhesives

A variety of acrylic copolymers are generally prepared by an addition polymerization. The acrylic monomers most commonly used in adhesives are ethyl acrylate, methyl acrylate, acrylic acid, methacrylic acid, acrylamide, and acrylonitrile. They are available as emulsions and dispersions. Water-based acrylic latexes offer the low cost adhesives with moderate performance properties. They are tremendously versatile due to the large number of different monomers and resins available. Waterborne acrylic laminating adhesives can provide bonds ranging from flexible and tough to hard and rigid depending on the formulation. Their advantages include moderate peel and impact strength, low shrinkage during cure, rapid bonding at room temperature, tolerance for oily surfaces and good environmental resistance (Ebnesajjad, 2010).



Figure 2.5 The synthesis route of polyacrylate or polymethacrylate with the acrylate linkage $-(\text{C}=\text{O})-\text{O}-$.

2.4 Structure of Adhesive Joints

Basically, the cohesive strength and the adhesion to substrates are factors affecting the good adhesive performance. As an illustration, the structure of adhesive joint indicates that the cohesion mechanism provides an internal strength of adhesive as a result of various interactions including chemical bonding, chemical crosslinking, intermolecular interaction and mechanical bonding between various molecules, while the adhesion mechanism is a force located on a boundary layer between substrate and adhesive itself, as indicated in Figure 2.6.

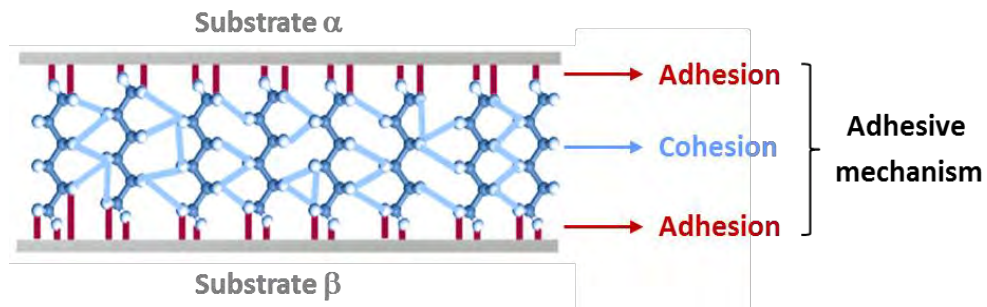


Figure 2.6 Adhesion and cohesion mechanisms within bonded joint (Adapted from: <http://www.adhesiveandglue.com/adhesive-definition.html>).

Currently, there are several theories attempting to explain the phenomenon of adhesion of the adhesive on the substrates, there is currently no unified theory to justify all cases. Now it is required to use the combination of different theories to explain them.

2.5 Definition of Adhesion

As mentioned above, the adhesion refers to the thin layer (boundary layer) between the substrate and the adhesive itself which holds the adhesive with each substrate. The definition of the adhesion is used to define two important concepts. First, the forces and mechanisms related to the forces created by the intermolecular interaction, chemical bonding, and anchoring mechanisms by roughness, adsorption and diffusion. Secondly, the boundary layer is concerned.

The adsorption phenomena occurs when part of adhesive polymers enter in contact with a substrate but not cross it, bonding to it by the action of intermolecular interaction and chemical bonding that develop in the area known as boundary layer or interface. The adsorption can be defined as the adhesion of the adhesive without penetration to the substrate.

In contrast, the diffusion phenomenon that forms part of the polymers which form the adhesive go through the substrate, resulting in the binding and anchorage points intertwining the two materials. Additionally, the boundary layer refers to the thin layer corresponding to the interfaces between the substrate and the adhesive,

where are all the forces as mentioned above. The adhesion is parameterized in two concepts:

2.5.1 Adhesion Energy

The adhesion energy represents the sum of all the energies produced through various interactions (chemical bonding, dipole-dipole moments, electrostatic forces, anchoring mechanisms, adsorption and diffusion.) These are developed in the boundary layer. The adhesion energy (E_A) is the energy which is released when one liquid or solid surface comes in contact with another liquid or solid surface to create a new interface, described by *Young-Dupré equation*:

$$E_A = -\gamma_{LV}(1 + \cos \theta) \quad (2.1)$$

Where, γ_{LV} is an interfacial tension between liquid and vapor; θ is a contact angle.

2.5.2 Reversible Work of Adhesion

The reversible work of adhesion represents the work that is applied to exceed the sum of all interactions or the boundary layer.

2.6 Adhesion Mechanisms

To emphasize on the adhesion mechanisms, these could be divided into five different types as an illustration (Figure 2.7):

2.6.1 Mechanical Adhesion

The mechanical adhesions are occurred by the adhesives flowing and penetrating microcavities of the surfaces and hold surfaces together by interlocking. When the adhesive then hardens, the substrates are held together mechanically. The adhesive must not only wet the substrate, but also have the rheological properties to penetrate pores and openings in a reasonable time. The surface of a substrate consists of a maze of peaks and valleys. According to the mechanical theory of adhesion, in

order to function properly, the adhesive must penetrate the cavities on the surface, displace the trapped air at the interface, and lock-on mechanically to the substrate.

2.6.2 Chemical Bonding

The chemical bonding theory of adhesion invokes the formation of covalent, ionic or hydrogen bonds across the interface. There is some evidence that covalent bonds are formed with silane coupling agents (or adhesion promoters), and it is possible that adhesives containing isocyanate groups react with active hydrogen atoms, such as hydroxyl groups, to form a permanent bond .

2.6.3 Physical Absorption

The adhesion results from molecular contacts between two substrates through van der Waals forces. For these forces to develop, the adhesive must make intimate molecular contact with the substrate. The process of establishing continuous contact between an adhesive and the adherent is known as wetting. The wetting can be determined by contact angle measurements.

2.6.4 Diffusive Adhesion

Some materials can merge at the bonded joint by diffusion. It occurs when the molecules of materials are mobile and soluble in each other. This would be effective with polymer chains where one end of the molecule diffuses into the other materials. When polymer granules are pressed together and heated, the atoms diffuse from one particle to the next. This joins the particles into one.

2.6.5 Electrostatic Adhesion

The basis of the electrostatic theory of the adhesion is the difference in electronegativities of adhering materials. Adhesive force is attributed to the transfer of electrons across the interface creating positive and negative charges that attract one another. The electrostatic theory originated in the proposal that if two metals are placed in contact, electrons will be transferred from one to the other so forming an electrical double layer, which gives a force of attraction. As polymers are insulators, it seems difficult to apply this theory to adhesives.

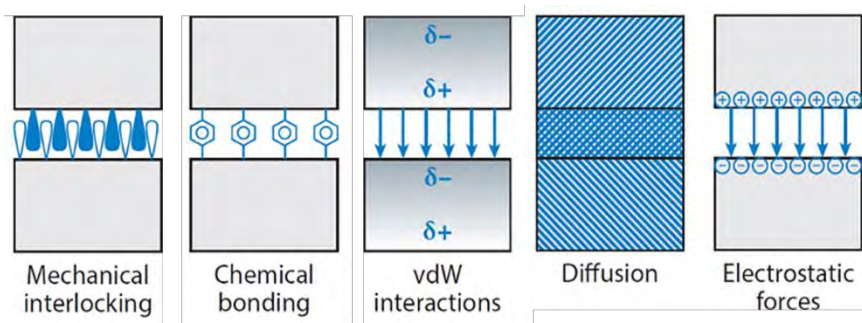


Figure 2.7 Adhesion mechanisms.

2.7 Failure Modes of Bonded Joints

For what concerns the mechanical behavior, an important analysis for the tested mechanical structures, adhesive joints included, is their failure modes. In the case of adhesives, the analysis of the failure mode is extremely important to verify if the considered adhesive fits with the intended application and also to understand the mechanical results. Visual inspection by means of an optical microscope, or a more precise equipment, is able to assess the failure mode. Figure 2.8 indicates the typical failures of adhesive-bonded structures.

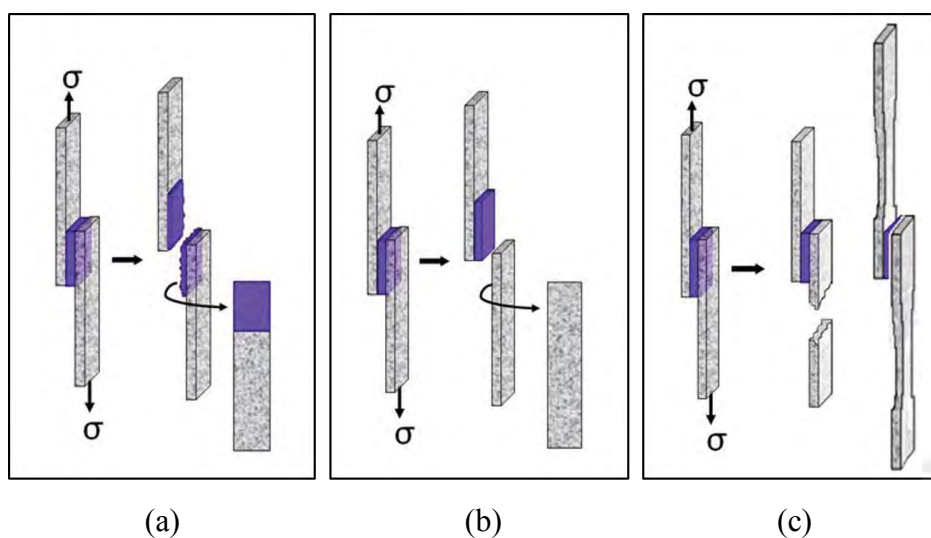


Figure 2.8 Failure modes of bonded joints: (a) cohesive failure (b) adhesive failure (c) structural failure.

The cohesive failure occurs in the adhesive layer, as shown in Figure 2.8(a). In this case, it is possible to find the clear presence of the adhesive material on both the two adherent faces. The adhesive failure presents a complete separation between the adhesive layer and one of the substrates, as shown in Figure 2.8(b). It should be mentioned that the combined modes also, i.e., with the presence of both adhesive and cohesive failures in the same joint, can be encountered. The last failure mode shows a failure in one of the two adherents which is the structural failure (Figure 2.8(c)). In laminating adhesives, the structural failure is the optimal bond strength.

2.8 Reinforcing Fillers

The waterborne polyurethane laminating adhesives and waterborne acrylate laminating adhesives were obtained the catastrophic failure in the bulk layer with a low-to-moderate peel strength values. Thus, their performance should be modified by reinforcing fillers. The reinforcing fillers are incorporated to provide improved peel strength, especially to low energy surfaces. They take on an important role in the composition of the adhesives. A number of functional fillers are available for various applications, including calcium carbonate, alumina trihydrate, barium sulfate, silica, and kaolin clay. In our research focuses on the modification of clay minerals to use as a specific filler in the water-based laminating adhesives.

2.9 Clay Minerals

The most predominant chemical weathering product of soil is clay mineral which is also known as a hydrous aluminium and/or magnesium phyllosilicate with a layered or plate-like structure. The fundamental units of silicate clay consist of individual tetrahedral and octahedral sheets. A tetrahedral sheet (silica tetrahedron) is a four-sided configuration of the silicon atom while an octahedral sheet (aluminium/magnesium octahedron) consists of eight-sided building block of either aluminium or magnesium atom (Pavlidou and Papaspyrides, 2008). The most common type of clay minerals is a 2:1 layered silicate e.g. smectite, vermiculite, illite, and chlorite which

its crystal lattice includes a central octahedral sheet bound between two external tetrahedral sheets by sharing the associated oxygen atoms, as indicated in Figure 2.9.

The layer thickness of silicate clays is around 1 nm led to a perfect crystalline structure. The aspect ratio (length/thickness ratio) is particularly high with values greater than 1000 (Solomon *et al.*, 2001). Likewise, clay particles are stacked in parallel layers which are slightly separated from each other with regular electrostatic and van der Waals interaction, called an interlayer or gallery of clay (Manias *et al.*, 2001; Ray and Okamoto, 2003; Pavlidou and Papaspyrides, 2008).

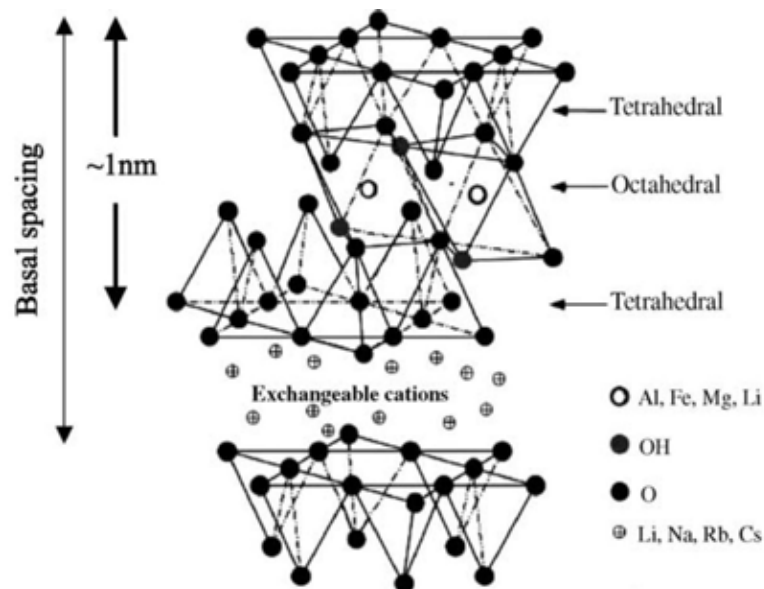


Figure 2.9 The structure of a 2:1 layered silicate (Pavlidou and Papaspyrides, 2008).

In nature, ions having nearly the same radius are able to fit within the layers (for example, Al^{3+} replaced by Mg^{2+} or Fe^{2+} ion) through an isomorphic substitution process. It generates negative charges that are counterbalanced by either alkali or alkaline earth cations situated inside the clay galleries. The cation exchange capacity (CEC), generally expressed as mequiv/100 g, is used to determine the number of exchangeable cations in the layered silicate. This charge is not locally constant, but varies from one layer to another, and must be considered as an average value over the entire crystal (Manias *et al.*, 2001; Ray and Okamoto, 2003).

Bentonite (BTN) is one of the most effective and powerful clay minerals consisting mostly of montmorillonite. It comes from naturally occurring volcanic ash in the presence of water. There are various types of BTN depending on the respective dominant elements, such as sodium (Na), aluminium (Al) potassium (K) and calcium (Ca) that may be attracted to the clay surfaces to neutralize the layer charges. The main uses of BTN are for reinforcing filler, drilling mud, purifier, and barrier due to unique water adsorbing and swelling characteristics.

2.10 Organomodified Layered Silicate (Organoclay)

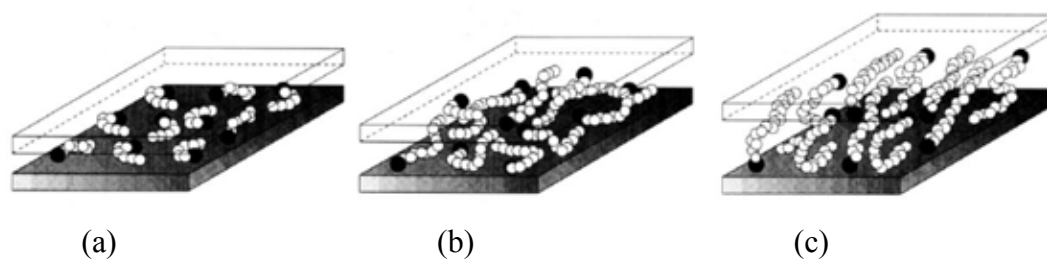


Figure 2.10 The alkyl chain aggregation models: (a) short chain length with isolated molecules (b) medium chain length with in-plane disorder and interdigitation to form the quasisdiscrete layers (c) long chain length with increased interlayer order (Mittal, 2009).

Organomodified layered silicate is an intercalation of an organic compound, typically quaternary alkylammonium salt, alkylphosphonium salt, biomolecules or surfactant, to interlayer spaces of clay minerals through a cationic exchange process. The separation from an initial basal spacing of 3 Å in the case of Na⁺ cations to the distances in the ranges of 10-40 Å was occurred depending upon alkyl chain length (Figure 2.10), packing density, and temperature. Moreover, the organic compound is located either parallel to the layered silicates or radiate away from them to generate an organophilic surface with covalently linked organic moieties as well as a change in chemical characteristics (Alexandre and Dubois, 2000; Ray and Okamoto, 2003; Bardzinski, 2014). In order to determine the orientation and its arrangement of the

organic compound in organoclays, a structural characterization is performed by X-ray diffraction (XRD) and Fourier transformed infrared spectroscopy (FT-IR). XRD pattern presents a d-spacing corresponding to a distance between clay intergalleries. As an increase in the organic compound loading, the (001) reflection peak is slightly shifted towards a lower 2θ angle which indicates the larger d-spacing through Bragg's relation. Likewise, the frequency shifts of both CH_2 stretching and bending vibrations are monitored via FTIR spectra due to the intercalated molecules existing in states with different degrees of order. The molecular environments vary from solid-like to liquid-like resulting from an increase in gauche/trans conformer ratio.

Recently, there are many examples of outstanding research that has been developed the organoclay for the specific application. In 2001, a nonionic surfactant, linear alcohol ethoxylate used as a household detergent with low toxicity, was used to prepare an organo-bentonite to improve an adsorption capacity and a chemical stability by Shen *et al.* In 2005, Zhang *et al.* synthesized a highly-ordered organoclay based on an alkylammonium salt to increase its basal spacing to 3.8 nm, afterwards. It was further used to prepare the polyethylene and polypropylene nanocomposites. Moreover, the modification of an organo-montmorillonite with the intercalation of quaternary phosphonium cations was studied by Patel *et al.* (2007). It indicated that higher thermal stability was observed in a melt processing of nanocomposites. For biomolecules, Ozturk *et al.* (2007) applied a histidine to the octahedral sheet of clay mineral to form the covalent bond. This organoclay revealed extraordinary properties as the adsorbent for purifying nanoclinal antibodies. Then, Gopinath and Sugunan (2007) immobilized the α -amylase, glucoamylase and invertase on acid-activated montmorillonite via adsorption and grafting to use for the enzyme immobilization and biosensing applications. Consequently, the organoclays are expected to be more advantageous beyond clay minerals as adsorbents, rheological control agents, paints, oil-based drilling fluids, personal care products, cosmetics, refractory varnishes, sensors, active and intelligent packages, etc.

In addition, organo-modified clays are now widely used to prepare a large variety of nanocomposite materials due to their low surface energy, great wetting characteristic and strong interfacial interaction with the polymer matrices. Polymer/organoclay nanocomposites exhibit an enhancement in physical, structural, thermal

and mechanical properties. For example, they could act as powerful polymer blend compatibilization agents and behave in a synergistic manner with standard flame retardant formulations, imparting self-extinguishing properties to a large class of polymers (Vaia *et al.*, 1993; Labidi *et al.*, 2010).

2.11 Porous Clay Heterostructure (PCH)

To enhance the particular properties beyond clay minerals and organoclays, a porous clay heterostructure (PCH) has been developed as a relatively new class of porous materials consisting of the lamellar framework with silica pillars. Its unique properties belong to the high specific surface area approximately 500 - 1000 m²/g with uniform pore diameters in the super micropore to mesopore range (1.5 - 3.0 nm) and high thermal stability. PCH was firstly discovered in 1995 by Galarnau *et al.* through the surfactant-directed assembly of silica species within the two-dimensional galleries of either natural or synthetic clay. The synthesis of thermally stable PCH consists of the following steps as presented in Figure 2.11.

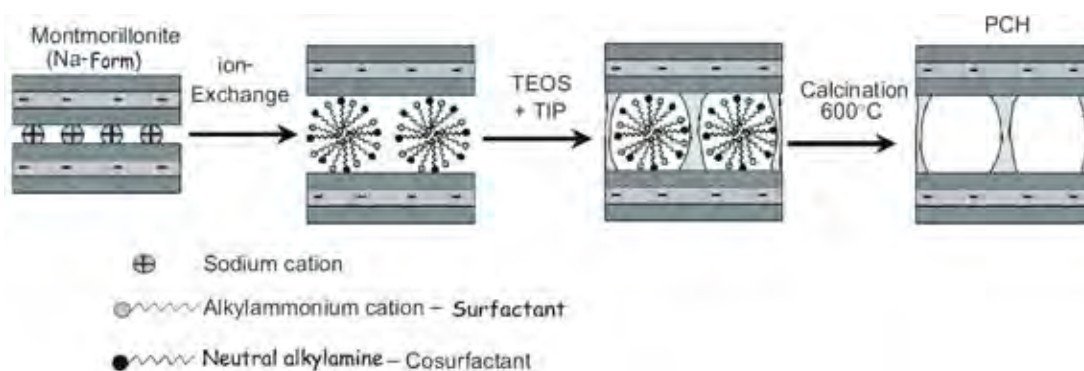


Figure 2.11 The synthesis mechanism of PCH (Chimiularz *et al.*, 2009).

Cationic templates and neutral amine co-templates are intercalated between the interlayer spaces of the host clay forming micelle structures. Subsequently, the silica pillars are created by in-situ polymerization of tetraethylorthosilicate (a silica source) around them. Then, the organic templates are removed from as-synthesized PCH by a classical calcination or a chemical extraction with an acidified solvent. The

negative charge of the clay layers is compensated by protons formed during the decomposition of the organic templates. Protons can migrate into unoccupied position in the clay layers (octahedral vacancies in di-octahedral clays or defects in tri-octahedral clays) and in consequence reduce a cationic exchange capacity (CEC) potential of PCH. This effect can be limited by exchanging the protons for NH_4^+ cations, which are too large to migrate in to the clay layers (Chimielarz *et al.*, 2006). The presence of these protons offers an interesting prospect for the modification of PCHs with different cations or transition metal ions in order to fine-tune them for specific adsorption or catalytic process. Up to now, many researches appeared on the synthesis and characterization of PCHs derived from fluorohectorite (Galarneau *et al.*, 1995; Galarneau *et al.*, 1997), synthetic saponite (Ahenach *et al.*, 2000), and natural montmorillonite (Ahenach *et al.*, 2000; Chimielarz *et al.*, 2009).

2.12 Applications of PCH

The new advanced materials are designed using PCH for a wide range of applications from the environment remediation to biomedicine. Due to the chemical functionalization of the intragallery framework walls while retaining efficient access to the active sites within the clay galleries, PCH attracts many researches in view to prepare clay-based materials. Recently, our group researches has previously reported the successful modification of PCH. In 2008, Srithammaraj *et al.* synthesized the mesoporous clay via the polymerization of the cationic surfactants in the presence of silica template between layers of sodium bentonite (BTN) clays. These mesoporous clays were further modified by a co-condensation reaction of dodecylamine (DDA) and tetraethoxysilane (TEOS) with methyl triethoxysilane in order to improve the hydrophobicity of PCH materials for an ethylene scavenger entrapping system in an active food packaging.

Mattayan *et al.* (2009) reported the surface modification of PCH with iron ions (Fe^{2+} and Fe^{3+}) to induce the magnetic properties. The results revealed that magnetic PCH exhibited the bacteriostatic effect against *Escherichia coli* and *Staphylococcus aureus*. Subsequently, magnetic PCH was blended with polylactide (PLA) to obtain PLA/clay nanocomposites using as an intelligent food packaging.

In 2010, Jindapech *et al.* studied a magnetic PCH by introducing manganese ion (Mn^{2+}) on the porous clay surface. The magnetic properties of Mn-PCH were significantly enhanced beyond Fe-PCH. Then, this magnetic PCH was used to produce the nanocomposite film for anti-corrosion in an active packaging.

Srithammaraj *et al.* (2011) prepared PCH through the surfactant directed assembly of mesostructured silica within the two-dimensional galleries of clays. In addition, PCH was modified its surface with the organic groups ((3-mercaptopropyl) triethoxysilane and methyl triethoxysilane) by a co-condensation method to produce organic-inorganic hybrid materials, MPPCH and HPCH respectively. Both MPPCH and HPCH indicated the higher efficiency in adsorbing an ethylene gas compared to PCH and also Na-BTN due to the hydrophobicity of organic groups. The synthesized MPPCH and HPCH were blended with polypropylene (PP) to obtain the composite films for ethylene scavenging packages.

Boonruang *et al.* (2012) modified PCH using the chromophore which was bromothymol blue for detecting the climacteric fruit freshness (banana). PCH-BTB was blended with low density polyethylene (LDPE), and compressed LDPE/PCH-BTB nanocomposites to a film. The color change of the nanocomposite film from green to yellow was observed corresponding to an increase in CO_2 levels during fruit ripening. This nanocomposite film was further used as a smart packaging in food industries.

Bunnak *et al.* (2014) produced the cationic-modified PCHs as a filler to improve the dielectric behaviors of the polymer-based nanoclay materials. It was found that the dielectric constant of modified PCHs was higher than that of unmodified PCHs, suggesting that the cationic ion was able to induce the polarity into PCH surface. Among all of these cationic species, Ba-PCH indicated the largest dielectric constant owing to the largest ionic radius of barium atoms (Ba). Therefore, this Ba-PCH was considered to be the effective filler in the nanocomposites for practical application as a capacitor.

2.13 3-Aminopropyl Triethoxysilane Functionalized PCH (APCH)

To enhance the physical and chemical properties of PCH, the incorporation of organic compounds on PCH surface is now interesting as the organic-inorganic hybrid structure. It can be divided into two methods: a post-synthesis modification (grafting method) and a co-condensation reaction. The organic modification provided a controllable surface area and pore size of the mesoporous materials led to the improvement in a capability for specific applications e.g. high adsorption and high selectivity. 3-Aminopropyl triethoxysilane (APTES) is usually used in the surface modification. There are many researches focused on the APTES functionalization on the surface of natural and synthetic silica sources.

In 2006, Wu *et al.* modified the surface of submicron silica spheres from TEOS with aminopropyl and phenyl groups through the one-step process. The silica particles modified with aminopropyl groups showed higher organic dyes (brilliant blue FCF or BBF) adsorption compared with pure TEOS particle and the particle modified with phenyl groups. Due to the protonation of silanol groups and amine groups on the silica surfaces created the electrostatic and hydrophobic attractions with BBF anions as shown in Figure 2.12, the adsorption capacity of APTES was strongly increased.

Araki *et al.* (2009) synthesized the aminopropyl-functionalized mesoporous silica microspheres (AF-MSM) by one-step method. The mesoporous silica surface was modified by the co-condensation reaction of TEOS, DDA, and APTES. FT-IR spectra was used to confirm the presence of aminopropyl groups in AF-MSM through a broad band extending from 2800 to 3400 cm^{-1} corresponding to the stretching vibration of NH_3^+ . The intensity of these peaks increased with increasing APTES contents. Consequently, AF-MSM was applied to the CO_2 adsorbent.

To improve the properties of PCH for a desirable application, Boonruang *et al.* (2012) functionalized PCH with amino groups of APTES, called APPCH. The surface area and pore volume of APPCH were decreased as an increase in APTES contents. In addition, the adsorption capability on either methyl red or bromothymol blue was expanded in the case of APPCH in which the protonation of NH_2 led to

an increment in the electrostatic attraction between APPCH and dyes. The composite of PP/APPCH was further used as a colorimetric indicator in food packaging.

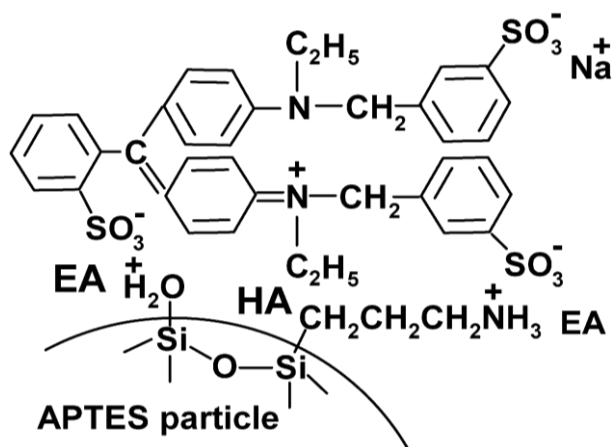


Figure 2.12 Schematic diagrams for the adsorption of BBF on the acidified APTES particles (EA = electrostatic attraction and HA = hydrophobic attraction).

2.14 Polymer/Layered Silicate Nanocomposites

The Polymers are traditionally reinforced with the inorganic fillers in order to enhance their properties as well as reduce costs. These conventional fillers include talc, calcium carbonate, fiber, clay, etc. The particle-filled polymer is normally called a nanocomposite material. The nanocomposite is a multiphase solid material which at least one dimension of dispersed phase is in a nanometer scale (less than 100 nm). Nanoparticles often strongly influence the properties of the composites at very low volume fractions. Besides, the geometrical shape of the particles plays an important role in determining properties of the composites (Mittal, 2009). The nanocomposite is attracting considerable attention in the academic and industrial polymer researches owing to the significant improvement in the superior properties such as dimensional stability, thermal stability, mechanical strength, stiffness, gas barrier, flame retardant, and electrical conductivity beyond the conventional microcomposites.

Polymers incorporating layered silicates are among the first nanomaterials to emerge on the market demand as advanced products. In order to take advantage of

the addition of these fillers, a homogeneous dispersion within the polymer matrix must be efficiently obtained. It requires sufficiently favorable enthalpic factors which are achieved due to the strength of interfacial interaction between two phases. In their pristine form, layered silicates are hydrophilic in nature, so they are very difficult to disperse into polymers. The surface modification of these materials is necessary to obtain organically modified silicates which are more compatible with the organic polymer matrices.

Depending on the nature of the components and the method of preparation, there are three categories of polymer/layered silicate nanocomposites as depicted in Figure 2.13 (Manias *et al.*, 2001; Beyer, 2002; Ray and Okamoto, 2003; Pavlidou and Papispyrides, 2008). In some cases, layered silicates are flocculated because of a hydroxylated edge-edge interaction leading to a phase separated (unintercalated) composite. Its property remain in the same range as the traditional microcomposites. Over this classical family of composites, two types of composites can be recovered. First, intercalated structures are formed in which an insertion of the polymer matrix into the galleries of silicate structure occurs in a crystallographic regular fashion. The result is a well ordered multilayer structure of the alternating organic and inorganic layers caused of less than 20 - 30 Å separation between platelet with the electrostatic force. The properties of the intercalated nanocomposites typically resemble those of ceramic materials. Moreover, the composite microstructure is classified as exfoliated or delaminated when the individual silicate layers are uniformly dispersed in the continuous polymer matrices. The electrostatic forces of the interaction between the platelets have been overcome by polymer chains in the nanocomposites led to the phase separation of 80 - 100 Å. The silicate contents of the exfoliated composite are much lower than that of intercalated nanocomposite.

The two complementary techniques are generally used to investigate the structures of nanocomposites including wide angle X-ray diffraction (WAXD) and transmission electron microscopy (TEM) as indicated in Figure 2.14 (LeBaron *et al.*, 1999; Vaia *et al.*, 1999). Because of its easiness and availability, WAXD is most commonly used to probe the different types of nanocomposite structures. Besides, this technique allows the determination of the interlayer spacing (d) between silicate layers utilizing Bragg's law: $\sin\theta = n\lambda/2d$. For immiscible polymer/layered silicates,

the structure of layered silicate is not affected leading to unchanged basal reflection and also d-spacing. On the other hand, the d-spacing of intercalation structure increases and the diffraction peak shifts toward lower angle. In the exfoliated nanocomposite, the extensive layer separation associated with the delamination of the original layered silicate in polymer matrix results in an eventual disappearance of the diffraction pattern and a disruption of any coherent layer stacking.

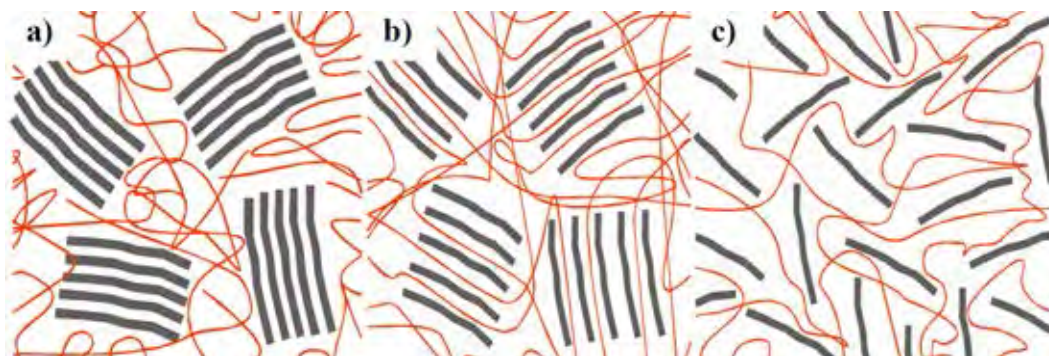


Figure 2.13 Schematic illustration of the different types of nanocomposites based on interactions between polymers and layered silicates: (a) phase separated composite, (b) intercalated composite and (c) exfoliated composite (Zádrapa and Maláč, 2011).

Some layered silicates do not exhibit well-defined basal reflections. Thus, the decreased peak broadening and intensity are very difficult to study. TEM is used to determine the nanocomposite structures. It allows qualitative understanding of the internal structure and can directly provide information in real space, in a localized area, on morphology and defect structures.

In fact, the preparation method of polymer/layered silicate nanocomposite is another influence in its structure. There are several strategies considered to produce nanocomposites. Four processes are extremely used: in-situ polymerization is the first method in which the layered silicate is swollen within the monomer solution. Polymerization can be initiated either by heat or radiation and occurred within the galleries of layered silicates. In solvent method, a polar solvent, toluene or N,N-dimethylformamide, is able to participate in whole synthesis steps of the composites. Polymer and layered silicates are dissolved in the solvent via in-situ polymerization

as the previous method. The advantages of the second method is that intercalated nanocomposites can be formed; however this approach is difficult to use in industry caused the use of large quantities of solvents. Melt intercalation is the blending of the molten thermoplastic with the layered silicates in order to optimize the composites. The polymer chains have the significant loss of conformational entropy during the intercalation thus either intercalated or exfoliated nanocomposite could be formed. Owing to its great potential in the industrial applications, this method has become increasingly popular (Alexandre and Dubois, 2000).

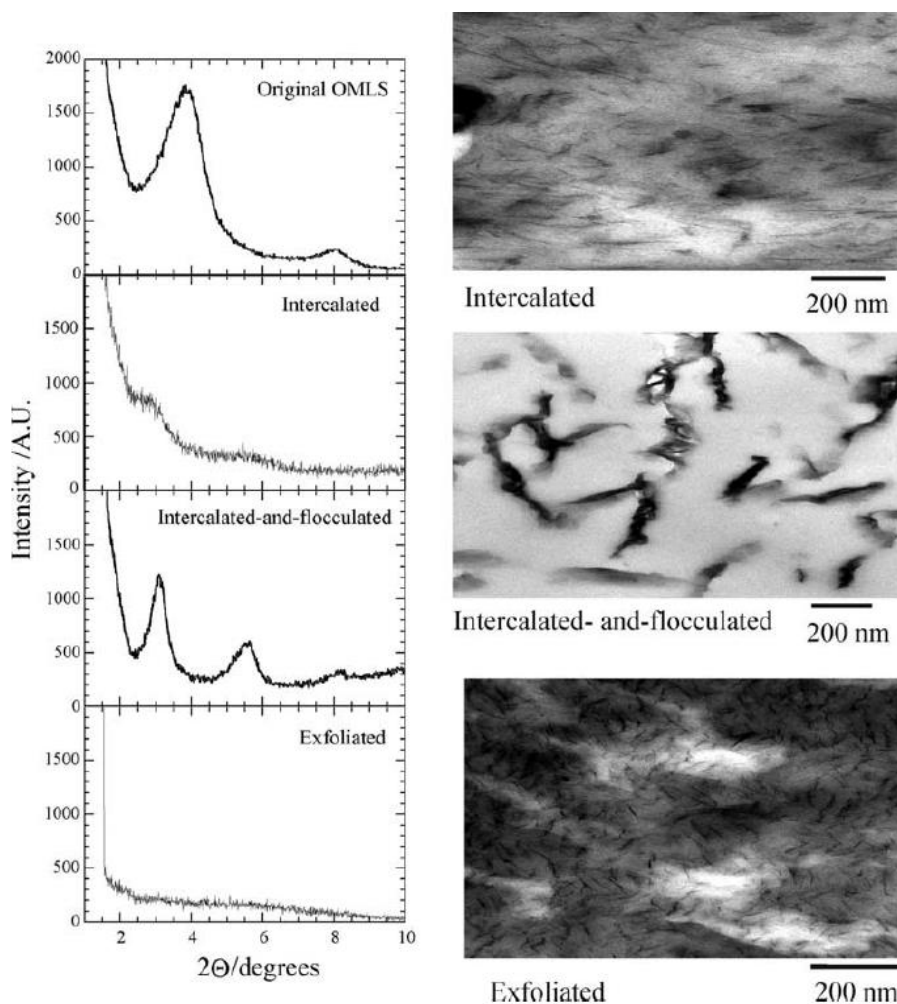


Figure 2.14 Typical XRD patterns and TEM micrographs of three distinct types of polymer/layered silicate nanocomposites (Ray and Okamoto, 2003).

Table 2.1 The adhesive lamination process

	Process	Description	Application Equipment	Typical Adhesives
Dry Process	Dry Bond Laminating	Liquid adhesive coated on substrate, dried with heat/air flow, and then laminated to a second substrate via a heated compression nip	Gravure application cylinder	<ul style="list-style-type: none"> - Polyurethane dispersions - Acrylic emulsions or solvent - Water-based polyvinyl alcohol - Ethylene vinyl acetate polymer - High solids silicone solvent
	Hot Melt Seal Coating	Low viscosity hot melt adhesives are applied to substrate	Heated rotogravure cylinder, extruder	<ul style="list-style-type: none"> - Ethylene vinyl acetate - Modified polyolefin - Polyesters
	Cold Seal	Liquid adhesives applied, dried by heat or air, and bonded with slight pressure so tack to non-cold seal surfaces is minimized	Gravure application cylinder	<ul style="list-style-type: none"> - Synthetic rubber - Acrylic - Natural rubber
Wet Process	Wet Bond Laminating	Liquid adhesive applied to substrate, then immediately laminated to the second layer via nip, followed by drying with heat/air flow (one substrate must be porous to allow evaporation of water or solvent)	Gravure cylinder or smooth roll	<ul style="list-style-type: none"> - Polyurethane dispersions - Acrylic emulsions - Ethylene vinyl acetate polymers - Polyesters - Starch, dextrin, latex - High solids silicone solvent
	Solventless Lamination	Adhesives are metered on substrate in a liquid form, then mated to a second layer via heated nip	Multiple application roll configurations	<ul style="list-style-type: none"> - Polyurethanes - Polyesters

CHAPTER III EXPERIMENTAL

3.1 Materials

The water-based polyurethane adhesives were synthesized using isophorone diisocyanate (IPDI) of 98 wt% purity (mixture of *cis/trans* isomers), poly(propylene glycol) (PPG) with a M_n of 2000 and hydroxyl value of 56 mg KOH/g (dried under vacuum at 120 °C), and 2,2-bis(hydroxymethyl)propionic acid (Bis-MPA; 98 wt% purity). The chain extender, catalyst and neutralizing agent used were 1,4-butanediol (BDO; 99 wt% purity), dibutyltin dilaurate (DBTDL) and triethylamine (TEA; 99 wt% purity), respectively. N-methyl-2-pyrrolidone (NMP) with a purity greater than 99 wt% was obtained, along with all of the other chemical reagents, from Aldrich Chemicals and were used as received without any further purification.

The water-based polyacrylate adhesives were synthesized using monomers, including 2-ethylhexyl acrylate (EHA), styrene, ethylene glycol methyl ether acrylate (EGMA), 2-(hydroxyethyl) methacrylate (HEMA), 1,3-butanediol dimethacrylate (BDMA), butyl acrylate (BA), acrylic acid, methyl methacrylate (MMA) and styryl acrylate (STA). All Monomers were purchased from Aldrich Chemicals and purified by using an inhibitor removal resin (Alfa Aesar) to remove contaminants. TritonTM X-100, TritonTM X-200 and sodium dodecyl sulfate (SDS) as surfactants; ammonium persulfate (APS) and potassium persulfate (KPS) as initiators; sodium bicarbonate (NaHCO₃) as a buffer were purchased from Aldrich Chemicals.

Commercial sodium-activated bentonite (Na-BTN), with cationic exchange capacity of 44.5 mmol/100 g, was supplied by Thai Nippon Chemical Industry Co., Ltd. Cetyltrimethylammonium chloride (CTAC) was provided from Italmar Co., Ltd. The co-surfactants, 3-aminopropyltriethoxysilane (APTES), dodecylamine, tetraethyl orthosilicate (TEOS) and 3-(trimethoxysilyl)propyl methacrylate (TSPM), were then purchased from Aldrich Chemicals. The dispersing medium, 37% hydrochloric acid (HCl) and methanol (CH₃OH), were acquired from RCI Labscan Ltd. All chemical reagents were used as received without any further purification.

3.2 Experimental

3.2.1 Preparation of Porous Clay Heterostructure

3 g of Na-BTN was added into 50 ml of 0.1 M CTAC solution. The mixture was continuously stirred at 50 °C for 24 h to ensure the cationic exchange had reached equilibrium. The organo-modified BTN (OBTN) was filtered and then washed with deionized water and methanol (1:1 (v/v) ratio) until at pH 9 to remove excess surfactant. The OBTN was dried at 60 °C for 24 h, ground into fine particles using a centrifugal ball mill at 400 rpm for 30 min, and screened through a mesh size of #325. The OBTN was stirred at 50 °C for 30 min in dodecylamine to form micelle structures in the clay galleries, followed by TEOS to derive the co-condensation at room temperature for 4 h (OBTN: dodecylamine: TEOS (v/v/v) of 1: 20: 150). The as-synthesized product was purified by solvent extraction (CH₃OH: HCl (v/v) ratio of 9:1) after drying at 60 °C. The solution was filtered, washed with CH₃OH, and then allowed to dry overnight before screening through a mesh size of #325 to yield the PCH.

3.2.2 Preparation of Amino-Functionalized PCH (APCH)

The mesoporous material was prepared as follows: approximately 50 g of Na-BTN was dispersed into 0.1 M CTAC solution and held at 50 °C for 24 h to ensure the cationic exchange had reached equilibrium. The OBTN was filtered and washed with deionized water and methanol (1:1 (v/v) ratio) until at pH 9 to remove excess surfactant. The dried OBTN was agitated at 50 °C for 30 min in dodecylamine (neutral amine) to form micelle structures in the clay galleries, and then a mixture of TEOS and 5 wt% APTES was added to derive the co-condensation at 25 °C for 4 h with a 1:20:150 molar ratio of OBTN: dodecylamine: TEOS+APTES. The products were purified via a solvent extraction (CH₃OH: HCl (v/v) ratio of 9:1) after drying at 60 °C. The solution was filtered, washed with excess CH₃OH, and then allowed to dry overnight before screening through a mesh size of #325 to yield the APCH.

3.2.3 Preparation of Methacrylate-Functionalized PCH (MPCH)

Mesoporous materials were accomplished as follows: approximately 50 g of Na-BTN was dispersed into 0.1 M CTAC solution at 50 °C for 24 h to ensure the cationic exchange had reached equilibrium. The synthesized product was filtered and then washed with a mixture of deionized water and methanol (1:1) until at pH of 9. The OBTN was agitated in dodecylamine at 50 °C for 30 min, followed by TEOS to derive the co-condensation at 25 °C for 4 h (OBTN: dodecylamine: TEOS (v/v/v) of 1:20:150). The air-dried OBTN was purified via solvent extraction (CH₃OH: HCl (v/v) of 9:1) and screened through a mesh size of #325 to obtain the PCH with an apparent density of 1.99 g/cm³. The PCH was then suspended in a freshly prepared solution of 5% (v/v) TSPM in 0.05 M sodium acetate buffer at pH of 4.0. Silylation processes were proceeded at 70 °C for 4 h. The obtained MPCH was then thoroughly washed with excess deionized water to remove the residual unlinked TSPM.

3.2.4 Preparation of Water-Based Polyurethane (WPU) Adhesives

The WPU adhesives were synthesized by prepolymer mixing process with appropriate NCO/OH ratio of 1.0. IPDI and PPG were added in a 1000-mL five-necked flange reaction flask equipped with a mechanical stirrer at 350 rpm, reflux condenser and thermometer. The synthesis reaction was placed in an electromantle at 80 °C for 2 h under nitrogen (N₂) atmosphere, and then DBTDL was slowly dropped in. Bis-MPA was well dispersed in NMP at 60 °C and was added to the mixture. The reaction was continued for another 2 h until the residual -NCO reached the expected content (as determined by the standard dibutylamine back-titration method (David and Stanley, 1969)). The prepolymer was cooled down to 50 °C and its chains were then extended using 2 wt% BDO. The carboxyl functional group in Bis-MPA was gently neutralized by the addition of 100 mL of TEA solution (in deionized water) through a dropping funnel regulating the pH at 7.0 and the WPU adhesives were then obtained with a 40 wt% solid content. The Bis-MPA contents of 1, 3, 5 and 7 wt% were varied in polyurethane ionomers, while the molar ratio of isocyanate/hydroxyl groups (hard/soft segments) of 1, 3, 4 and 5 was varied.

3.2.5 Preparation of WPU Hybrid Adhesives

The WPU hybrid adhesives were synthesized by a prepolymer mixing process at the appropriate -NCO/-OH molar ratio of 1.0. IPDI and PPG were added in a 1000-mL five-necked flange reaction flask equipped with a mechanical stirrer at 350 rpm, thermometer and reflux condenser. The synthesis reaction was placed in an electromantle at 80 °C for 2 h under a N₂ atmosphere, and then DBTDL was slowly dropped in. The 5 wt% Bis-MPA (with respect to the prepolymer weight) was well dispersed in NMP at 60 °C and was added into the prepolymer mixture, followed by APCH at various weight fractions including 0, 0.5, 1, 2 and 3 wt%. The reaction was performed for another 2 h until the residual -NCO reached the expected contents (as determined by the standard dibutylamine back-titration method (David and Stanley, 1969)). The prepolymer was cooled down to 50 °C and its chains were extended by 2 wt% BDO. The carboxyl functional group in Bis-MPA was gently neutralized by the addition of 100 mL of TEA solution through a dropping funnel for 1 h regulating the pH at 7.0 and the WPU hybrid adhesives were obtained with a 40 wt% solid content.

3.2.6 Preparation of Water-Based Polyacrylate (WAC) Adhesives

The WAC adhesives were then synthesized by the batchwise emulsion polymerization process. The pre-emulsion was prepared by dissolution of surfactant and buffer in deionized water, and charged to a 1000-mL five-necked flange reaction flask equipped with a thermometer, reflux condenser and a mechanical stirrer at 350 rpm. The synthesis reaction was placed in an electromantle at 80 °C for 2 h under N₂ atmosphere. The mixture of monomers were then charged to the reaction, followed by the dropwise addition of initiator solution (in deionized water) through a dropping funnel. The temperature was carefully raised to 80 °C, avoiding overheating from the exothermic reaction, and held for 4 h to ensure the maximal conversion. The pH was regulated to 7.0 using 0.5 M TEA. The variations of surfactant types (SDS, TritonTM X-100 and TritonTM X-200), surfactant concentration (0.05, 0.06, 0.08 and 0.15 M), initiator types (APS and KPS), monomer types (EHA, EGMA, SR, HEMA, AA, BA, MMA, STA, and BDMA), natural thickeners (nanosilica, calcium carbonate, PCH and Na-BTN) and wetting agent types were investigated.

3.2.7 Preparation of WAC Hybrid Adhesives

The WAC hybrid adhesives with a molecular weight (M_w) of 309,128 g/mol were synthesized through batchwise emulsion polymerization. Briefly, MPCH at various weight fractions (0, 0.5, 1.0, 1.5 and 2.0 wt%) was dispersed in monomers using an ultrasonic bath (Fisher Scientific FS20) for 50 min. The pre-emulsion was then prepared by homogeneous dissolution of 0.08 M surfactants and 0.7 g buffer in deionized water, and charged to Optimax™ 1001 working station (Mettler Toledo) equipped with a thermocouple, reflux condenser and a mechanical stirrer at 350 rpm. The polymerization was performed at 70 °C under N₂ protection and slowly initiated by the dropwise addition of 0.45 M APS solution (a feeding rate of 0.2 mL/min). The temperature was carefully raised to 80 °C, avoiding overheating from the exothermic reaction, and held for 4 h to ensure maximal conversion. The WAC hybrid adhesives were successfully obtained with a 50 wt% solid content (according to ISO124:1997) and the pH was regulated to 7.0.

3.2.8 Preparation of Water-Based Core-Shell (CS) Adhesives

CS laminating adhesives were synthesized using a two-stage seeded-semibatch emulsion polymerization under a N₂ protection, which were performed in the 1000-mL Optimax™ 1001 working station (Mettler Toledo) equipped with reflux condenser, a mechanical agitator at 300 rpm, a thermocouple for controlling reaction temperature at 75 °C, and two feeding inlets for pre-emulsion and initiator solution, respectively. The peristaltic pumps were used to control an even feeding rate. polyurethane laminating adhesives.

3.2.8.1 *Preparation of Seed Latex*

Poly(styrene-co-ethylhexyl acrylate) seed latex was prepared using the batchwise emulsion polymerization. The pre-emulsion including monomers (21.79 wt% of EHA and 18.21 wt% of styrene), 0.17 M SDS and 0.02 g NaHCO₃ was prepared. A mixture of 0.05 M SDS and 0.33 g NaHCO₃ was initially charged to the Optimax™ reactor, followed by a dropwise addition of the pre-emulsion and 0.1 M APS solution at feeding rate of 0.75 and 0.22 mL/min, respectively. After feeding, the reaction was held for 4 h to ensure maximal conversion. The as-synthesized seed

latex was obtained with 40 wt% solid content which is identical to the theoretical design value (according to ISO124:1997).

3.2.8.2 *Preparation of Core Latex*

10 wt% of seed latex was initially charged to the Optimax™ reactor, followed by the dropwise addition of pre-emulsion and 0.05 M APS solution at a feeding rate of 1.0 and 0.5 mL/min, respectively. The pre-emulsion was prepared by a homogeneous dissolution of monomers (28.5 wt% of EHA and 17.5 wt% of styrene), 0.28 M SDS, 0.16 g Triton™ X-100 and 0.35 g NaHCO₃. After complete feeding, the reaction was held for 4 h to ensure maximal conversion. The core latex was then obtained with 50 wt% solid content which is identical to the theoretical design value.

3.2.8.3 *Preparation of CS Latex*

A core latex was initially charged to the Optimax™ reactor, followed by dropwise addition of a shell pre-emulsion and APS solution at a feeding rate of 0.75 and 0.2 mL/min, respectively. Each of shell pre-emulsions was prepared by dissolving surfactants, buffer and monomers (EHA, EGMA, HEMA styrene, and acrylic acid) in deionized water. After complete feeding, the reaction was held for 4 h to ensure maximal conversion. The CS adhesives were obtained with 50 wt% solid content which is identical to the theoretical design value and the conversions were approximately 99% (no residual monomer at the end of polymerization process). The pH was regulated to 7.0 using monoethanolamine.

3.2.9 Film Preparation

The adhesive films were prepared by casting the latexes (20 mL) on a polytetrafluoroethylene (PTFE) surface. The remaining trapped water was allowed to completely evaporate at 60 °C for 24 h in a vacuum drying oven. The obtained film (typically of 0.5 mm thickness) was then stored in a desiccator to avoid any moisture at ambient temperature prior to characterization.

3.3 Characterization Techniques

3.3.1 Brookfield Viscosity

The viscosity characteristics of latexes were determined by Brookfield viscometer (model DV-III programmable rheometer) with a SC4-27 spindle. The test temperature, shear rate and rotational speed were set at 25 °C, 85 s⁻¹ and 250 rpm, respectively. The thixotropic behavior was obtained by increasing the shear rate from 5 s⁻¹ to 85 s⁻¹ and maintaining for 300 s in order to provide a homogeneous emulsion. Then, the shear rate was gradually decreased from 85 s⁻¹ to 5 s⁻¹. Arrows show the measurements corresponding to the increased and decreased shear rate.

3.3.2 CHNS Elemental Analysis

The elemental quantity was evaluated by a CHNS elemental analyzer (Leco® Truspec). The electrical furnace was operated at 950 °C and the sample was introduced and immediately combusted.

3.3.3 Contact Angle Measurement

The contact angle (θ) of latexes was carried out through Krüss drop shape analysis system (model DSA 10 Mkz), which is a quantitative measurement of the wettability using a syringe to pump the latexes steadily into the sessile drop on a substrate surface.

3.3.4 Differential Scanning Calorimetry (DSC)

The glass transition temperature (T_g) was characterized using DSC204 F1 Phoenix® NETZSCH instrument, measuring an inflection point of the second scan over a temperature range from -100 °C to 100 °C at a heating rate of 20 °C/min. The temperature program was designed for heat-cool-heat under a N₂ purge gas at a flow rate of 50 mL/min. Approximately 5 mg of each sample was sealed in a hermetic aluminium crucible of 25 μ L.

3.3.5 Dynamic Light Scattering (DLS)

The mean particle size and its distribution were determined by a DLS using NanoBrook ZetaPALS Potential Analyzer (Brookhaven Instruments). Latexes were diluted to 0.5 wt% in an aqueous solution of SDS and NaHCO₃. Samples were measured at room temperature through 90° scattering angle. The statistical averages of three replicates were presented.

3.3.6 Dynamic Mechanical Analyzer (DMA)

The DMA instrument (EPLEXOR® 100 N, GABO) was programmed to determine the temperature dependence of storage modulus (E'), loss modulus (E'') and loss factor (tanδ), operating in tension mode at a mechanical vibration frequency of 1 Hz. The temperature range of -80 °C to 30 °C was used at a heating rate of 2 °C/min. The rectangular-shaped specimen (10 mm × 40 mm) was then prepared with a thickness of 1 mm.

3.3.7 Electrolytic Stability Measurement

The electrolytic stability was measured by homogeneous dispersion of latexes in deionized water. The aqueous solution of 2 M NaCl was slowly dropped to the mixture until the coagulation was obtained. The electrolytic stability was defined by the volume of NaCl necessary to coagulate the latexes. The statistical averages of three replicates were presented.

3.3.8 Energy Dispersive X-Ray Analysis (EDX)

The elemental composition in the adhesive films was identified using EDX, which was operated in conjunction with FE-SEM (as per section 3.3.10), at an accelerating voltage of 20.0 kV and a working distance of 15.0 mm. The quantitative analysis was performed via mapping and point & ID modes.

3.3.9 Emulsion Stability Measurement

The stability of the latexes was evaluated by monitoring its Brookfield viscosity (as per section 3.3.1) over 30 d. Each sample bottle was sealed and stored at

ambient temperature until analysis. A shear rate of 85 s^{-1} , a test temperature of $25 \text{ }^{\circ}\text{C}$ and rotational speed of 250 rpm were used with the SC4-27 spindle.

3.3.10 Field Emission Scanning Electron Microscopy (FE-SEM)

The surface morphology of the adhesive film was observed by FE-SEM (Hitachi S-4800 model) with an accelerating voltage of 5.0 kV. The specimen coating was applied by platinum sputtering for 150 s to reduce the surface charging during electron irradiation.

3.3.11 Fourier Transform Infrared Spectroscopy (FTIR)

The structural properties were investigated through FTIR on Thermo Scientific Nicolet iS5 instrument with attenuated total reflectance (ATR) iD7 mode to identify the functional groups of the adhesive films. The spectra were accurately recorded in a transmission mode over the wavenumber region of $4000\text{-}500 \text{ cm}^{-1}$ with 16 scans and a resolution of 4 cm^{-1} . Prior to the characterization, samples were stored in a vacuum oven at 60°C to prevent any moisture adsorption.

3.3.12 Gel Permeation Chromatography (GPC)

The weight average molecular weight (M_w) was measured by using a high-performance GPC instrument (EcoSEC HLC-8320GPC) from Tosoh Co., Japan with RI detector. Tetrahydrofuran (THF) was used as the mobile phase. The adhesive films were dissolved in THF of HPLC grade (RCI Labscan Ltd.) for 24 h, and then filtered through a disposal $0.45 \text{ }\mu\text{m}$ PTFE syringe filter prior to characterization. A test temperature of $40 \text{ }^{\circ}\text{C}$ and a flow rate of 1.0 mL/min were used. The result was calibrated according to polystyrene (PS) standards.

3.3.13 N_2 Adsorption-Desorption Analysis (SAA)

The Quantachrome Autosorb-1 was used to define the N_2 adsorption-desorption isotherm at 77 K. Each powder sample was degassed at 423 K for 17 h under vacuum prior to analysis. The specific surface area, pore volume and pore size were calculated using the Brunauer-Emmett-Teller (BET) equation (Brunauer *et al.*, 1938), while the pore size distribution was defined based on the Barrett, Joyner, and

Halenda (BJH) method (Barrett *et al.*, 1951) using the adsorption branch of the N₂ isotherm. All experiments were repeated three times and the statistical averages were reported.

3.3.14 180° Peel Strength Measurement

The adhesion property of the adhesives was investigated in terms of their 180° peel strength according to ASTM D1876 using Tensiometer-Instron 5567 instrument equipped with a 100 N static load cell, a crosshead speed of 150 mm/min, and a gauge length of 50 mm. The rectangular-shaped specimen (25 mm × 300 mm) was prepared. The latexes were then applied on paper using a drawdown bar with a coating thickness of 24 μm and suddenly laminated to an untreated OPP film. The OPP/adhesive/paper joints were allowed to dry at 60 °C.

3.3.15 pH Measurement

The pH values of the latexes were explored at ambient temperature in a pH meter (EUTECH pH 510 instrument) using a silver reference electrode. The pH was calculated as the average of three experimental determinations.

3.3.16 Simultaneous Thermal Analysis (STA)

The thermal decomposition of adhesive films was examined by high resolution STA449 F3 Jupiter[®] NETZSCH instrument under a N₂ atmosphere at a purge rate of 50 mL/min, and then switching to an O₂ atmosphere at the same purge rate at high temperature (600-800 °C). The temperature range was performed under a dynamic condition from 40 to 800 °C at a heating rate of 10 °C/min. Approximately 10 mg of each sample was loaded on an alumina crucible.

3.3.17 Solid Content

The solid content measurements were accurately performed according to the ISO124:1997 standard. Approximately 1.5 g of latexes was placed in a 60-mm diameter aluminium tray and weighed three times before and after water evaporation.

The solid content was calculated by the following equation as the average of three replicates:

$$\% \text{ Solid content} = \frac{\text{Mass of dried sample}}{\text{Mass of initial sample}} \times 100 \quad (3.1)$$

3.3.18 Surface Tension Measurement

Measurement of the surface tension was performed using a DuNouy tensiometer from CSC scientific Co., Inc., and was then reported in the CGS unit of dyne/cm.

3.3.19 Thermogravimetric Analysis (TGA)

The thermal decomposition was studied using a high resolution TGA model TA Q50 instrument (TA instruments) under a continuous N₂ atmosphere at a purge rate of 40 mL/min over the temperature range of 50-800 °C at a heating rate of 10 °C/min. Approximately 10 mg of each sample was loaded on a platinum crucible.

The grafting ratio (R_g) was calculated from the following equation (Kango *et al.*, 2013);

$$R_g = \left(\frac{W_1'}{W_1} - \frac{W_0'}{W_0} \right) \times 100\% \quad (3.2)$$

where W_1 is the starting weight of modified materials; W_1' is the residual weight of modified materials at 750 °C; W_0 is the starting weight of neat materials; and W_0' is the residual weight of neat materials at 750 °C.

3.3.20 Transmission Electron Microscopy (TEM)

The latex microstructure was observed by TEM using a JEOL JEM-2100 electron microscope with an accelerating voltage of 160 kV. The latexes were dialyzed to remove surfactant and buffer molecules, then diluted to 0.1 wt% solid content in DIW and deposited a drop of the diluted latex on a carbon-coated grid. Preferential staining with ruthenium tetroxide (RuO₄) was used to distinguish soft

and hard phases before TEM examination. The TEM images were captured under a magnification of 50 kx.

3.3.21 True Density

The true density was measured by Quantachrome, Ultrapycnometer-1000 with helium as the purge gas. The sample was previously dried under vacuum at 60 °C for 24 h.

3.3.22 X-Ray Diffraction (XRD)

The crystal structures of the adhesive film were analyzed through a small/wide angle X-ray scattering system, (Rigaku SmartLab) with Ni-filtered $\text{CuK}\alpha$ radiation, operated at 40 kV and 30 mA. The samples were scanned at 2θ ranges of 2-80° with a scan step of 0.01° and a scan speed of 0.5°/min.

CHAPTER IV
SYNTHESIZED AMINO-FUNCTIONALIZED POROUS CLAY
HETEROSTRUCTURE AS AN EFFECTIVE THICKENER IN
WATERBORNE POLYURETHANE HYBRID ADHESIVES
FOR LAMINATION PROCESSES

4.1 Abstract

The use of waterborne polyurethane (WPU) adhesives with non-volatile organic compounds (non-VOCs) has essentially expanded in laminating adhesive applications due to stringent environmental regulations, including on the release of VOCs. To function well, the inferior properties of WPUs should be overcome with good adhesion and cohesion mechanisms. High-performance WPU adhesives were synthesized by incorporating an amino-functionalized porous clay heterostructure (APCH) into the WPU to increase its internal strength via formation of urea linkages between fillers and the polymer matrix, to yield an organic/inorganic hybrid adhesive with greater cohesion. Urea linkages, as characterized by Fourier-self deconvolution of the C=O stretching vibration region ($1600-1800\text{ cm}^{-1}$), increased with increasing APCH content. In addition, APCH significantly enhanced the adhesion properties of bonded joints together with an improved thermal stability of the adhesive, affirmed by the DSC analysis and higher viscosity observed by a Brookfield viscometer. The highest peel strength (126 N/m) was achieved with WPU hybrid adhesive containing 2.0 wt% APCH, that can be used for application in untreated oriented polypropylene (OPP) lamination.

Keywords: Waterborne polyurethane adhesive, Polypropylene lamination, Porous clay heterostructure

4.2 Introduction

Polyurethane materials have been extensively used in adhesive and coating industries, where their key benefits include flexibility, strength, durability, absorption

of stresses, adhesiveness and thermal transfer, depending on the chemical species (Wirpsza, 1993; Malucelli *et al.*, 2005). Due to the presence of highly polar urethane (carbamate) linkages, polyurethane adhesives will permanently adhere to different substrates, such as metals, textiles, paper, wood, plastics and concrete, through an intermolecular interaction (Van der Waals force and/or hydrogen bonding) (Ciullo, 1996). With respect to environmental legislation, waterborne polyurethane (WPU) adhesives are now an interesting alternative to the current solvent-based adhesives for reducing emissions of Volatile Organic Compounds (VOCs) to the atmosphere (Dieterich, 1981; Lichman, 1990; Ebnesajjad, 2009).

WPU adhesives are formed by an exothermic reaction between diisocyanate (-NCO) and more than one reactive hydroxyl (-OH) group per molecule within the continuous aqueous media. The segmental structure, hard/soft molar ratio, molecular weight and ionic group content can significantly influence its individual properties (Cakić *et al.*, 2013). However, the mechanical and adhesion properties of WPU adhesives do not go beyond that of traditional ones. To develop high-performance WPU adhesives, investigated changes have included increasing the hard segment content (Tawa and Ito, 2006), changes in the polyol (Kim and Kim, 2005; Cakić *et al.*, 2013), use of different amounts of ionic compounds (Turri *et al.*, 2004; Pérez-Limiñana *et al.*, 2005) or neutralizing agent types (Yang *et al.*, 2002), crosslinking (Mequanint and Sanderson, 2003; Rahman *et al.*, 2007a) and the addition of fillers/additives (Wang and Pinnavaia, 1998; Kim *et al.*, 2003; Kuan *et al.*, 2005; Rahman *et al.*, 2007b; Cao *et al.*, 2007). The efforts to improve the internal strength of WPU adhesives have usually been made by the use of fillers.

Fillers (e.g., CaCO₃, SiO₂, Al₂O₃ and clay minerals) have always played an important role in the adhesive formulations, since they result in a lower cost product with equivalent/improved property. Generally, their desirable characteristics should include a ready availability, low oil absorption, good surface wetting and bonding, good chemical resistance and high strength (Katz and Milewski, 1987; Licari and Swanson, 2011). Recently, porous clay heterostructure (PCH) has attracted attention as a relatively new class of mesoporous materials with several of the desired features mentioned above. In place of clay minerals, PCH is frequently used as an inorganic filler within polymer nanocomposites for applications in food packaging, electronic

capacitors and radio-frequency identification because of its high specific surface area (approximately 500-1000 m²/g) with uniform pore diameters and small particle sizes (Srithamaraj *et al.*, 2012; Bunnak *et al.*, 2013). For this purpose, the interfacial polymer-filler interactions should be induced by the use of various types of surface modifications (Kango *et al.*, 2013). Among them, chemical treatment is a suitable method to enhance the compatibility and dispersion stability of nanoparticles into the matrix, by introducing an organosilane precursor. The 3-aminopropyltriethoxysilane (APTES) is one of the most commonly used aminosilanes, and is comprised of both alkoxy and amino end-groups that are able to react with the silanol surfaces and -NCO chains, respectively. Consequently, organic/inorganic hybrid adhesives can be prepared in a one-step procedure with remarkable results (Wu *et al.*, 2006; Bertuoli *et al.*, 2014).

The objectives of the present study were to synthesize WPU hybrid adhesive for oriented polypropylene (OPP) lamination and to select the optimal amount of a natural thickener additive to achieve the best adhesion properties in the laminated films. The thickener additive used in this study was an amino-functionalized porous clay heterostructure (APCH), derived from a sodium-activated bentonite clay (Na-BTN) after initial modification through the surfactant-directed assembly of APTES and tetraethoxysilane (TEOS) as silica sources. During the emulsion polymerization process, WPU matrix was able to chemically couple with APCH via the formation of stable urea linkages. The cohesion mechanisms of WPU hybrid adhesives strongly depend on the interfacial interaction between those two phases. The effects of APCH concentration on the crystallinity, structural, rheological and thermal properties were then examined by X-ray diffraction (XRD), Fourier transform infrared spectroscopy (FTIR), Brookfield viscosity, simultaneous thermal analysis (STA) and differential scanning calorimetry (DSC) analyses, respectively, while the mechanical properties were evaluated by 180° peel strength tests.

4.3 Experimental

4.3.1 Materials

The commercial Na-BTN, with a cationic exchange capacity (CEC) of 44.5 mmol/100 g of clay, was used as the starting material to synthesize APCH, and was supplied by the Thai Nippon Chemical Industry Co., Ltd. The cationic surfactant cetyltrimethylammonium chloride (CTAC) was purchased from Italmar Co., Ltd. The co-surfactants TEOS, APTES and dodecylamine were purchased from Aldrich Chemicals. Methanol (CH₃OH), sodium hydroxide (NaOH) and 37% hydrochloric acid (HCl) were provided by RCI Labscan Ltd.

WPU hybrid adhesives were prepared by a reaction of a macroglycol, an internal emulsifier, an isocyanate and a chain extender. Isophorone diisocyanate (IPDI) of 98 wt% purity (mixture of *cis/trans* isomers) was used as the isocyanate, while poly(propylene glycol) (PPG) as the macroglycol, with a M_n value of 2000 and a hydroxyl value of 56 mg KOH/g, was dried under vacuum at 120 °C prior to use. 2,2-Bis(hydroxymethyl)propionic acid (Bis-MPA; 98 wt% purity) and 1,4-butanediol (BDO; 99 wt% purity) were obtained as the internal emulsifier and chain extender, respectively. The catalyst was dibutyltin dilaurate (DBTDL). Triethylamine (TEA) as a neutralizing agent and n-methyl-2-pyrrolidone (NMP) with a purity greater than 99 wt% were obtained, together with all of the other chemical reagents, from Aldrich Chemicals and were used as received without any further purification.

4.3.2 Preparation of the APCH

The mesoporous materials were prepared as follows: approximately 50 g of Na-BTN was dispersed into 0.1 M CTAC solution and held at 50 °C for 24 h to ensure cationic exchange had reached equilibrium. The obtained organo-modified BTN (OBTN) was filtered and then washed with deionized water and methanol (1:1 (v/v) ratio) until at pH 9 to remove excess surfactant. The air-dried OBTN was then agitated at 50 °C for 30 min in dodecylamine to form micelle structures in the clay galleries, and a mixture of TEOS and 5 wt% APTES was freshly added to derive the co-condensation at room temperature for 4 h with a 1:20:150 molar ratio of OBTN: dodecylamine: TEOS+APTES. The as-synthesized products were purified by solvent extraction (CH₃OH: HCl (v/v) ratio of 9:1) after drying at 60 °C. The solution was

filtered, washed with CH₃OH, and then allowed to dry overnight before screening through a mesh size of #325 to yield the APCH.

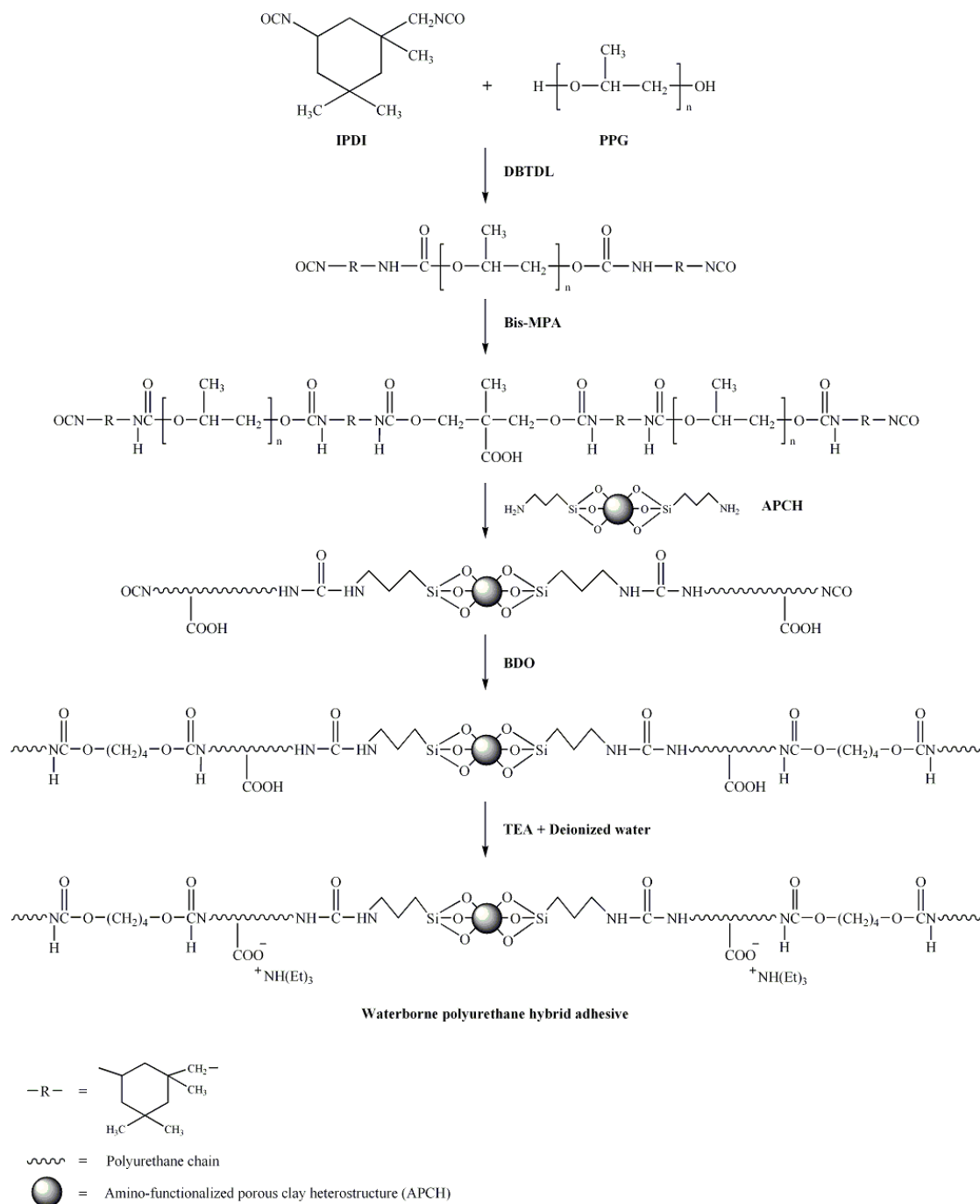


Figure 4.1 The synthesis route of WPU-x hybrid adhesives.

4.3.3 Preparation of WPU Hybrid Adhesives

The WPU hybrid adhesives were synthesized by a prepolymer mixing process at the appropriate -NCO/-OH molar ratio of 1.0 (Figure 4.1). The IPDI and PPG were added in a 1000-mL five-necked flange reaction flask equipped with the mechanical stirrer at 350 rpm, thermometer and reflux condenser. The reaction was placed in an electromantle at 80 °C for 2 h under a nitrogen (N₂) atmosphere, then DBTDL was slowly dropped in. The 5 wt% Bis-MPA (with respect to a prepolymer weight) was dispersed in NMP at 60 °C and was added into the mixture, followed by APCH at various weight fractions, including 0, 0.5, 1, 2 and 3 wt%. The reaction was then performed for another 2 h until the residual -NCO reached the expected content (determined by the standard dibutylamine back-titration method (David and Stanley, 1969)). The resulting prepolymer was cooled down to 50 °C and its chains were then extended using 2 wt% BDO. The carboxyl functional group in Bis-MPA was gently neutralized by the addition of 100 mL of TEA solution (in deionized water) through a dropping funnel for 1 h regulating the pH at 7.0 and WPU hybrid adhesives were then obtained with a 40 wt% solid content, and are referred to hereafter as WPU-x, where x is the wt% APCH.

4.3.4 Film Preparation

The WPU-x hybrid adhesive films were prepared by casting aqueous emulsion (20 mL) on a polytetrafluoroethylene surface. The remaining trapped water was allowed to completely evaporate at 60 °C for 24 h in vacuum oven. The obtained film (typically 0.5 mm thickness) was stored in a desiccator at ambient temperature, in order to avoid any moisture, prior to characterization.

4.3.5 Characterization Techniques

4.3.5.1 *Solid Content*

Solid content measurements were performed according to the ISO124:1997 standard. Approximately 1.5 g of WPU-x hybrid adhesive was placed in a 60-mm diameter aluminium tray and weighed three times before and after water evaporation.

4.3.5.2 *Fourier Transform Infrared Spectroscopy (FTIR)*

FTIR spectra were obtained using Thermo Scientific Nicolet iS5 instrument with attenuated total reflectance (ATR) iD7 mode to exactly identify the functional groups of adhesive films. The spectra were recorded in transmission mode over a wavenumber region of 650-4000 cm^{-1} with 16 scans and a resolution of 4 cm^{-1} .

4.3.5.3 *True Density Analysis*

The true density of APCH was measured by Quantachrome, Ultrapycnometer-1000 with helium (He) as a purge gas. The sample was previously dried under vacuum at 60 °C for 24 h.

4.3.5.4 *CHNS Elemental Analysis*

The apparent nitrogen level in APCH, which correlated with the level of amino groups (-NH₂), was evaluated using a CHNS elemental analyzer (Leco® Truspec). The electrical furnace was operated at 950 °C and the sample was introduced and immediately combusted.

4.3.5.5 *Transmission Electron Microscopy (TEM)*

The topography and particle size of APCH were monitored by TEM using a JEOL JEM-2100 electron microscope with an accelerating voltage of 160 kV. The sample was suspended in dispersing medium and then dropped onto a molybdenum grid.

4.3.5.6 *Surface Area Analysis*

The N₂ adsorption-desorption isotherm was determined via Quantachrome Autosorb-1 at 77 K. Each powder sample was degassed at 423 K for 17 h under vacuum prior to analysis. The specific surface area, pore volume and pore size were calculated using the Brunauer Emmett Teller (BET) equation (Brunauer *et al.*, 1938), while the pore size distribution was defined based on the Barrett, Joyner, and Halenda (BJH) method (Barrett *et al.*, 1951) using the adsorption branch of the N₂ isotherm.

4.3.5.7 *Field Emission Scanning Electron Microscopy (FE-SEM)*

The surface morphology of the adhesive film and APCH was clearly observed by FE-SEM (Hitachi S-4800 model) with an accelerating voltage of

5.0 kV. The specimen coating was applied by platinum sputtering for 150 s to reduce surface charging during electron irradiation.

4.3.5.8 Energy Dispersive X-ray Analysis (EDX)

Elemental composition of the adhesive films were identified by EDX, which was operated in conjunction with FE-SEM (as per section 4.3.5.10), at an accelerating voltage of 20.0 kV and working distance of 15.0 mm. Quantitative analysis was performed via mapping and point & ID modes.

4.3.5.9 X-ray Diffraction (XRD)

The crystal structures of the adhesive films and APCH were analyzed through a wide angle X-ray scattering system (Rigaku SmartLab) with Ni-filtered $\text{CuK}\alpha$ radiation, operated at 40 kV and 30 mA. The samples were scanned at 2θ ranges of 2-80° with a scan step of 0.01° and a scan speed of 0.5°/min.

4.3.5.10 Brookfield Viscosity

The viscosity characteristics of the aqueous emulsion were determined using a Brookfield viscometer (model DV-III programmable rheometer). The viscosity was specified with the Brookfield spindle SC4-27 at a test temperature of 25 °C. The shear rate was increased from 5 s⁻¹ to 85 s⁻¹ and maintained for 300 s to provide a homogeneous emulsion. Then, the shear rate was gradually decreased from 85 s⁻¹ to 5 s⁻¹ to obtain a thixotropic behavior.

4.3.5.11 Emulsion Stability Measurement

The stability of the aqueous emulsion was evaluated through monitoring its Brookfield viscosity (as per section 4.3.5.10) over 30 d. Each sample bottle was sealed and stored at ambient temperature until analysis. A shear rate of 85 s⁻¹ and rotational speed of 250 rpm were used with the SC4-27 spindle.

4.3.5.12 Differential Scanning Calorimetry (DSC)

The glass transition temperature (T_g) was characterized using a DSC204 F1 Phoenix® NETZSCH instrument, by measuring the inflection point of the second scan over a temperature range from -100 °C to 100 °C at a heating rate of 20 °C/min. The temperature program was specially designed for heat-cool-heat under a N₂ purge gas at a flow rate of 50 mL/min. Approximately 5 mg of each sample was sealed in an aluminium crucible of 25 µL.

4.3.5.13 Simultaneous Thermal Analysis (STA)

The thermal decomposition of adhesive films was studied by a high resolution STA449 F3 Jupiter[®] NETZSCH instrument under a continuous N₂ atmosphere at a purge rate of 50 mL/min, and then switching to an O₂ atmosphere at the same purge rate at a high temperature (600–800 °C). The temperature range was performed under a dynamic condition between 40 and 800 °C at a heating rate of 10 °C/min. Approximately 10 mg of each sample was loaded on an alumina crucible.

4.3.5.14 Measurement of the 180° Peel Strength

The adhesion property of the WPU-x hybrid adhesives was investigated in terms of their 180° peel strength according to ASTM D1876 using a rectangular-shaped specimen (25 mm × 300 mm). The measurement was performed in a LLOYD instrument equipped with a 500 N load cell, a crosshead speed of 50 mm/min and a gauge length of 50 mm. The aqueous emulsion was then applied on paper with a coating thickness of 24 μm and suddenly laminated to an untreated OPP film. The OPP/WPU hybrid adhesive/paper joints were allowed to dry at 60 °C for 2 min.

4.4 Results and Discussion

4.4.1 Characterization of the Synthesized APCH

The true particle density is a fundamental and unchanging property of mineral fillers. Generally, high-density filler particles ($> 1.50 \text{ g/cm}^3$) are desirable as a thickener additive within waterborne emulsion adhesive and sealants (Ciullo, 1996; Rothon, 2003). The synthesized APCH had an apparent density of 1.99 g/cm^3 , which was lower than that of the Na-BTN clay (2.45 g/cm^3) due to the presence of porous structures in the clay galleries, as confirmed by TEM. The TEM analysis of APCH (Figure 4.2) revealed a dry particle morphology with quite round-shaped particles having diameters of approximately $612.5 \pm 26.3 \text{ nm}$.

The N₂/77 K adsorption-desorption isotherm analysis was performed to investigate the surface morphology and physical properties of the APCH. A type IV isotherm was exhibited (Figure 4.3), according to the Brunauer-Deming-Deming-

Teller (BDDT) classification (Brunauer *et al.*, 1940), indicating mesoporous material with a strong affinity. Additionally, from the IUPAC notation (Sing *et al.*, 1985), the formation of a type-H3 hysteresis loop without any limiting adsorption at a high relative pressure (P/P_0) was observed, which can be attributed to the presence of slit-shaped pores with wide bodies and narrow short necks. A linear relation of the BET equation (Brunauer *et al.*, 1938) in the P/P_0 range of 0.05-0.30 was used to determine the monolayer adsorption capacity (V_m) of APCH using Eq. (4.1);

$$\frac{P}{V_{ads}(P_0 - P)} = \frac{1}{V_m C} + \frac{(C - 1)P}{V_m C P_0} \quad (4.1)$$

where V_{ads} is the adsorption volume of N_2 , P is the equilibrium pressure, P_0 is the saturation pressure and C is a parameter related to the gas-solid interactions.

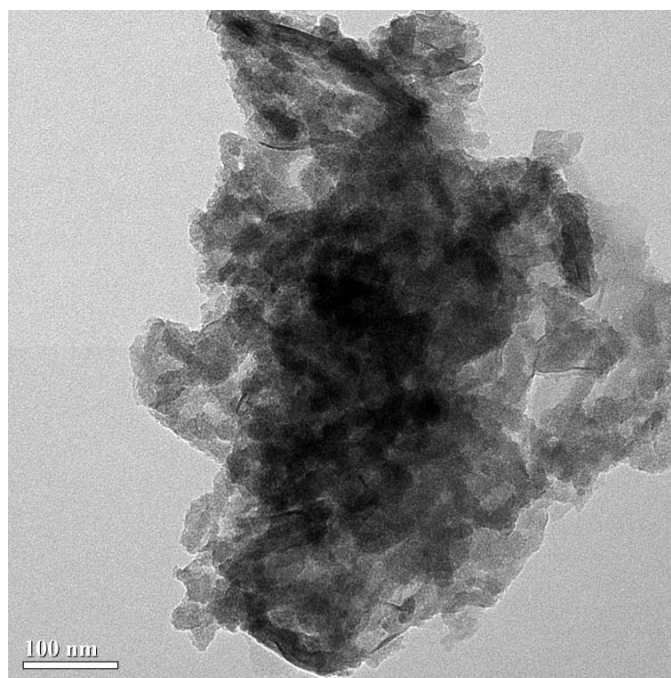


Figure 4.2 TEM micrograph (25.0 kx magnification, scale bar = 100 nm) of APCH.

The specific surface area (S_{BET}) of APCH was obtained from the V_m values using Eq. (4.2);

$$S_{BET} = \frac{a_m V_m N_A}{V_M} \quad (4.2)$$

where a_m is the cross-section of the N_2 molecule ($16.2 \times 10^{-20} \text{ m}^2$), N_A is Avogadro's number and V_M is the molar volume of N_2 ($22,414 \text{ cm}^3/\text{mol}$).

The application of the BET equation gave a specific surface area of $129.1 \text{ m}^2/\text{g}$ and a C_{BET} parameter of 63.1 for the APCH, which is typical of a strong solid-gas interaction in mesoporous materials, and a BJH pore diameter of 9.75 nm and pore volume of 0.39 cc/g (calculated from the adsorption branches of isotherm). The relatively high specific surface area as compared with Na-BTN clay ($34.5 \text{ m}^2/\text{g}$) is due to its porous structure at a nanometer scale.

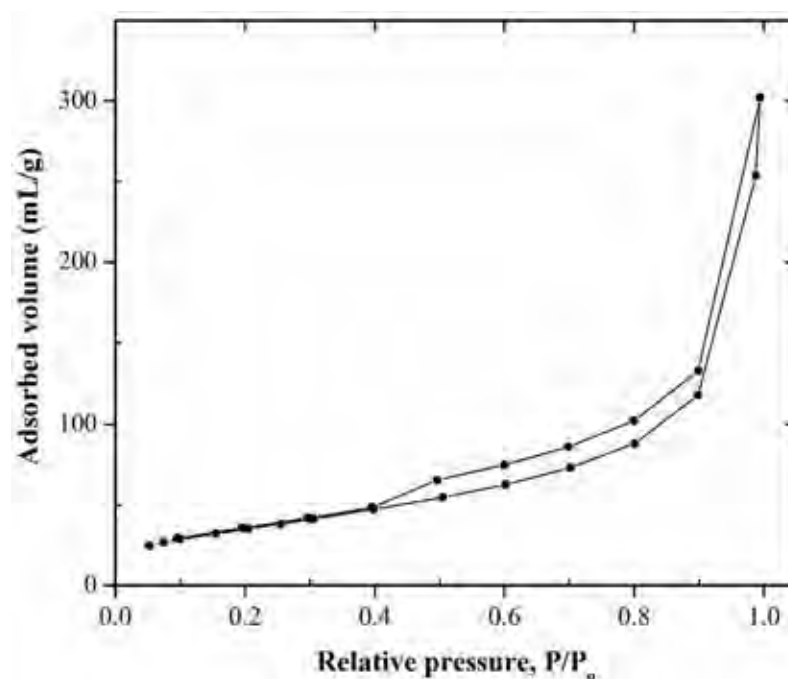


Figure 4.3 $N_2/77\text{K}$ adsorption-desorption isotherm of APCH.

The typical infrared spectrum of the synthesized APCH (Figure 4.4) revealed the stretching vibrations of Si-O-Si linkages in asymmetric and symmetric modes centered at 1070 cm^{-1} and 800 cm^{-1} , respectively. The weak transmission band

at around 1610 cm^{-1} was assigned to the -NH_2 stretching in primary amines, indicating the presence of α -amino groups on the APCH surface. Moreover, CHNS elemental analysis was performed to confirm the existence of α -amino groups. The conversion of the nitrogen content to α -amino groups gave an α -amino group level in APCH of 10.1 mmol/g sample, which are available to form a strong bond with residual -NCO groups within the WPU matrix, forming urea linkages.

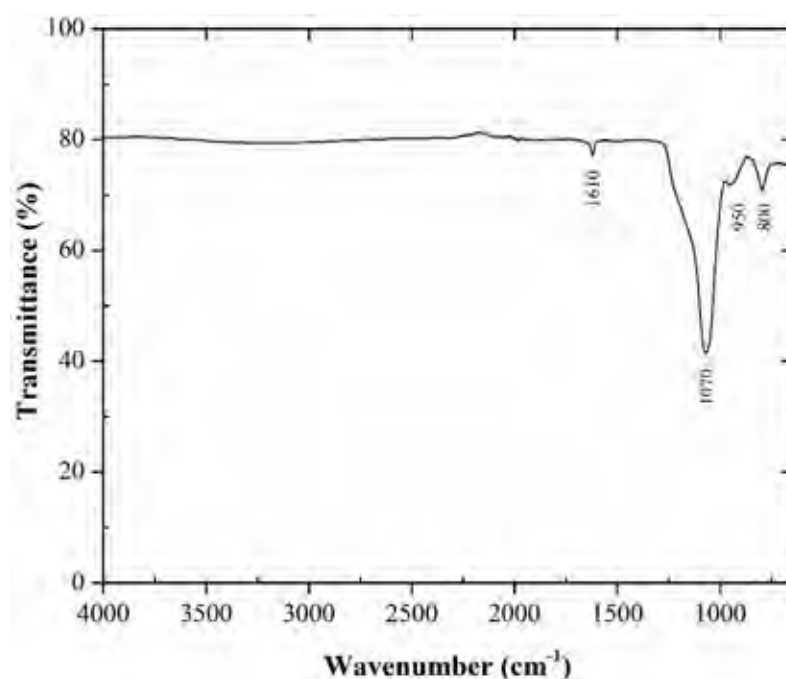


Figure 4.4 ATR-FTIR spectrum of APCH.

4.4.2 Characterization of the WPU-x Hybrid Adhesives

Surface morphologies of the APCH and WPU-x hybrid adhesives were analyzed through FE-SEM (Figure 4.5), where APCH was observed to exhibit a rough surface, due to the formation of porous structures in the clay galleries. After synthesis of the WPU-x hybrid adhesives, the presence of APCH was observed to have an even distribution and dispersion throughout the polyurethane matrix, especially for WPU-2.0. The EDX analysis was used to identify the quantitative elemental composition in the hybrid adhesives, and revealed that the surface of WPU-2.0 was explicitly covered with silicon atoms (Si) at 2.3% of the total surface

area (Figure 4.5d), with very clear evidence of a good distribution of APCH (green dots) in the WPU-2.0 hybrid adhesive.

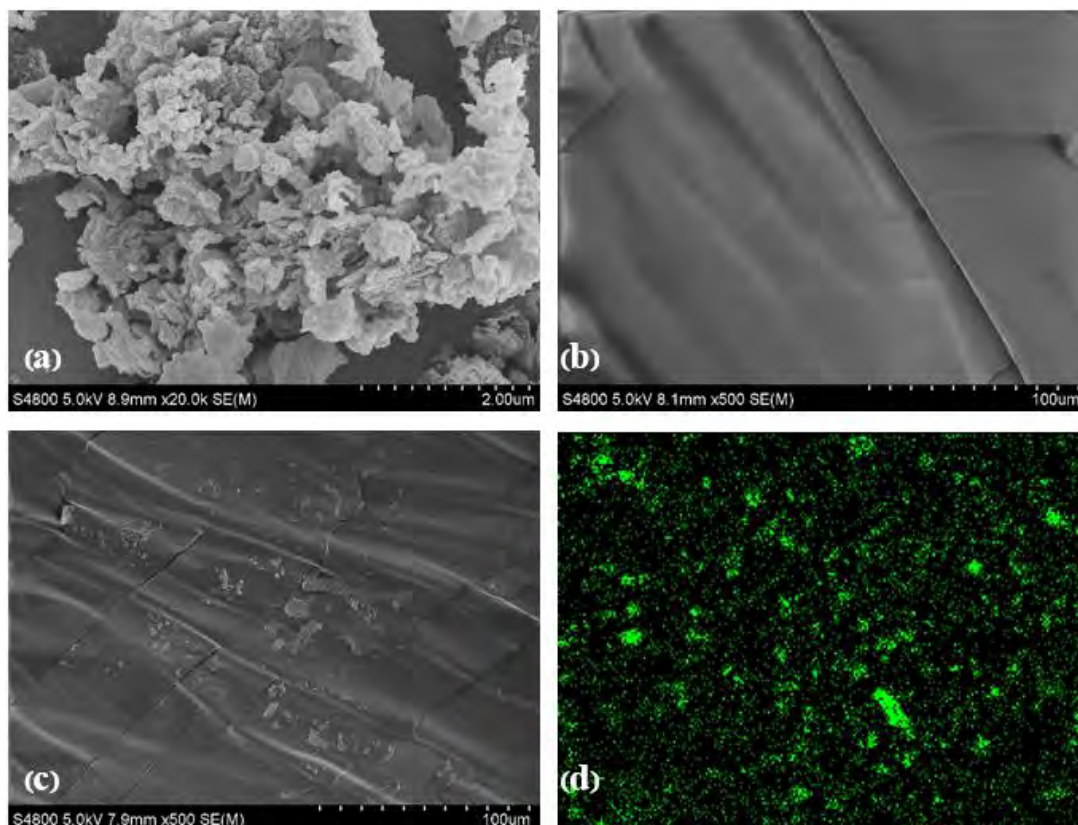


Figure 4.5 Representative FE-SEM images showing the surface morphology of the (a) APCH (20.0 kx magnification, scale bar = 2 μm), (b) WPU-0.0, (c) WPU-2.0 (500 x magnification, scale bar = 100 μm) and (d) a silicon mapping of WPU-2.0.

Normally, viscosity of waterborne adhesives behave like a Newtonian fluid, where the viscosity is independent of the shear rate. However, some have been reported to display a change in viscosity with an increasing shear rate, called a non-Newtonian fluid (Kästner, 2001; Licari and Swanson, 2011). The natural thickener, a rheological modifier for WPU adhesives, is used to provide non-Newtonian behavior together with a low penetration into the absorbent substrate, good applicability, non-sag property and a high emulsion stability (Ciullo, 1996). The significant variation in the viscosity as function of the shear rate of those WPU-x hybrid adhesives is shown

in Figure 4.6. A thixotropic system (pseudoplasticity) was imparted to these hybrid adhesives with an APCH content of > 1 wt%, in which the up and down curves do not coincide due to the reversible structural properties. So, the viscosity is drastically decreased while increasing the shear rate. Technically, the existence of thixotropy can be ascribed to the creation of interactions between the WPU adhesives, APCH and water (polyurethane-thickener interactions) (Barnes, 1997; Orgilés-Calpena *et al.*, 2009). The viscosity of adhesives was enhanced with increasing APCH contents (Table 4.1) with a long-term shelf stability.

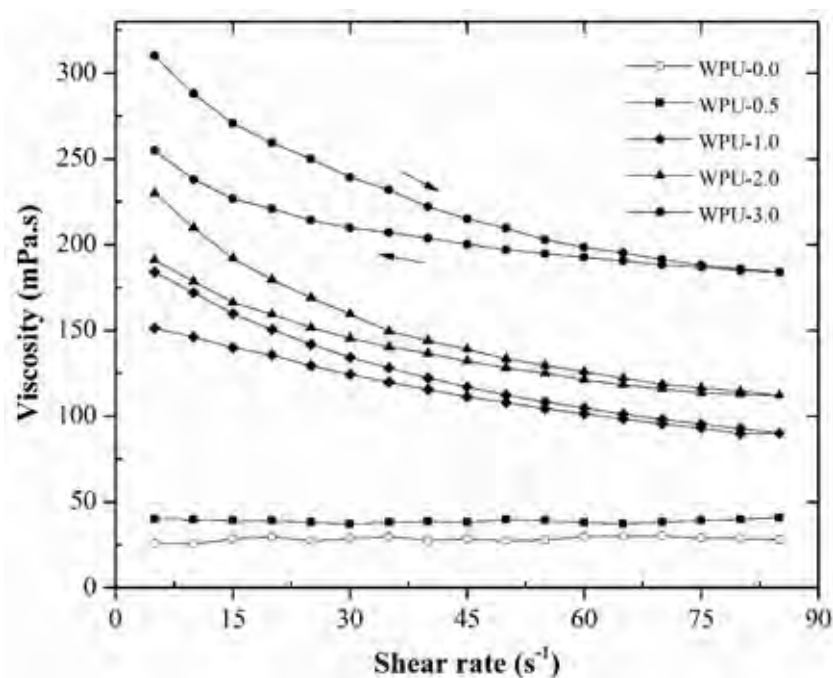


Figure 4.6 The variation of viscosity as a function of shear rate for WPU-x hybrid adhesives. Arrows show the measurements corresponding to increased and decreased shear rate.

The chemical structure of the WPU-x hybrid adhesives was analyzed by ATR-FTIR, where the spectra (Figure 4.7) of different WPU-x hybrid adhesives were relatively similar. The assignment of the most intensive transmission bands is given in Table 4.2 (Pérez-Limiñana *et al.*, 2005; Fang *et al.*, 2014), and consisted of N-H stretching at 3330 cm^{-1} , C-N stretching coupled with N-H bending at 1540 cm^{-1} ,

C-H stretching of hydrocarbon chains at 2970–2860 cm^{-1} and C=O stretching in the region from 1800–1600 cm^{-1} . Moreover, the N-H bending mode can be determined as a fingerprint region (770 and 650 cm^{-1}). The absence of the N=C=O stretching at 2270 cm^{-1} supports that the -NCO groups had completely reacted in the WPU hybrid adhesives. The Si-O-Si stretching band (1070 cm^{-1}) of APCH was also not seen, but this was due to the masking effect of the strong intensity of the C-O-C stretching (1095 cm^{-1}) at a similar position. Thus, the existence of APCH within the hybrid adhesives was studied by confirming the creation of urea bonds between the -NCO and -NH₂ groups.

Table 4.1 Viscosity of WPU-x hybrid adhesives at temperature of 25 °C and shear rate of 85 s^{-1}

WPU hybrid adhesives	Viscosity (mPa.s)
WPU-0.0	28
WPU-0.5	41
WPU-1.0	90
WPU-2.0	112
WPU-3.0	184

The urethane, urea and carbonyl functional groups participated in the hydrogen bonding (H-bonding) processes in which the N-H groups are proton donors and C=O groups are proton acceptors. The comparative analysis of C=O stretching vibration band in the spectral region of 1800-1600 cm^{-1} can be used to estimate the actual bonding in the WPU hybrid adhesives. Hence, the C=O stretching band was deconvoluted into five components using OriginPro 8.6 as a curve fitting simulation. The Gaussian peaks centered at 1730, 1710, 1690, 1665 and 1640 cm^{-1} were then designed as the C=O stretching bands in free urethane, H-bonded urethane, free urea, disordered H-bonded urea (C=O groups interacted with one adjacent N-H group) and

ordered H-bonded urea (C=O groups interacted with both adjacent N-H groups), respectively (Queiroz *et al.*, 2003; Cakić *et al.*, 2013).

Table 4.2 The most characteristic ATR-FTIR bands of the WPU-x hybrid adhesives

Wavenumber (cm ⁻¹)	Assignment
3300	st N-H (bonded)
2970-2860	st C-H
2270	st N=C=O
1730	st C=O (free urethane)
1710	st C=O (bonded urethane)
1690	st C=O (free urea)
1665	st C=O (bonded disordered urea)
1640	st C=O (bonded ordered ure)
1530	st C-N + δ N-H
1460	δ CH ₂
1372-1342	δ sym CH ₃
1238	st asym N-CO-O + st C-O-C
1095, 925	st C-O-C
1015	st sym N-CO-O
770, 650	δ N-H

st: stretching, δ : bending, sym: symmetric, asym: asymmetric

The fractions of each spectral component in the C=O stretching region are then depicted in Figure 4.8 in which frequencies (ν) remain essentially constant. The relative areas (A) of all deconvoluted bands in the WPU hybrid adhesives, as listed in Table 4.3, revealed that the H-bonded urethane linkage (1730 cm⁻¹) was the major component in all the WPU-x adhesives. With increasing APCH contents, the relative area of the free urea band at 1690 cm⁻¹ was clearly enhanced, which is due to

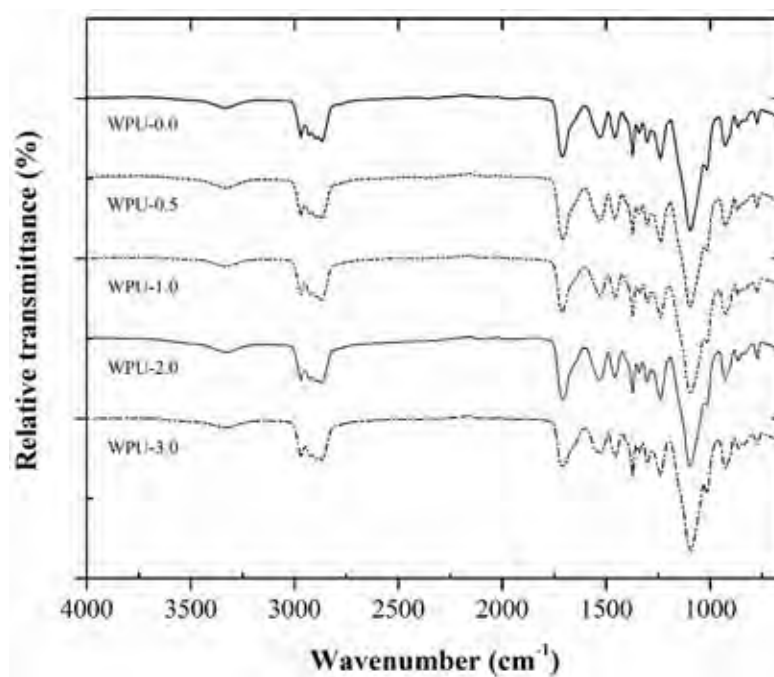


Figure 4.7 ATR-FTIR spectra of the WPU-x hybrid adhesives.

Table 4.3 The frequency (ν) and relative area (A) of the five spectral components in the C=O stretching region

WPU hybrid adhesives	Urethane				Urea					
	free		H-bonded		free		H-bonded			
							disordered		ordered	
	ν (cm ⁻¹)	A (%)	ν (cm ⁻¹)	A (%)	ν (cm ⁻¹)	A (%)	ν (cm ⁻¹)	A (%)	ν (cm ⁻¹)	A (%)
WPU-0.0	1729	7	1713	55	1690	15	1666	14	1640	9
WPU-0.5	1729	14	1712	42	1690	21	1666	13	1642	10
WPU-1.0	1728	16	1714	39	1691	23	1665	13	1641	9
WPU-2.0	1727	20	1711	31	1691	26	1665	12	1643	11
WPU-3.0	1728	21	1713	29	1691	28	1666	12	1642	10

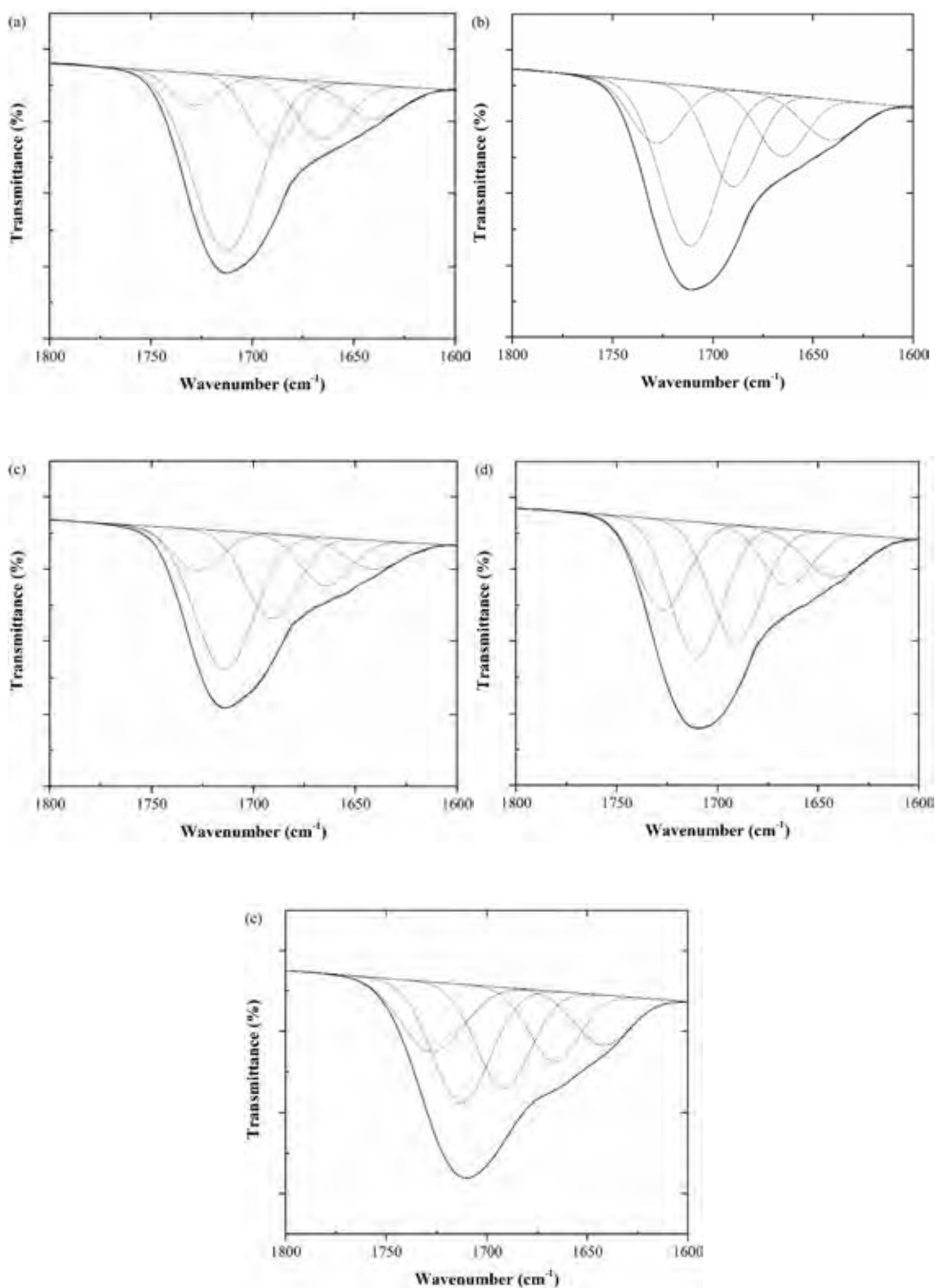


Figure 4.8 Partially enlarged details of the WPU-x hybrid adhesives in the C=O stretching vibration of WPU-x with APCH contents of (a) 0, (b) 0.5, (c) 1.0, (d) 2.0 and (e) 3.0 wt%.

the formation of urea linkages between APCH filler and its polyurethane matrix. The strength of the hard-hard segment is stronger than that of the hard-soft segment. It can be verified that the obtained urea linkages do not exhibit H-bonding because the APCH particles obstructed the intermolecular interactions to a great extent (steric hindrance effect). Moreover, the relative area of the free urethane band (1730 cm^{-1}) also increased with respect to that of the free urea band.

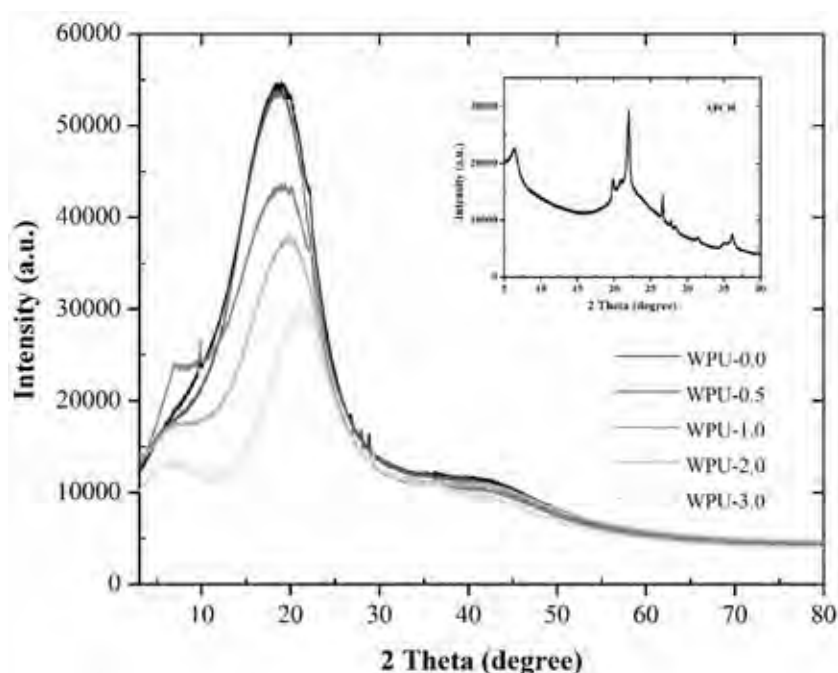


Figure 4.9 XRD patterns of WPU-x hybrid adhesives with different APCH contents.

The WPU-x hybrid adhesive is amorphous in nature and as such can commonly be divided into the three types of rigid, semi-rigid and soft polyurethane (Trovati *et al.*, 2010). In the present study, there were three diffraction peaks of the soft WPU adhesives at 2θ values of 6° , 18.5° (the major diffraction peak) and 42.0° , indicating some degree of crystallinity, as shown in Figure 4.9. Generally, the degree of crystallinity, ascribed to the ordered arrangement of soft segments in polyurethane chains (Xu *et al.*, 2014), could be lowered by the dispersion of hard segments. The greatest intensity of major diffraction peak was found in the WPU without APCH, because of the highest ordered soft segments in the adhesive structure (Fang *et al.*,

2014; Xu *et al.*, 2014). As expected, its intensity was weakened in the presence of included APCH because of the steric hindrance by APCH particles to the structural regularity of the soft segments, and also the higher level of hard segments dispersing into the soft segments (correlated with the deconvolution of C=O stretching in the urea linkages), which lead to a decreased level of crystallinity. The main diffraction peaks in these adhesives were slightly shifted towards higher 2θ values following APCH addition, in which its characteristic peak was previously found at 2θ values of 6.1° and 22.0° .

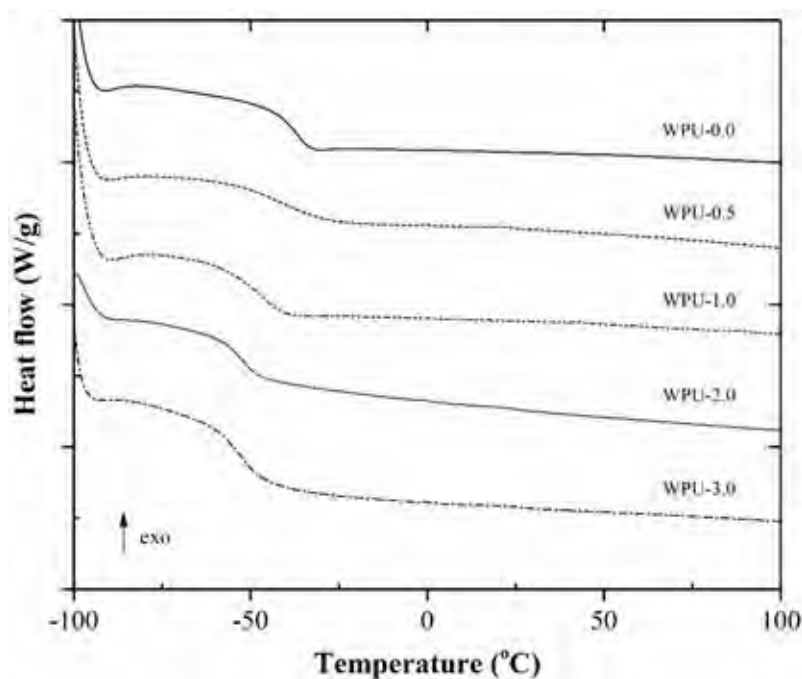


Figure 4.10 DSC thermograms of WPU-x hybrid adhesives with different APCH contents. Thermograms were taken from the second heating scan.

The DSC thermograms of the WPU-x hybrid adhesives (Figure 4.10) showed a strong soft phase transition as a function of the temperature. During the heating process, a single low temperature T_g was observed, which is expected for an exothermic process. The T_g values of the WPU-x hybrid adhesives with increasing APCH contents were slightly shifted to a lower temperature from -44.6°C for WPU-0.0 to -58.1°C for WPU-3.0 (Table 4.4), which was due to the formation of the urea

linkages as hard segments in the polyurethane chains. Meanwhile, the increased hard segment contents with decreasing crystallinity (as supported by the XRD analysis) was likely to be associated with the enlarged hard segments dispersing into the soft segment microdomain (Garrett et al. 2003). There was no melting temperature (T_m) detected in the WPU-x hybrid adhesives because a slow crystallization process followed the weak phase separation between the hard and soft polyurethane segments (Fang *et al.*, 2014).

Table 4.4 Glass transition temperature (T_g), decomposition temperature (T_d), and weight loss of the WPU-x hybrid adhesives

WPU hybrid adhesives	T_g (°C)	First decomposition		Second decomposition		Third decomposition	
		T_1 (°C)	Weight loss (%)	T_2 (°C)	Weight loss (%)	T_3 (°C)	Weight loss (%)
WPU-0.0	-44.6	257.9	5.9	304.2	28.7	357.1	64.6
WPU-0.5	-49.9	258.3	6.2	308.4	29.1	359.7	63.7
WPU-1.0	-53.5	255.9	6.3	311.1	32.9	360.9	58.8
WPU-2.0	-57.5	259.4	6.6	313.0	35.6	363.4	55.3
WPU-3.0	-58.1	260.1	6.8	321.0	41.7	367.8	47.9

T_1 , T_2 , and T_3 are onset temperatures for the first, second, and third decomposition.

Generally, the degradation mechanism of polyurethane is a complex heterogeneous process due to the different features of its hard and soft segments. Therefore, it is necessary to understand the structure-property relationship through the thermal degradation behavior. The thermal stability of WPU-x hybrid adhesives was evaluated by TG analysis utilizing gas switching from N_2 to O_2 at a very high temperature (600-800 °C), with the results shown in Figure 4.11. The vaporization of residual water, oligomers and silane coupling agents occurred at 100-200 °C, and thereafter three steps of partial thermal decomposition were observed. With respect

to the urethane and urea formations (two kinds of hard segments) in the WPU-x hybrid adhesives, urea linkages have a better thermal resistance than urethane (Pérez-Limiñana *et al.*, 2005; Fang *et al.*, 2014). Accordingly, the first decomposition stage at around 260 °C was due to the urethane hard segments, while the second stage at 300-320 °C was associated with decomposition of the urea hard segments. Finally, the chain scission of soft segments occurred at 360-370 °C (Yeh *et al.*, 2008; Cakić *et al.*, 2012). In an oxidizing atmosphere, the WPU-x hybrid adhesives were further decomposed, eliminating the residual hydrocarbons at temperatures of >500 °C. The percent char residue was related to the amount of added APCH during the emulsion polymerization process, with a higher percentage of char residue with increasing APCH contents.

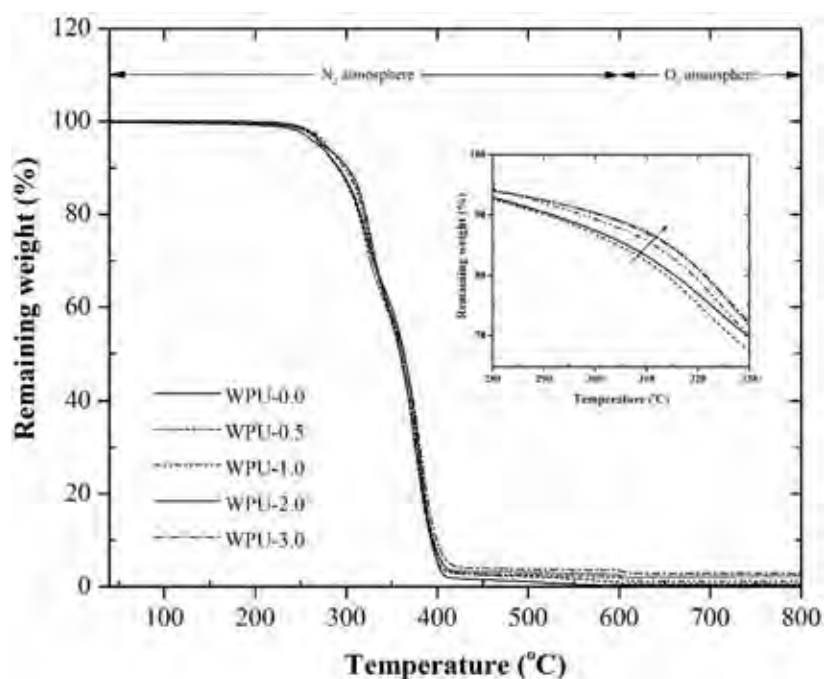


Figure 4.11 TG curves of WPU-x hybrid adhesives with different APCH contents.

The TG curves shifted to higher temperatures with increasing APCH contents (Figure 4.11), which was because of the higher bonding energy of the Si-O bond compared to the C-C and C-O bonds. Additionally, APCH acted as a thermal insulator retarding the heat transfer in the polyurethane matrix that was generated

during a degradation process. Table 4.4 indicates the decomposition temperature and weight loss of the WPU-x hybrid adhesives. The percentage of the hard segments (both urethane and urea) and soft segment was proportional to the weight loss during the degradation. With respect to the increased APCH level, the amount of urea hard segments were certainly much higher than that for urethane ones, resulting in a good thermal stability of the WPU-x hybrid adhesives, and supporting the formation of the urea linkages.

4.4.3 Adhesion Properties

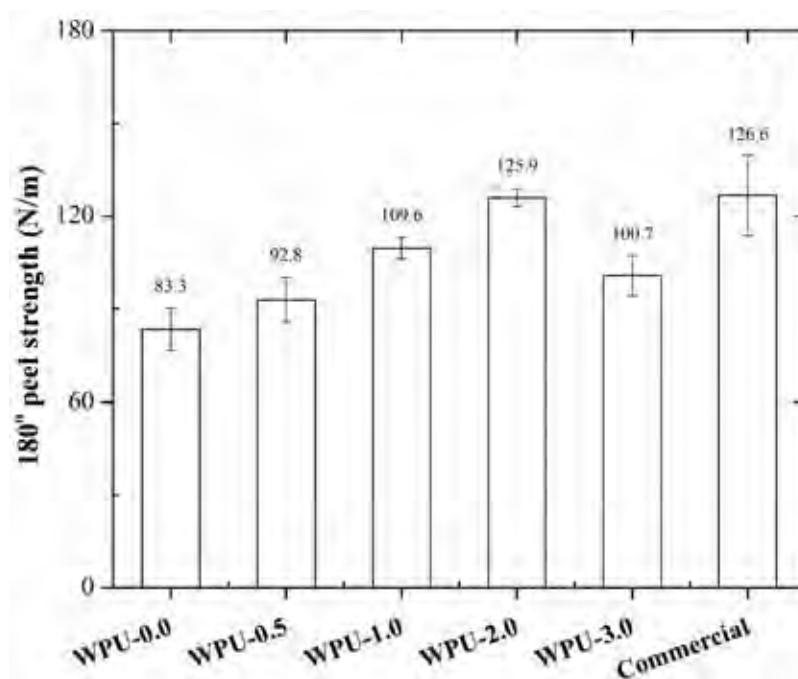


Figure 4.12 The 180° peel strength of the WPU-x hybrid adhesives with different APCH contents.

The adhesion properties of the WPU-x hybrid adhesives with different APCH contents were examined in terms of the 180° peel strength of OPP/adhesive/paper joint. The strength of the bonded joints was acquired by both of the adhesion (including transition zone) and cohesion mechanisms, whereas undesirable cohesive failure usually happened in a bulk layer of the WPU-0.0 due to the lack of elasticity

and also internal strength in its structure. In accordance with Figure 4.12, significant change in the mechanical properties was obtained with the addition of 2 wt.% APCH to the WPU, where a maximum peel strength (126 N/m) was obtained, which is in an acceptable range compared to commercial adhesives (100-130 N/m). Therefore, the addition of APCH strengthens the cohesion of the WPU-x hybrid adhesives, which is due to the presence of urea linkages (additional types of hard segment) dispersed in the soft segment, that leads to a higher internal strength within the adhesive structure. Likewise, the dispersive adhesion mechanism to the adherent surfaces via Van der Waals forces is efficiently displayed.

4.5 Conclusion

Mesoporous APCH was synthesized and used as an additive with α -amino end group (-NH₂) to enhance the internal strength of the polyurethane matrix through urea linkages. The presence of the urea linkages (hard segments) was well dispersed in the soft segments of WPU, as confirmed by the Fourier-self deconvolution of the C=O stretching band and XRD analyses. The surface morphology of each WPU-x hybrid adhesive with ACPH exhibited a good distribution and dispersion of APCH, especially for that with 2 wt% ACPH. The good performance, in terms of the thermal stability, viscosity behavior as a thickener and mechanical property, of the WPU-x hybrid adhesives was improved by the addition of ACPH, indicating an improved adhesion mechanism to the laminated joints. The optimal level of ACPH was 2 wt.%, giving the 180° peel strength of 126 N/m, which was in the acceptable range for a waterborne adhesive. The crystallinity and T_g were slightly lowered by the inclusion of ACPH because of the changes in the poly(urethane-urea) structure (higher hard segments dispersed in the soft segments). Overall evaluations imply that this WPU hybrid adhesive with 2 wt% ACPH is applicable as a commercial waterborne adhesive for OPP laminations.

4.6 Acknowledgement

This research was financially supported by Research and Researchers for Industries (RRI), the Thailand Research Fund (TRF) and Nateethong Polymer Company, Thailand. Special thanks give to Dr. Robert Butcher of the Publication Counseling Unit, Science Department, Chulalongkorn University for proofreading the manuscript.

4.7 References

- Barnes, H.A. (1997) Thixotropy - a review. Journal of Non-Newtonian Fluid Mechanics, 70, 1-33.
- Barrett, E.P., Joyner, L.G. and Halenda, P.P. (1951) The determination of pore volume and area distributions in porous substances. I. computations from nitrogen isotherms. Journal of the American Chemical Society, 73(1), 373-380.
- Bertuoli, P.T., Piazza, D., Scienza, L.C. and Zattera, A.J. (2014) Preparation and characterization of montmorillonite modified 3-aminopropyltriethoxysilane. Applied Clay Science, 87, 46-51.
- Brunauer, S., Deming, L.S., Deming, W.E. and Teller, E. (1940) On a theory of the van der Waals adsorption of gases. Journal of the American Chemical Society, 62(7), 1723-1732.
- Brunauer, S., Emmett, P.H. and Teller, E. (1938) Adsorption of gases in multimolecular layers. Journal of the American Chemical Society, 60, 309-319.
- Bunnak, N., Laoratanakul, P., Bhalla, A.S. and Manuspiya, H. (2013) Dielectric properties improvement of polymer composite prepared from poly(vinylidene difluoride) and barium-modified porous clay heterostructure. Electronic Materials Letters, 9, 315-323.
- Cakić, S.M., Ristić, I.S., Marinović-Cincović, M. and Špirková, M. (2013) The effects of the structure and molecular weight of the macrodiol on the

- properties polyurethane anionic adhesives. International Journal of Adhesion and Adhesives, 41, 132-139.
- Cakić, S.M., Ristić, I.S. and Ristić, O.Z. (2012) Thermal analysis of polyurethane dispersions based on different polyols. Licensee InTech. [Chapter 5]
- Cao, X., Dong, H. and Li, C.M. (2007) New nanocomposite materials reinforced with flax cellulose nanocrystals in waterborne polyurethane. Biomacromolecules, 8(3), 899-904.
- Ciullo, P.A. (1996) Industrial minerals and their uses: a handbook and formulary. Westwood, New Jersey: Noyes Publications.
- David, D.J. and Stanley, H.B. (1969) Analytical chemistry of polyurethanes, High polymer series, XVI, Part III. New York: Wiley-Interscience.
- Dieterich, D. (1981) Aqueous emulsions, dispersions, and solutions of polyurethanes: synthesis and properties. Progress in Organic Coatings, 9(3), 281-340.
- Ebnesajjad, S., editor. (2009) Adhesive technology handbook. New York: William Andrew Inc.
- Fang, C., Zhou, X., Yu, Q., Liu, S., Guo, D., Yu, R. and Hu, J. (2014) Synthesis and characterization of low crystalline waterborne polyurethane for potential application in water-based ink binder. Progress in Organic Coatings, 77, 61-71.
- Garrett, J.T., Xu, R., Cho, J. and Runt, J. (2003) Phase separation of diamine chain-extended poly(urethane) copolymers: FTIR spectroscopy and phase transitions. Polymer, 44, 2711-2719.
- Kango, S., Kalia, S., Celli, A., Njuguna, J., Habibi, Y. and Kumar, R. (2013) Surface modification of inorganic nanoparticles for development of organic-inorganic nanocomposites-A review. Progress in Polymer Science, 38, 1232-1261.
- Kästner, U. (2001) The impact of rheological modifiers on water-borne coatings. Colloids and Surface A: Physicochemical and Engineering Aspects, 183-185, 805-821.
- Katz, H.S. and Milewski J.V., editors. (1987) Handbook of fillers for plastics. New York: Van Nostrand Reinhold.

- Kim, B.K., Seo, J.W. and Jeong, H.M. (2003) Morphology and properties of waterborne polyurethane/clay nanocomposites. European Polymer Journal, 39, 85-91.
- Kim, B.S. and Kim, B.K. (2005) Enhancement of hydrolytic stability and adhesion of waterborne polyurethanes. Journal of Applied Polymer Science, 97, 1961-1969.
- Kuan, H.C., Ma, C.C.M., Chuang, W.P. and Su, H.Y. (2005) Hydrogen bonding, mechanical properties, and surface morphology of clay/waterborne polyurethane nanocomposites. Journal of Polymer Science Part B: Polymer Physics, 43, 1-12.
- Licari, J.J. and Swanson, D.W. (2011) Adhesives technology for electronic applications: materials, processing, reliability, 2nd ed. New York: Elsevier Inc.
- Lichman, J. (1990) Water-based and solvent-based adhesives. In: Skeist I, (Ed.). Handbook of adhesives. New York: Van Nostrand Reinhold. [Chapter 44].
- Malucelli, G., Priola, A., Ferrero, F., Quaglia, A., Frigione, M. and Carfagna, C. (2005) Polyurethane resin-based adhesives: curing reaction and properties of cured systems. International Journal of Adhesion and Adhesives, 25, 87-91.
- Mequanint, K. and Sanderson, R. (2003) Nano-structure phosphorus-containing polyurethane dispersions: synthesis and crosslinking with melamine formaldehyde resin. Polymer, 44(9), 2631-2639.
- Orgilés-Calpena, E., Arán-Aís, F., Torró-Palau, A.M., Orgilés-Barceló, C. and Martín-Martínez, J.M. (2009) Addition of different amounts of a urethane-based thickener to waterborne polyurethane adhesive. International Journal of Adhesion and Adhesives, 29, 309-18.
- Pérez-Limiñana, M.A., Arán-Aís, F., Torró-Palau, A.M., Orgilés-Barceló, A.C. and Martín-Martínez, J.M. (2005) Characterization of waterborne polyurethane adhesives containing different amounts of ionic groups. International Journal of Adhesion and Adhesives, 25, 507-517.

- Queiroz, D.P., Pinho, M.N. and Dias, C. (2003) ATR-FTIR studies of poly(propylene oxide)/polybutadiene bi-soft segment urethane/urea membranes. Macromolecules, 36, 4195-4200.
- Rahman, M.M., Kim, E.Y., Kwon, J.Y., Yoo, H.J. and Kim, H.D. (2007) Cross-linking reaction of waterborne polyurethane adhesives containing different amount of ionic groups with hexamethoxymethyl melamine. International Journal of Adhesion and Adhesives, 28, 47-54.
- Rahman, M.M., Yoo, H.J., Mi, C.J. and Kim, H.D. (2007) Synthesis and characterization of waterborne polyurethane/clay nanocomposite-effect on adhesive strength. Macromolecular Symposia, 249-250, 251-258.
- Rothon, R.N., editor. (2003) Particulate-filled polymer composites. Shrewsbury: Rapra Technology Limited.
- Sing, K.S.W., Everett, D.H., Haul, R.A.W., Moscou, L., Pierotti, R.A., Rouquérol, J. and Siemieniewska, T. (1985) Reporting physisorption data for gas/solid systems with special reference to the determination of surface area and porosity. Pure and Applied Chemistry, 57(4), 603-619.
- Srithammaraj, K., Magaraphan, R. and Manuspiya, H. (2012) Modified porous clay heterostructures by organic-inorganic hybrids for nanocomposite ethylene scavenging/sensor packaging film. Packaging Technology and Science, 25, 63-72.
- Tawa, T. and Ito, S. (2006) The role of hard segments of aqueous polyurethane-urea dispersion in determining the colloidal characteristics and physical properties. Polymer Journal, 38, 686-693.
- Trovati, G., Sanches, E.A., Neto, S.C., Mascarenhas, Y.P. and Chierice, G.O. (2010) Characterization of polyurethane resins by FTIR, TGA, and XRD. Journal of Applied Polymer Science, 115, 263-268.
- Turri, S., Levi, M. and Trombetta, T. (2004) Waterborne anionomeric polyurethane-ureas from functionalized fluoropolyethers. Journal of Applied Polymer Science, 93, 136-144.
- Wang, Z. and Pinnavaia, T.J. (1998) Nanoclay reinforcement of elastomeric polyurethane. Chemistry of Materials, 10, 3769-3771.

- Wirpsza, Z. (1993) Polyurethanes: chemistry, technology, and applications. London: PTR Prentice Hall.
- Wu, Z., Xiang, H., Kim, T., Chun, M.S. and Lee, K. (2006) Surface properties of submicrometer silica spheres modified with aminopropyltriethoxysilane and phenyltriethoxysilane. Journal of Colloid and Interface Science, 304, 119-124.
- Xu, C., Cai, Z., Xing, J., Ren, Y., Xu, W. and Shi, W. (2014) Synthesis of polypropylene carbonate polyol-based waterborne polyurethane modified with polysiloxane and its film properties. Fibers and Polymers, 15(4), 665-671.
- Yang, J.E., Lee, Y.H., Koo, Y.S., Jung, Y.J. and Kim H.D. (2002) Preparation and properties of waterborne poly(urethane-urea) ionomers-effect of the type of neutralizing agent. Fibers and Polymers, 3, 97-102.
- Yeh, J.M., Yao, C.T., Hsieh, C.F., Yang, H.C. and Wu, C.P. (2008) Preparation and properties of amino-terminated anionic waterborne-polyurethane-silica hybrid materials through a sol-gel process in the absence of an external catalyst. European Polymer Journal, 44, 2777-2783.

CHAPTER V
IN-SITU EMULSION POLYMERIZATION OF WATER-BASED
POLYACRYLATE LAMINATING ADHESIVES UTILIZING
ULTRASONIC-DISPERSED NATURAL THICKENERS

5.1 Abstract

A novel water-based polyacrylate laminating adhesive was synthesized by incorporating the natural thickeners, including bentonite, porous clay heterostructure, calcium carbonate and nanosilica, with different loading levels. Particularly, natural thickeners were dispersed in reaction monomers via ultrasonic to reduce the particle agglomeration. The *in-situ* emulsion polymerization of 2-ethylhexyl acrylate, acrylic acid, styrene, ethylene glycol methyl ether acrylate, 2-(hydroxyethyl) methacrylate, together with the natural thickeners was performed and then investigated the specific properties of the laminating adhesives. Interestingly, with increasing the porous clay heterostructure and CSC1 calcium carbonate, the adhesion property, in terms of 180° peel strength measurement (as followed ASTM D1876), was slightly increased up to 119 N/m at 0.5 wt% loading levels. The introduction of natural thickeners induced a significant improvement in the glass transition temperature (T_g) of the water-based polyacrylate laminating adhesives.

Keywords: Water-based polyacrylate adhesive, Polypropylene lamination, Natural thickeners

5.2 Introduction

Today's environmentally-friendly polymer latexes are of great interest as a raw material for many industrial processes. About 23% of polymer latexes are used for adhesive industries (Landfeater, 2003). Specially-developed adhesives based on semi- or fully synthetic products are interesting. The monomers typically used to produce the commercial latex adhesives are n-butyl acrylate (BA) and 2-ethylhexyl acrylate (EHA) which produce high molar mass, permanently tacky polymers and

very low glass transition temperature (T_g) (Satas, 1989). The carboxylic containing monomers, such as methacrylic acid (MMA) and acrylic acid (AA), are included at very low levels because, after neutralization, the acid groups enhance latex colloidal stability, facilitate stronger bonds to polar substrates and provide intermolecular interaction or physical crosslinking via ion clustering (Foster *et al.*, 2009). Recently, the use of water-based latexes is widespread due to the limitation on solvent-based laminating adhesives, which favor low volatile organic compounds (VOCs) (Romo-Urbe *et al.*, 2016). However, their performances do not go beyond the traditional products.

Recently, the organic/inorganic hybrid materials have attracted considerable attention as they present excellent physical, chemical and mechanical properties (Pavlidou *et al.*, 2008; Wang *et al.*, 2008; Vodnik *et al.*, 2010; Silani *et al.*, 2012). Clearly, the obtained materials might offer the opportunity to combine the desirable properties of both organic polymer and inorganic solid (Xiang *et al.*, 2016). There are two kinds of the organic-inorganic nanocomposites. Class I is the physical blend, wherein weak physical interactions exist between organic and inorganic phases e.g. hydrogen bonds or van der Waals forces. Class II is the strong chemical covalent or ionic bond between organic and inorganic phases (Lin *et al.*, 2012; Campos *et al.*, 2014; Chang *et al.*, 2014).

The number of inorganic particles added to polymeric matrix has increased over the years. Some inorganic particles act as a thickener (a substance which can increase the viscosity of a latex without substantially changing its other properties). There are a variety of thickeners (thixotropes) designed for different applications. In latex adhesives and sealants, such as polyacrylate, polyurethane, polyvinyl acetate and natural rubber, frequently used types include: cellulose, starches, bentonite, gum, fumed silica, precipitated silica and organo-modified clay.

In present study, class I organic/inorganic polyacrylate laminating adhesives based on copolymers of 2-ethylhexyl acrylate (EHA), 2-(hydroxyethyl) methacrylate (HEMA), ethylene glycol methyl ether acrylate (EGMA), acrylic acid (AA) and styrene (SR) were successfully produced by incorporating natural thickeners, such as bentonite (BTN), porous clay heterostructure (PCH), calcium carbonate (CSC1 and Calofil800) and nanosilica. The effect of natural thickener concentration on physical,

thermal and adhesion properties of the laminating adhesives was investigated using Brookfield viscosity, dynamic light scattering (DLS), DuNoüy surface tension and differential scanning calorimetry (DSC). The mechanical properties in terms of 180° peel strength measurement on an untreated oriented polypropylene (OPP) lamination was then characterized.

5.3 Experimental

5.3.1 Materials

Sodium-activated bentonite (BTN) with a cationic exchange capacity (CEC) of 44.5 mmol/100 g was supplied by Thai Nippon Chemical Industry Co., Ltd. Cetyltrimethylammonium chloride, from Italmar Co. Ltd.; dodecylamine and tetraethoxysilane from Sigma Aldrich were used as cationic surfactant, co-surfactant and silica source, respectively. Nanosilica was purchased from General Engineering & Research. Calcium carbonate (CSC1 and Calofil800) was supported by Sand and Soils industrial Co., Ltd. Monomers, including EHA, EGMA, HEMA, styrene and acrylic acid, were purchased from Sigma Aldrich. All monomers were purified using an inhibitor removal resin (Alfa Aesar) to remove any contaminants. Triton™ X-100, sodium dodecyl sulfate (SDS), ammonium persulfate (APS) and sodium bicarbonate (NaHCO₃) were purchased from Sigma Aldrich as surfactants, initiator and buffer in the *in-situ* emulsion polymerization process, respectively.

5.3.2 Preparation of Water-Based Polyacrylate Laminating Adhesives

The water-based polyacrylate laminating adhesives with a molecular weight (M_w) of 309,128 g/mol were then synthesized through the *in-situ* emulsion polymerization. The natural thickeners at various weight fractions (0, 0.5, 1.0, 2.0 and 3.0 wt%) were dispersed in entire monomers using an ultrasonic bath (Fisher Scientific FS20) for 50 min. Pre-emulsion was prepared by homogeneous dissolution of monomers, 0.08 M surfactant and 0.7 g buffer in deionized water (DIW), and then charged to the Optimax™ 1001 working station (Mettler Toledo) equipped with a thermocouple, reflux condenser and a mechanical stirrer at 350 rpm. Polymerization process was performed at 70 °C under nitrogen (N₂) protection and slowly initiated

by the dropwise addition of 0.45 M APS solution with a feeding rate of 0.2 mL/min. The reaction temperature was then carefully raised to 80 °C, avoiding overheating from the exothermic reaction, and held for 4 h to ensure maximal conversion. The water-based polyacrylate laminating adhesives were obtained with a 50 wt% solid content (according to the ISO124:1997) and the pH was regulated to 7.0.

5.3.3 Film Preparation

The water-based polyacrylate laminating adhesives were prepared by casting 20 mL latexes on a PTFE surface. The remaining trapped water was allowed to completely evaporate at 60 °C for 48 h in the vacuum drying oven. The obtained films (~0.5 mm thickness) were then stored in a desiccator at ambient temperature in order to avoid any moisture prior to characterization.

5.3.4 Characterization Techniques

5.3.4.1 *Solid Content*

The solid content measurements were accurately carried out according to the ISO124:1997 standard. Approximately 1.5 g of latex was placed in an aluminium tray with a diameter of 60 mm. The solid content was then calculated by a following equation as the average of three replicates of weight before and after water evaporation.

5.3.4.2 *Structural Properties by FTIR Analysis*

The structural properties of adhesives were investigated using FTIR on a Thermo Scientific Nicolet iS50 instrument with an ATR (attenuated total reflectance) Smart iTX-diamond mode. The FTIR spectra were accurately recorded in an absorption mode over the wavenumber region of 4000-500 cm⁻¹ with 16 scans and a resolution of 4 cm⁻¹.

5.3.4.3 *Surface Area Analysis*

The N₂ adsorption-desorption isotherms were determined via a Micromeritics TriStar II at 77 K following sample preparation at 423 K for 15 h under vacuum (Micromeritics FlowPrep™ 060). Specific surface area, pore volume and pore size were calculated through the Brunauer-Emmett-Teller (BET) equation (Brunauer *et al.*, 1938). The pore size distribution was defined based on the Barrett-

Joyner-Halenda (BJH) method (Barrett *et al.*, 1951) using the adsorption branch of the isotherm.

5.3.4.4 *Brookfield Viscosity Measurement*

The viscosity characteristics were inspected using Brookfield viscometer (model DV-II+ Pro) with LV-25 spindle, Brookfield engineering LABS. INC. The test temperature and speed were set at 25 °C and 100 rpm, respectively.

5.3.4.5 *Particle Size Analysis by DLS*

Particle size and its distribution were determined via DLS using a NanoBrook ZetaPALS Potential Analyzer (Brookhaven Instruments). The latex samples were diluted to 0.5 wt% in an aqueous solution of SDS and NaHCO₃. Samples were measured at room temperature through a 90° scattering angle.

5.3.4.6 *Latex Morphology by TEM Analysis*

The latex microstructures were observed by TEM using a Hitachi-S4800 microscope operated at an accelerating voltage of 100 kV. The latexes were dialyzed to remove surfactant and buffer molecules, then diluted to 0.1 wt% solid content in DIW and deposited a drop of the diluted latex on a carbon-coated grid. Preferential staining with ruthenium tetroxide (RuO₄) was used to distinguish soft and hard phases before TEM examination.

5.3.4.7 *T_g Analysis by DSC*

T_g was examined by DSC using a model Q2000 instrument (TA instruments). The inflection point of the second heating scan was measured in a temperature range between -80 °C to 120 °C at a heating rate of 20 °C/min. The temperature program was designed for a heat-cool-heat system under a N₂ purge rate of 50 mL/min. Approximately 5 mg of sample was sealed in a hermetic aluminium crucible of 40 µL.

5.3.4.8 *Measurement of the 180° peel strength*

Adhesion properties of water-based polyacrylate laminating adhesives was investigated in terms of their 180° peel strength according to ASTM D1876 using a Tensiometer-Instron 5567 instrument equipped with a 100 N load cell, a crosshead speed of 150 mm/min, and a gauge length of 50 mm. A rectangular-shaped specimen (25 mm × 300 mm) was prepared. The latex adhesives were applied

on paper using a drawdown bar with a coating thickness of 24 μm and suddenly laminated to an untreated OPP film.

5.4 Results and Discussion

5.4.1 Investigation on Natural Thickeners

The natural thickeners consisted of bentonite clay (BTN), porous clay heterostructure (PCH), calcium carbonate (CSC1 and Calofil800) and nanosilica. The different vibration modes of chemical groups in BTN, PCH, CSC1, Calofil800 and nanosilica were assigned from the FTIR spectra (Figure 5.1).

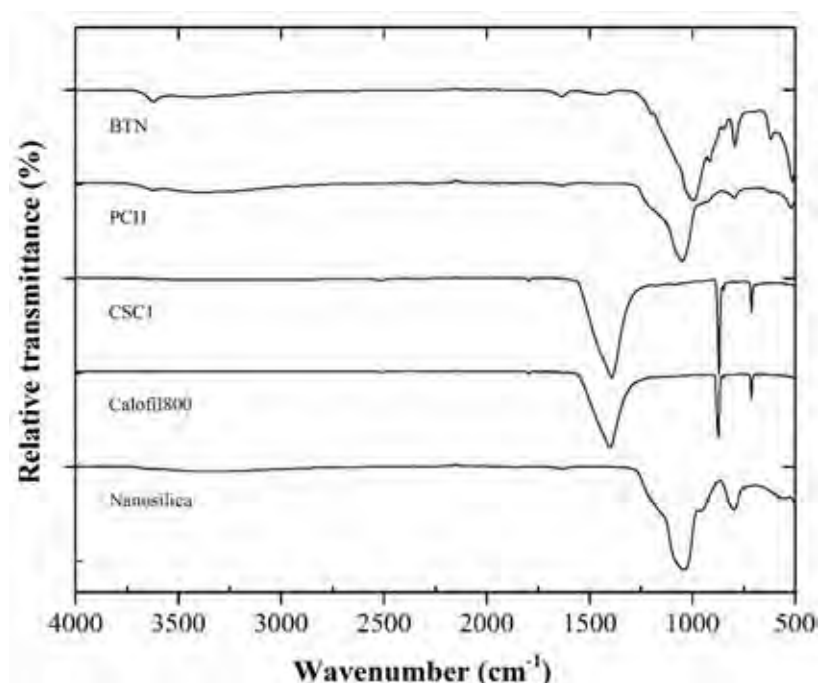


Figure 5.1 ATR-FTIR spectra of the natural thickeners.

The characteristic FTIR bands of BTN, PCH and nanosilica indicated that stretching vibrations of Si-O-Si linkages in asymmetric and symmetric modes were centered at 1000-1100 cm^{-1} and 796 cm^{-1} , respectively. The broad band at 3440 cm^{-1} was then ascribed to stretching vibration of Si-OH of hydrogen-bonded surface silanol groups. While, the characteristic FTIR bands of calcium carbonate indicated

that stretching vibrations of C-O was located at 1390 cm^{-1} . So, the natural thickeners used in the research can be divided into two types: silica-based natural thickeners and calcium carbonate-based natural thickeners.

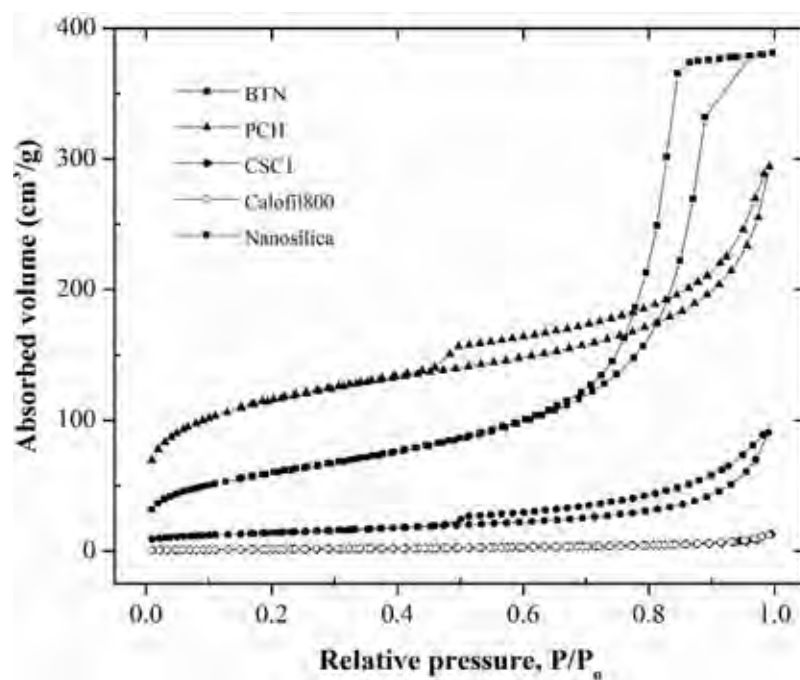


Figure 5.2 $\text{N}_2/77\text{K}$ adsorption-desorption isotherms of natural thickeners.

Table 5.1 Specific surface area of natural thickeners

Natural thickeners	Surface area (m^2/g)
BTN	48.4
PCH	415.8
CSC1	4.0
Calofil800	4.4
Nanosilica	209.4

Figure 5.2 exhibited the measurement of N_2 adsorbed over a range of partial pressures at 77 K gave the $\text{N}_2/77\text{K}$ adsorption-desorption isotherms, which

were used to describe the surface morphology and physical properties of the porous materials. According to the Brunauer-Deming-Deming-Teller (BDDT) classification (Brunauer *et al.*, 1940), a type-IV isotherms were exhibited by BTN and PCH which is a feature of mesoporous materials with a strong adsorbate-adsorbent interaction. A type-V isotherm was exhibited by nanosilica which is a characteristic of mesoporous materials with a weak adsorbate-adsorbent interaction. Additionally, its adsorption and desorption branches do not coincide, indicating the hysteresis loop at a high relative pressure (P/P_o). From the IUPAC classification (Sing *et al.*, 1985), a type-H3 loop can be attributed to the slit-shaped pores with wide bodies and narrow short necks. In case of calcium carbonate, A type-II isotherms were exhibited for the non-porous solids.

The linear relation of the BET equation (Brunauer *et al.*, 1938; Vega-Baudrit *et al.*, 2006) in the P/P_o range of 0.05-0.30 is mainly used to determine the monolayer adsorption capacity (V_m) of materials, using Eq. (5.1);

$$\frac{P}{V_{ads}(P_o - P)} = \frac{1}{V_m C} + \frac{(C - 1)P}{V_m C P_o} \quad (5.1)$$

where V_{ads} is the adsorption volume of N_2 , P is the equilibrium pressure, P_o is the saturation pressure, and C is a parameter related to the heat of adsorptive interactions of monolayer.

The specific surface area (S_{BET}) is obtained from the V_m values by applying Eq. (5.2);

$$S_{BET} = \frac{a_m V_m N_A}{V_M} \quad (5.2)$$

where a_m is the cross-section of the N_2 molecule ($16.2 \times 10^{-20} \text{ m}^2$), N_A is Avogadro's number and V_M is the molar volume of N_2 ($22,414 \text{ cm}^3/\text{mol}$).

The application of the BET equation presented a S_{BET} (Table 5.1). The highest specific surface area belonged to PCH, nanosilica, BTN, calofil800 and CSC1, respectively.

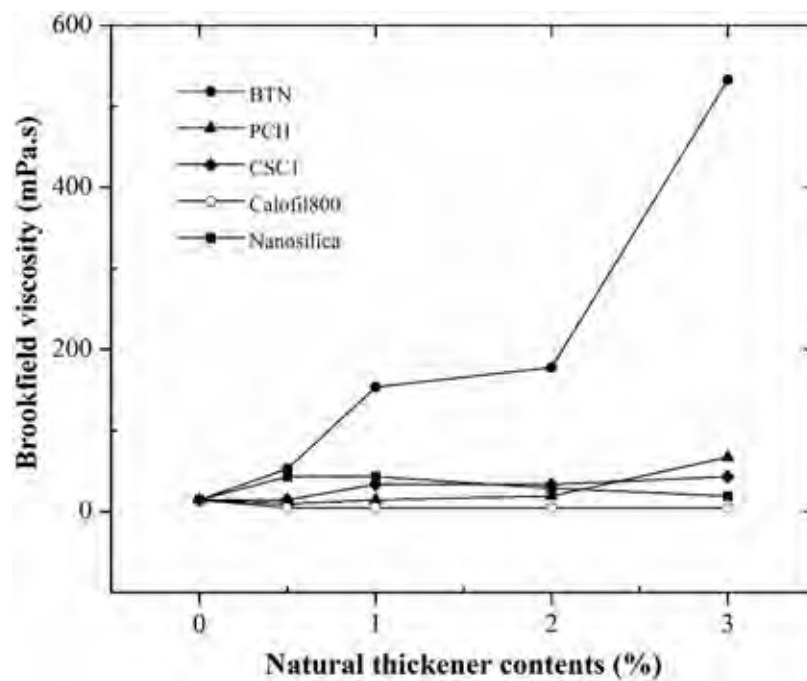


Figure 5.3 Brookfield viscosity of water-based polyacrylate laminating adhesives incorporated with the natural thickeners.

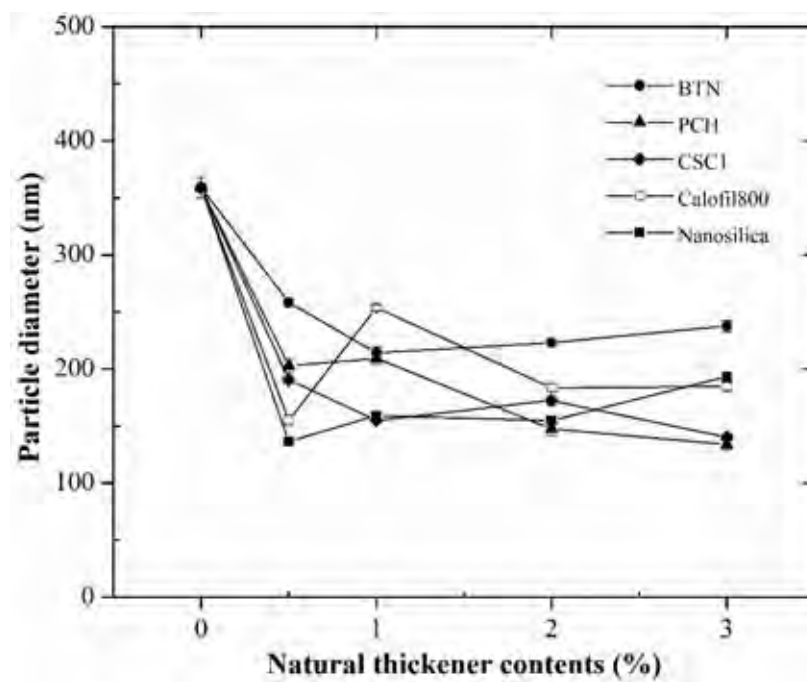


Figure 5.4 The particle diameter of water-based polyacrylate laminating adhesives incorporated with the natural thickeners.

5.4.2 Characteristics of Water-Based Laminating Adhesives

The natural thickeners are substances which can increase the viscosity of latexes without substantially changing its other properties. Moreover, the emulsion stability can be improved. As indicated in Figure 5.3, the Brookfield viscosity was increased with increasing natural thickener contents. Especially in 3 wt% BTN, the viscosity was dramatically enhanced up to 532.7 mPa.s., which was 37 times higher than the neat water-based polyacrylate laminating adhesives. The DLS curves of the water-based polyacrylate laminating adhesives exhibited a single narrow peak. They indicated a monodisperse particle size distribution of the synthesized latex adhesives. The average particle diameters were significantly decreased, with increasing in the natural thickener concentrations (Figure 5.4). The obstruction of the natural thickener particles during the emulsion polymerization process led to a chain scission. The polyacrylate chains were broken at a random point in the backbone to form two-mostly still highly molecular-fragments.

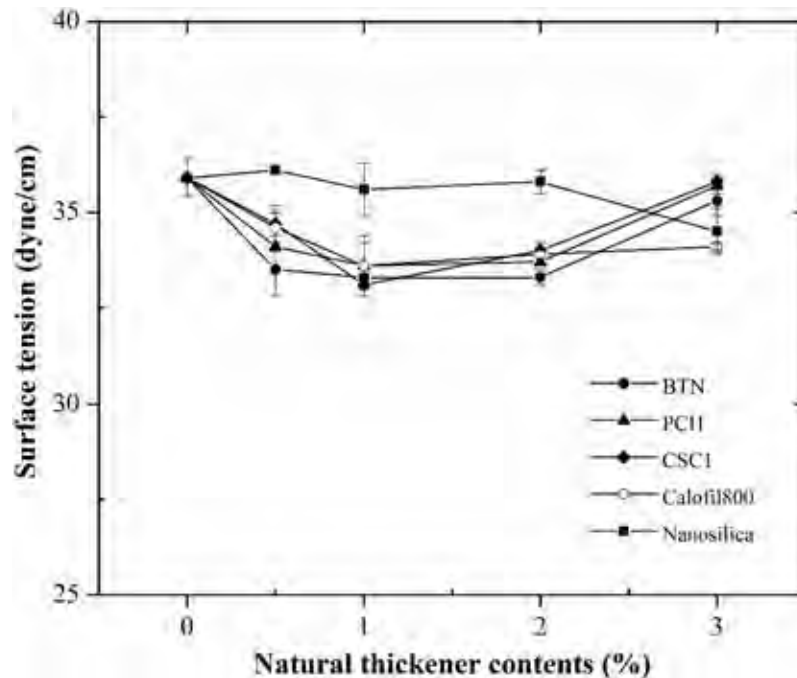


Figure 5.5 The surface tension of the water-based polyacrylate laminating adhesives incorporated with the natural thickeners.

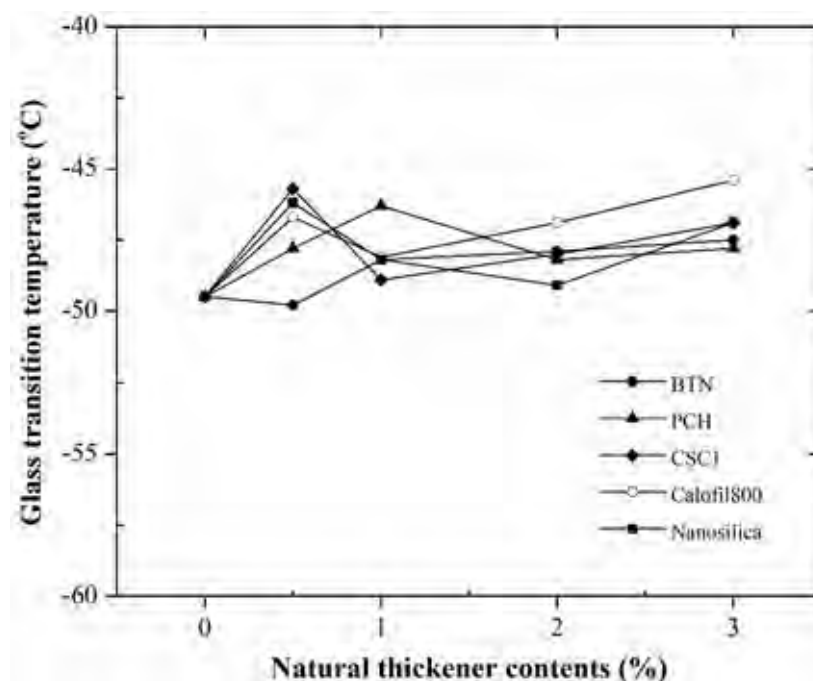


Figure 5.6 T_g plot of water-based polyacrylate laminating adhesives incorporated with the natural thickeners.

Table 5.2 T_g values of water-based polyacrylate laminating adhesives incorporated with the natural thickeners

Natural thickeners (wt%)	T_g (°C)				
	BTN	PCH	CSC1	Calofil800	Nanosilica
0	-49.5	-49.5	-49.5	-49.5	-49.5
0.5	-49.8	-47.8	-45.7	-46.7	-46.2
1.0	-48.2	-46.3	-48.9	-48.1	-48.2
2.0	-47.9	-48.2	-48.0	-46.9	-49.1
3.0	-47.5	-47.8	-46.9	-45.4	-46.9

The surface tension of water-based polyacrylate laminating adhesives incorporated with the natural thickeners was presented in Figure 5.5. It revealed that the natural thickeners had no influence on the surface tension. The representative

DSC thermograms of water-based polyacrylate laminating adhesives are indicated in Figure 5.6. During heating, a single low centered T_g was obtained, consistent with an exothermic process. The T_g values of water-based polyacrylate laminating adhesives are effected by the natural thickener concentrations (Mahkam and Vakhshouri, 2010). With the addition of natural thickeners, the T_g values were gradually shifted to a higher temperature range. The highest T_g value of -45.4 °C was the water-based polyacrylate laminating adhesives incorporated with 3 wt% Calofil800 (Table 5.2). So, the reduction in flexibility of their microdomain and the ability of the natural thickeners to inhibit polymer motion presumably through the covalent attachment were achieved, resulting in the enhanced T_g .

5.4.3 Adhesion Properties

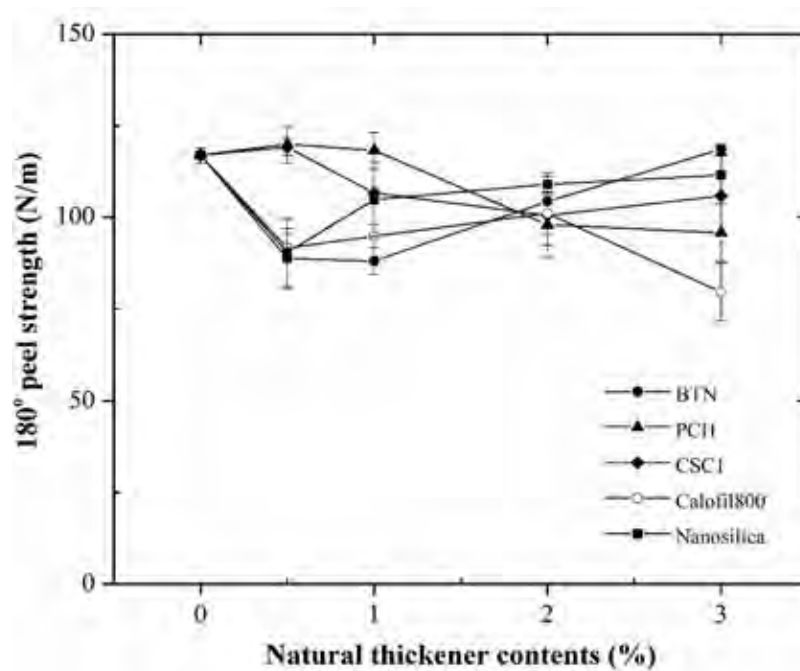


Figure 5.7 Average 180° peel strength of the water-based polyacrylate laminating adhesives incorporated with the natural thickeners.

The 180° peel strength measurement, defined as the average load at plateau, is a reliable method for studying the adhesion property of OPP/adhesives/

paper joints with good sensitivity. The effect of the natural thickener concentration on the adhesion properties of the water-based polyacrylate laminating adhesives incorporated with the natural thickeners was evaluated and is shown in Figure 5.7. All adhesively-bonded joints had an undesirable cohesive failure in its bulk layer due to the lack of cohesive (internal) strength. Both the cohesive and adhesive strengths could be improved by reinforcing the interfacial bond strength via the thickeners. With increasing natural thickener concentrations, the 180° peel strength value was slightly increased up to 119 N/m at 3 wt% BTN, 0.5 wt% PCH and 0.5 wt% CSC1, but then sharply decreased. An excess of natural thickeners reduced flexibility and as a consequence, adhesion performance (decreased peel strength).

5.5 Conclusion

A series of water-based polyacrylate laminating adhesive was successfully synthesized by incorporating the natural thickeners, including bentonite, porous clay heterostructure, calcium carbonate and nanosilica, with different loading levels (0, 0.5, 1, 2 and 3 wt%). The ultrasonic can be used to increase the degree of dispersion of thickener particles into the adhesive matrices. The *in-situ* emulsion polymerization of 2-ethylhexyl acrylate, ethylene glycol methyl ether acrylate, 2-(hydroxyethyl) methacrylate, acrylic acid, styrene, as well as the natural thickeners was performed. With increasing the natural thickeners, the Brookfield viscosity and T_g values were increased, confirming that BTN, PCH, CSC1, Calofil800 and nanosilica exhibited its thickening behavior. On the other hand, the particle diameter was decreased due to the chain scission process (steric hindrance) during an emulsion polymerization. 180° Peel strength of water-based polyacrylate laminating adhesives incorporated with the natural thickeners was enhanced up to 119 N/m at 3 wt% BTN, 0.5 wt% PCH and 0.5 wt% CSC1. However, it does not much different from neat water-based polyacrylate laminating adhesives. Therefore, further development of this adhesive by increasing the compatibility between matrix and filler should be concerned.

5.6 Acknowledgement

This research was financially supported by Research and Researchers for Industries (RRI), The Thailand Research Fund (TRF) Grant number PHD56I0019. Additionally, the authors are thankful for the utilization of the experimental facilities at the Department of Polymer Engineering, the University of Akron. The chemical support from Sand and Soils Co., Ltd was appreciated.

5.7 References

- Barrett, E.P., Joyner, L.G. and Halenda, P.P. (1951) The determination of pore volume and area distributions in porous substances. I. computations from nitrogen isotherms. Journal of the American Chemical Society, 73(1), 373-380.
- Brunauer, S., Deming, L.S., Deming, W.E. and Teller, E. (1940) On a theory of the van der Waals adsorption of gases. Journal of the American Chemical Society, 62(7), 1723-1732.
- Brunauer, S., Emmett, P.H. and Teller, E. (1938) Adsorption of gases in multimolecular layers. Journal of the American Chemical Society, 60, 309-319.
- Campos, C.H., Urbano, B.F. and Rivas, B.L. (2014) Synthesis and characterization of organic-inorganic hybrid composites from poly(acrylic acid)-[3-(trimethoxysilyl)propyl methacrylate]-Al₂O₃. Composites Part B: Engineering, 57, 1-7.
- Chang, C.C., Oyang, T.Y., Chen, Y.C., Hwang, F.H. and Cheng L.P. (2014) Preparation of hydrophobic nanosilica-filled polyacrylate hard coatings on plastic substrates. Journal of Coatings Technology and Research, 11, 381-386.
- Ciullo, P.A. (1996) Industrial minerals and their uses: a handbook and formulary. Westwood, New Jersey: Noyes Publications.

- Foster, A.B., Lovell, P.A. and Rabjohns, M.A. (2009) Control of adhesive properties through structured particle design of water-borne pressure-sensitive adhesives. Polymer, 50, 1654-1670.
- Landfester, K. (2003) Polymer dispersions and their industrial applications. Macromolecular Chemistry and Physics, 204(3), 542.
- Lin, W.C., Yang, C.H., Wang, T.L., Shieh, Y.T. and Chen W.J. (2012) Hybrid thin films derived from UV-curable acrylate-modified waterborne polyurethane and monodispersed colloidal silica. Express Polymer Letter, 6, 2-13.
- Mahkam, M. and Vakhshouri L. (2010) Colon-specific drug delivery behavior of pH-responsive PMAA/perlite composite. International Journal of Molecular Sciences, 11, 1546-1556.
- Pavlidou, S. and Papaspyrides, C.D. (2008) A review on polymer-layered silicate nanocomposites. Progress in Polymer Science, 33(12), 1119-1198.
- Rahman, M.M., Yoo, H.J., Mi, C.J. and Kim, H.D. (2007) Synthesis and characterization of waterborne polyurethane/clay nanocomposite-effect on adhesive strength. Macromolecular Symposia, 249-250, 251-258.
- Rothon, R.N., editor. (2003) Particulate-filled polymer composites. Shrewsbury: Rapra Technology Limited.
- Romo-Uribe, A., Arcos-Casarrubias, J.A., Hernandez-Vargas, M.L., Reyes-Mayer, A., Aguilar-Franco, M. and Bagdhachi, J. (2016) Acrylate hybrid nanocomposite coatings based on SiO₂ nanoparticles by *in-situ* batch emulsion polymerization. Progress in Organic Coatings, 97, 288-300.
- Satas, D. (1989) Handbook of Pressure Sensitive Adhesive Technology. New York: Van Nostrand Reinhold.
- Silani, M., Ziaei-Rad, S., Esfahanian, M. and Tan, V.B.C. (2012) On the experimental and numerical investigation of clay/epoxy nanocomposites. Composite Structures, 94(11), 3142-3148.
- Sing, K.S.W., Everett, D.H., Haul, R.A.W., Moscou, L., Pierotti, R.A., Rouquérol, J. and Siemieniewska, T. (1985) Reporting physisorption data for gas/solid systems with special reference to the determination of surface area and porosity. Pure and Applied Chemistry, 57(4), 603-619.

- Vodnik, V.V., Božanić, D.K., Džunuzović, E., Vuković, J., and Nedeljković, J.M. (2010) Thermal and optical properties of silver-poly(methylmethacrylate) nanocomposites prepared by in situ radical polymerization. European Polymer Journal, 68(8), 1225-1230.
- Wang, Y., Shen, Y., Pei, X., Zhang, S., Liu, H., and Ren, J. (2008) Poly(styrene-co-maleic anhydride)/SiO₂ hybrid composites via “grafting onto” strategy based on nitroxide-mediated radical polymerization. Reactive and Functional Polymers, 68(8), 1225-1230.
- Xiang, B. and Zhang, J. (2016) Using ultrasound-assisted dispersion and in situ emulsion polymerization to synthesize TiO₂/ASA (acrylonitrile-styrene-acrylate) nanocomposites. Composites Part B: Engineering, 99, 196-202.

CHAPTER VI
WATERBORNE ACRYLIC HYBRID ADHESIVES
BASED ON A METHACRYLATE-FUNCTIONALIZED POROUS CLAY
HETEROSTRUCTURE FOR POTENTIAL LAMINATION APPLICATION

6.1 Abstract

A new waterborne acrylic (WAC) hybrid adhesive was evaluated for an untreated polypropylene lamination. The WAC hybrid adhesive was formulated with a new class of mesoporous clay heterostructure (PCH), which was modified with 3-(trimethoxysilyl)propyl methacrylate (as a coupling agent) to promote the chemical bonding with the acrylic matrix to form a methacrylate-functionalized PCH (MPCH). The WAC hybrid adhesive was based on copolymers (2-ethylhexyl acrylate, ethylene glycol methyl ether acrylate, 2-(hydroxyethyl) methacrylate, styrene and acrylic acid) with varying amounts of MPCH. The SEM micrographs revealed the presence of a well dispersed MPCH distributed throughout the matrix. Thus, the optimal adhesive performance, in terms of the 180° peel strength of bonded joints, of 140.2 N/m was achieved using 1.5 wt% of MPCH, while the thermal stability of the adhesives was improved with increasing MPCH loading levels.

Keywords: Adhesion, Adhesive, Strength

6.2 Introduction

Solventborne laminating adhesives are dominant in manufacturing processes especially for the flexible packaging. However, as highlighted by the Environmental Protection Agency, volatile organic compound (VOC) emissions from anthropogenic sources are in urgent need of restriction since they are hazardous air pollutants (US EPA, 2015). As a consequence, the waterborne acrylics (WACs) are currently being explored as a replacement for the solventborne adhesives. These adhesives offer the excellent durability, optical clarity, UV resistance, toughness and also oil tolerance (Huang *et al.*, 2004; Ebnesajjad, 2009; Romo-Uribe *et al.*, 2016). On the other hand,

on occasion waterborne adhesives have been reported to have a catastrophic loss of adhesion, resulting in a failure of bonded joint (Packham, 1992). So, new approaches are needed for the waterborne adhesives to replace the solventborne systems. As one possible solution to the serious debonding problem, WAC adhesives based on an organic/inorganic hybrid structure are being developed (Sanchez *et al.*, 2005).

Generally, a small percentage (less than 5 wt%) of nano-inorganic fillers, including clay mineral (Diaconu *et al.*, 2008; Mičušík *et al.*, 2012; Solhi *et al.*, 2012), titania (Xiang and Zhang, 2016), alumina (Rong *et al.*, 2002; Campos *et al.*, 2014), nanosilica (Lin *et al.*, 2008; Chang *et al.*, 2014) and calcium carbonate (Gumfekar *et al.*, 2011), are mechanically blended into the adhesive matrix resulting in dramatic enhancement of the adhesive properties with clay being the most favorable. In case of pressure-sensitive adhesives (PSAs), Bonnefond *et al.* studied the morphology and properties of the waterborne films from n-butyl acrylate/methyl methacrylate/Nanmontmorillonite clay (MMT) hybrid adhesives in 2013. The peel resistance increased for the formulations containing MMT. The most remarkable result was obtained for 2% weight based on monomers (wbm%) of MMT, 0.23 wbm% of allyl methacrylate and 0.15 wbm% of n-dodecyl mercaptan with 180° peel strength of 250 N/m. In 2013, acrylic/MMT PSAs were synthesized by Oh *et al.* through *in-situ* emulsion polymerization and mechanical blending. A greater dispersion of MMT and higher peel strength of 370 gf was reported by using an *in-situ* emulsion polymerization technique where the polymerization was performed in the presence of the clay additive. In other work, a solventless UV-crosslinkable acrylic approach was taken to formulate PSAs (Kajtna *et al.*, 2014). With increasing MMT, a maximum of 1000 N/m peel strength was achieved with 3-5 wt% of MMT Cloisite depending on type. However, there has been a lack of systematic development of waterborne laminating adhesives that can give definitive direction for the flexible packaging industry. In a previous report, a relatively new class of mesoporous materials, named porous clay heterostructure (PCH), with a specific surface area of approximately 500-1000 m²/g, was used successfully in the waterborne polyurethane laminating adhesives. After modification, the amino-functionalized PCH was reported to greatly improve the Brookfield viscosity, thermal and adhesion properties of waterborne polyurethane

hybrid adhesives, as well as lowering crystallinity and glass transition temperature (T_g) of the polyurethane matrix.

In this study, the synthetic strategy for generating the effective WAC hybrid adhesives is the combination of an acrylic polymeric matrix (a soft domain with flexibility and ductility) and inorganic filler (a hard domain with rigidity and thermal stability) through a covalent bond. The PCH nanoparticles were functionalized using a silylation reaction with 3-(trimethoxysilyl)propyl methacrylate (TSPM) acting as a coupling agent (Kango *et al.*, 2013), where the resultant methacrylate-functionalized PCH (MPCH) can covalently bond with the acrylic matrix reducing any tendency for macroscopic phase separation between filler and matrix (Guo *et al.*, 2008; Mičušík *et al.*, 2012). A new acrylic latex adhesive matrix was designed using mostly of 2-ethyl hexyl acrylate (EHA) and ethylene glycol methyl ether acrylate (EGMA), with small quantities of styrene, 2-(hydroxyethyl) methacrylate (HEMA) and acrylic acid. The acrylic acid on the latex particle surfaces was used to facilitate the emulsion stability and, after film formation, the physical crosslinking via the ionic clusters (Landfester, 2003; Foster *et al.*, 2009). The *in-situ* emulsion polymerization of these monomers in the presence of MPCH was designed to be industrially scalable (Araújo *et al.*, 1999). The influence of MPCH concentration on the morphology, structural, physical and thermal properties of the WAC hybrid adhesives was investigated using Fourier transform infrared spectroscopy (FTIR), scanning electron microscopy (SEM), energy dispersive X-ray analysis (EDX), Brookfield viscosity, DuNouy surface tension, dynamic light scattering (DLS), differential scanning calorimetry (DSC) and thermogravimetric (TG) analyses. The adhesion properties of the synthesized WAC hybrid adhesive on oriented polypropylene (OPP)/paper lamination were determined by measurement of their 180° peel strength.

6.3 Experimental

6.3.1 Materials

Commercial sodium-activated bentonite (BTN) was supplied by Thai Nippon Chemical Industry Co., Ltd with the cationic exchange capacity (CEC) of 44.5 mmol/100 g. Cetyltrimethylammonium chloride (CTAC), from Italmar Co. Ltd.,

was used as the cationic surfactant, while TSPM and tetraethoxysilane (TEOS) were purchased from Sigma Aldrich, US as silica sources. Dodecylamine, sodium acetate trihydrate ($\text{CH}_3\text{COONa}\cdot 3\text{H}_2\text{O}$) and acetic acid (CH_3COOH) were obtained from Sigma Aldrich, and used as the dispersing medium. Methanol (CH_3OH) and 37% hydrochloric acid (HCl) were acquired from RCI Labscan Ltd. Monomers, including EHA, EGMA, HEMA, styrene and acrylic acid, were purchased from Sigma Aldrich. All monomers were purified using an inhibitor removal resin (Alfa Aesar) to remove contaminants. TritonTM X-100, sodium dodecyl sulfate (SDS), sodium bicarbonate (NaHCO_3) and ammonium persulfate (APS) were purchased from Sigma Aldrich as the surfactants, buffer and initiator in emulsion polymerization process, respectively.

6.3.2 Preparation of MPCH

Mesoporous materials were accomplished as follows: approximately 50 g of BTN was dispersed in 0.1 M CTAC solution at 50 °C for 24 h until an equilibrium to obtain the cationic exchange reaction. The synthesized product was filtered and then washed with a mixture of deionized water and methanol (1:1) until at pH of 9. Organo-modified BTN (OBTN) was agitated in dodecylamine at 50 °C for 30 min, followed by TEOS to derive the co-condensation at room temperature for 4 h (OBTN: dodecylamine: TEOS (v/v/v) of 1:20:150). The dried OBTN was purified via solvent extraction (CH_3OH : HCl (v/v) of 9:1) and screened through a mesh size of #325 to obtain the PCH with an apparent density of 1.99 g/cm³. The PCH was then suspended in a freshly prepared solution of 5% (v/v) TSPM in 0.05 M sodium acetate buffer (pH = 4.0) and the silylation process proceeded at 70 °C for 4 h. The obtained MPCH was then thoroughly washed with excess deionized water to remove the residual unlinked TSPM.

6.3.3 Preparation of the WAC Hybrid Adhesives

The WAC hybrid adhesives with a molecular weight (M_w) of 309,128 g/mol were synthesized through batchwise emulsion polymerization, as indicated in Figure 6.1. Briefly, MPCH at various weight fractions (0, 0.5, 1.0, 1.5 and 2.0 wt%) was dispersed in entire monomers using an ultrasonic bath (Fisher Scientific FS20)

for 50 min. The pre-emulsion was gently prepared by homogeneous dissolution of monomers, 0.08 M surfactant and 0.7 g buffer in deionized water, and then charged to Optimax™ 1001 working station (Mettler Toledo) equipped with a thermocouple, a reflux condenser and a mechanical stirrer at 350 rpm. The emulsion polymerization was performed at 70 °C under nitrogen (N₂) protection and slowly initiated by the dropwise addition of 0.45 M APS solution (a feeding rate of 0.2 mL/min). The reaction temperature was then carefully raised to 80 °C, avoiding overheating from the exothermic reaction, and held for 4 h to ensure maximal conversion. The WAC hybrid adhesives were obtained with a 50 wt% solid content measurement (according to ISO124:1997) and the pH was regulated to 7.0.

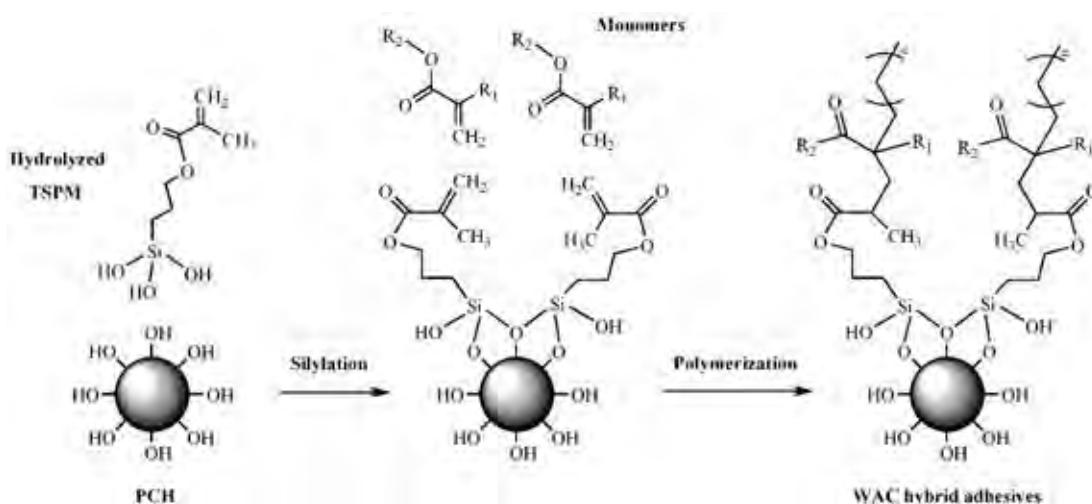


Figure 6.1 Schematic description of grafting-to approach for WAC hybrid adhesive.

6.3.4 Film Preparation

WAC hybrid adhesive films were prepared by casting latex adhesives (20 mL) on a polytetrafluoroethylene (PTFE) surface. The remaining trapped water was allowed to completely evaporate at 60 °C for 24 h in a vacuum drying oven. The obtained film (typically of 0.5 mm thickness) was then stored in a desiccator at ambient temperature prior to characterization.

6.3.5 Characterization Techniques

6.3.5.1 *Structural properties by FTIR analysis*

Structural properties were investigated by FTIR on a Thermo Scientific Nicolet iS50 instrument with an attenuated total reflectance (ATR) Smart iTX-diamond mode. The FTIR spectra were accurately recorded in an absorption mode over the wavenumber region of 4000-500 cm^{-1} with 16 scans and a resolution of 4 cm^{-1} .

6.3.5.2 *Surface Area Analysis*

The N_2 adsorption-desorption isotherms were determined by using a Micromeritics TriStar II at 77 K following sample preparation (Micromeritics FlowPrep™ 060) at 423 K for 15 h under vacuum. Specific surface area, pore volume and pore size were calculated through the Brunauer-Emmett-Teller (BET) equation (Brunauer *et al.*, 1938). The pore size distribution was defined based on the Barrett-Joyner-Halenda (BJH) method (Barrett *et al.*, 1951) using adsorption branch of the isotherm.

6.3.5.3 *Surface Morphology by Field Emission SEM Analysis*

The surface morphology of adhesives was observed by FE-SEM using a Hitachi S-4800 model microscope with a 5.0 KV accelerating voltage. The specimen was coated with platinum by sputtering for 200 s to reduce the surface charging during electron irradiation.

6.3.5.4 *Elemental Analysis by Energy Dispersive X-ray (EDX)*

Elemental composition within the adhesives was identified using EDX (operated together with the FE-SEM in section 6.3.5.3) at a 20.0 kV accelerating voltage and a working distance of 15.0 mm. The quantitative analysis was performed through mapping and point & ID modes.

6.3.5.5 *Brookfield Viscosity Measurement*

The viscosity characteristics were inspected using Brookfield viscometer (model DV-II+ Pro) with a LV-25 spindle from Brookfield engineering LABS. INC. The test temperature and rotational speed were set at 25 °C and 100 rpm, respectively.

6.3.5.6 Particle Size Analysis by DLS

Particle size and its distribution were determined by DLS using a NanoBrook ZetaPALS Potential Analyzer (Brookhaven Instruments). The latex samples were diluted to 0.5 wt% in an aqueous solution of SDS and NaHCO₃. Samples were measured at room temperature through a 90° scattering angle.

6.3.5.7 DuNouy Surface Tension

The measurement of the surface tension was performed using a DuNouy tensiometer from CSC scientific Co., Inc., and is reported in the CGS unit of dyne/cm.

6.3.5.8 T_g Analysis by DSC

The T_g was then characterized by DSC using a model Q2000 instrument (TA instruments). The inflection point of the second heating scan was measured in a temperature range between -80 °C to 120 °C at a heating rate of 20 °C/min. The temperature program was designed for a heat-cool-heat system under a N₂ purge rate of 50 mL/min. Approximately 5 mg of each sample was sealed in a hermetic aluminium crucible of 40 µL.

6.3.5.9 Thermal Stability and Grafting Ratio (R_g) Analysis by TGA

The thermal decomposition was studied by a high resolution TGA model TA Q50 instrument (TA instruments) under a continuous N₂ atmosphere at a purge rate of 40 mL/min over the temperature range of 50-800 °C at a heating rate of 10 °C/min. Approximately 10 mg of each sample was loaded on a platinum crucible.

The R_g of TSPM on the mesoporous surface was calculated from Eq. (6.1) from Kango *et al.*, 2013;

$$R_g = \left(\frac{W_1'}{W_1} - \frac{W_0'}{W_0} \right) \times 100\% \quad (6.1)$$

where W_1 is the starting weight of MPCH; W_1' is the residual weight of MPCH at 750 °C; W_0 is the starting weight of PCH; and W_0' is the residual weight of PCH at 750 °C.

6.3.5.10 Measurement of the 180° peel strength

The adhesion property of the WAC hybrid adhesives was investigated in terms of the 180° peel strength in tension testing mode according to ASTM D1876 using a Tensiometer-Instron 5567 instrument equipped with a 100 N static load cell, a crosshead speed of 150 mm/min, and a gauge length of 50 mm. Laminated test panels consisted of two rectangular-shaped adherends, paper and untreated OPP film, were properly prepared and then bonded together in accordance with the WAC hybrid adhesive. Specially prepared specimens 25 mm (1 in.) wide by 305 mm (12 in.) long, but bonded only over approximately 241 mm (9 in.) of their length. The WAC hybrid adhesive was applied on paper using a BYK drawdown bar with an average coating thickness of 24 μm and suddenly adhered to untreated OPP film. The OPP/WAC hybrid adhesive/paper laminated joints were post-cured at 60 °C. The 76 mm (3 in.) long unbounded ends bent apart, perpendicular to the glue line, for clamping in the grips of the testing machine. An autographic curve of peeling was calculated as the average peeling load in N/m of the specimen width required to separate the adherends.

6.4 Results and Discussion

The PCH was much better than clay mineral due to its lightweight and high porosity, acting as a desirable reinforcing filler. After modification by TSPM, the methacrylate groups were anchored either in the pores or on the surfaces of PCH, resulting in MPCH. Then, the acrylic monomers were able to polymerize with vinyl groups either in the pores or on the surfaces of MPCH as well. Thus, the internal strength was increased via a strong chemical bonding. Conversely, modifications of clay mineral by TSPM, the methacrylate groups were anchored on the surfaces. Thus, the reinforcement was not as strong as using MPCH.

6.4.1 Synthesis and characterization of MPCH

The different vibration modes of chemical groups in the PCH and MPCH materials were assigned from the ATR-FTIR spectra, as indicated in Figure

6.2. The characteristic FTIR bands of the stretching vibrations of Si-O-Si linkages in both asymmetric and symmetric modes were centered at 1042 cm^{-1} and 796 cm^{-1} , respectively, in PCH, while they were at 1039 cm^{-1} and 791 cm^{-1} , respectively, in MPCH. The bending vibrations of these linkages were located at 460 cm^{-1} . The broad absorptions at 3440 cm^{-1} and 1650 cm^{-1} were ascribed to the Si-OH stretching and the bending vibration modes of hydrogen-bonded surface silanol groups, which were physically adsorbed water (Hair, 1967; Bunnak *et al.*, 2013). Moreover, the reduction

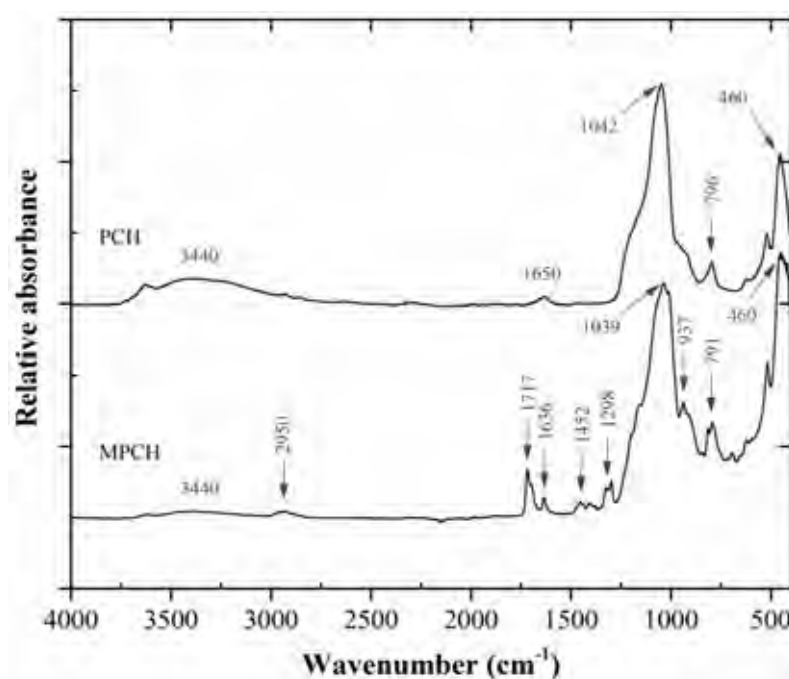


Figure 6.2 ATR-FTIR spectra of PCH and MPCH.

in intensity of these absorption bands in MPCH obviously indicates the total surface modification of PCH via the silylation reaction between the -OH groups on the PCH surface and the hydrolyzed TSPM (Kango *et al.*, 2003). After this silane treatment, C-H asymmetric and symmetric stretching vibrations at around $2900\text{--}2800\text{ cm}^{-1}$; C=O stretching vibrations at 1717 cm^{-1} associated with carbonyl ester compounds; C=C stretching vibrations at 1636 cm^{-1} ; -CH₂ and -CH₃ asymmetric deformations at 1452 cm^{-1} ; C-O-C asymmetric stretching vibrations at 1298 cm^{-1} ; and CH=CH₂ out of plane deformations in vinyl compounds at 937 cm^{-1} , were all in evidence. Thus,

the FTIR analysis revealed the successful functionalization of methacrylate groups on the surface silanol groups of PCH, confirming the formation of MPCH.

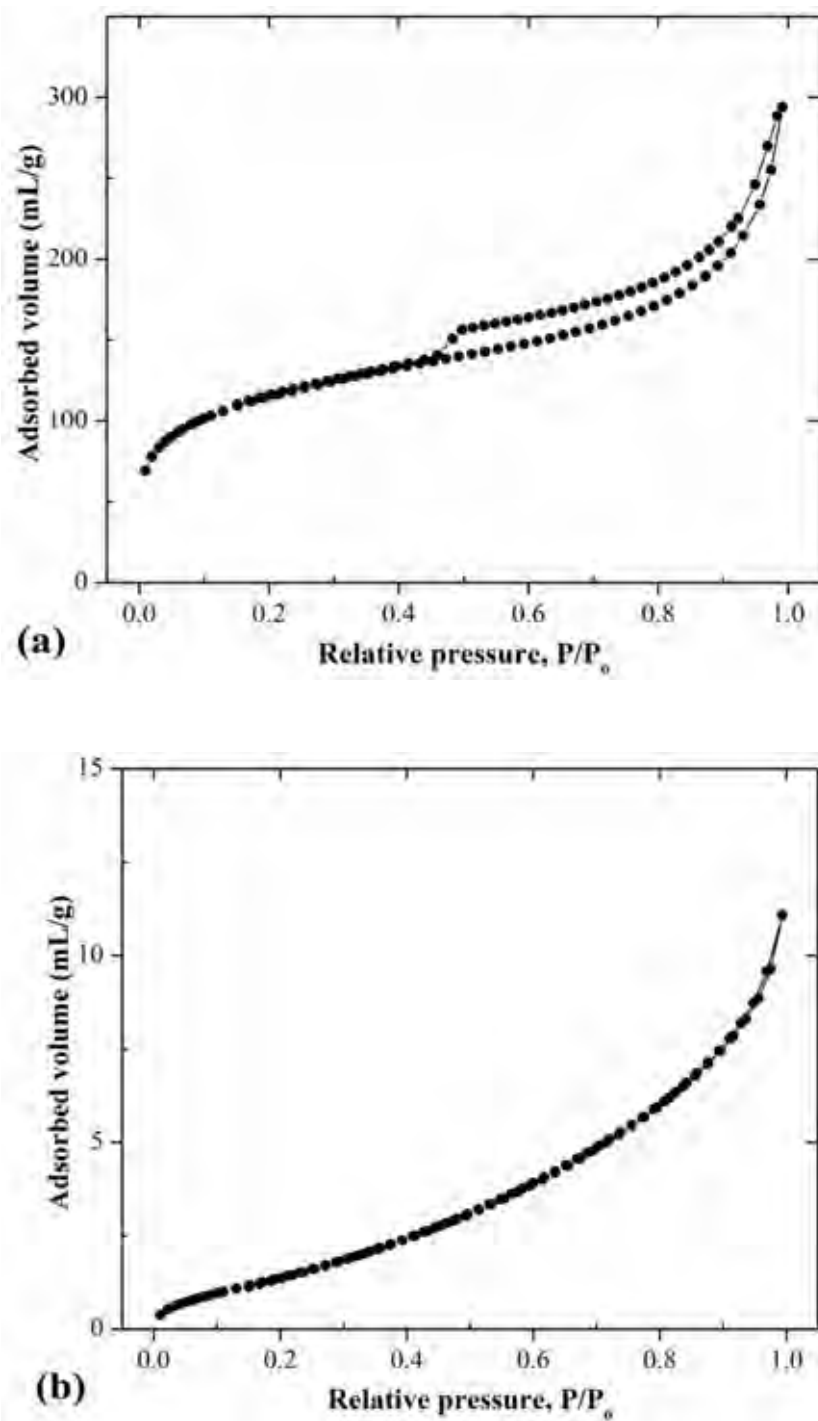


Figure 6.3 $N_2/77K$ adsorption-desorption isotherms of (a) PCH and (b) MPCH.

The exact amount of methacrylate groups anchored on MPCH was determined by TG analysis, where the decomposition ratio of organic compounds corresponds to their R_g values (Wenfang *et al.*, 2005). The greater the weight loss, the higher the obtained grafting level. The untreated PCH had a total weight loss of 8.8 wt% up to 200 °C, which was due to the elimination of the physically adsorbed water. Meanwhile, MPCH had a total weight loss of 34.8% at 387.8 °C, which was due to the degradation of covalently grafted methacrylate-functional silane groups on the surface (Kango *et al.*, 2013). In contrast, there was no adsorption of water on MPCH because of the replacement of the hydrophilic silanol groups of PCH with methacrylate groups in MPCH, as confirmed by the FTIR results. Therefore, the R_g , expressed as the percentage of add-on, and then calculated using Eq. (6.1) was 26.1% of methacrylate-functional silanes on MPCH.

The measurement of the amount of N_2 adsorbed over a range of partial pressures at 77 K gave the $N_2/77K$ adsorption-desorption isotherms, which were used to describe the surface morphology and physical properties of the porous materials. According to the Brunauer-Deming-Deming-Teller (BDDT) classification (Brunauer *et al.*, 1940), a type-IV isotherm was exhibited by the untreated PCH (Figure 6.3a), which is a characteristic of mesoporous materials with a strong adsorbate-adsorbent interaction. Additionally, its adsorption and desorption branches do not coincide, indicating the hysteresis loop at a high relative pressure (P/P_o). From the IUPAC classification (Sing *et al.*, 1985), a type-H3 loop can be attributed to the slit-shaped pores with the wide bodies and narrow short necks. A BDDT type-II isotherm was exhibited by MPCH (Figure 6.3b) which is typical of non-porous solid with capillary condensation at a P/P_o of 0.85, suggesting that the methacrylate groups replaced the continuous pore area of the PCH host material.

The linear relation of the BET equation (Brunauer *et al.*, 1938; Vega-Baudrit *et al.*, 2006) in the P/P_o range of 0.05-0.30 is mainly used to determine the monolayer adsorption capacity (V_m) of materials, using Eq. (6.2);

$$\frac{P}{V_{ads}(P_o - P)} = \frac{1}{V_m C} + \frac{(C - 1)P}{V_m C P_o} \quad (6.2)$$

where V_{ads} is the adsorption volume of N_2 , P is the equilibrium pressure, P_o is the saturation pressure, and C is a parameter related to the heat of adsorptive interactions of monolayer.

The specific surface area (S_{BET}) is then obtained from the V_m values by applying Eq. (6.3);

$$S_{BET} = \frac{a_m V_m N_A}{V_M} \quad (6.3)$$

where a_m is the cross-section of the N_2 molecule ($16.2 \times 10^{-20} \text{ m}^2$), N_A is Avogadro's number and V_M is the molar volume of N_2 ($22,414 \text{ cm}^3/\text{mol}$).

The application of the BET equation gave a S_{BET} and C_{BET} of $415.8 \pm 2.3 \text{ m}^2/\text{g}$ and 178.0, respectively, for untreated PCH with a BJH pore diameter and pore volume of 4.43 nm and 0.46 cc/g (calculated from the adsorption branches of isotherms), respectively. The S_{BET} of PCH was relatively high due to its porous structures at the nanometer scale. After modification of PCH to MPCH, the S_{BET} and C_{BET} values were significantly decreased (96.7- and 3.7-fold, respectively) to $4.3 \pm 0.1 \text{ m}^2/\text{g}$ and 48.6, respectively, indicating the small cavities, assumed then to be a non-porous material. In fact, when the porous material was fully filled cavities across its depth, its characteristic was changed to be the non-porous material with a very low S_{BET} . In the case of MPCH, the preferential adsorption of the long-chain methacrylate-functional silanes, either in the pores or on the surfaces of the PCH host material led to the significant changes in the surface morphology of MPCH and its S_{BET} . Finally, MPCH transformed into the non-porous material.

6.4.2 Hybrid WAC Adhesives

As a result of MPCH, the emulsion polymerization was then occurred between acrylic monomers and methacrylate groups of TSPM anchoring either in the pores or on the surfaces of MPCH. Therefore, the internal strength was increased by a strong chemical bonding. On the other hand, the modification of clay mineral by

TSPM caused the methacrylate groups anchoring on its surfaces so the reinforcement was not as strong as when using MPCH.

The characteristics of WAC hybrid adhesives prepared by batchwise emulsion polymerization, including the solid content, Brookfield viscosity, particle size and surface tension, are summarized in Table 6.1. First, the solid contents of the WAC adhesives, in terms of the ISO124:1997 standard, were almost identical to the theoretical designed value with ~99% conversion levels, which implies that there was no residual monomer at the end of the polymerization. The Brookfield viscosity of the latex adhesives exponentially increased from 14.4 to 62.4 mPa.s with increasing MPCH contents, which is due to the unfolding of the polymer molecules (thickening behavior). The Brookfield viscosity of latex adhesives is a function of the volume fraction of the dispersed phase (Arevalillo *et al.*, 2006). The presence of MPCH and its intramolecular interaction via chemical bonding within the WAC chains might considerably decrease the polymer chain entanglement, increase the effective volume fraction, and hence the viscosity of latex adhesives. A much larger volume fraction of MPCH led to an aggregation of MPCH and to undergo conformation changes, which are thought to result in unfolding the structure of the WAC hybrid adhesives.

Table 6.1 Physical characteristics of the WAC hybrid adhesives

WAC hybrid adhesives	Solid content (%)	Brookfield viscosity (mPa.s)	Particle diameter (nm)	Surface tension (dyne/cm)
0.0MPCH	50.4 ± 0.2	14.4	355.6 ± 2.9	50.4 ± 0.2
0.5MPCH	50.4 ± 0.3	24.0	281.4 ± 3.2	34.0 ± 0.2
1.0MPCH	50.2 ± 0.5	28.8	314.9 ± 5.1	34.1 ± 0.4
1.5MPCH	50.0 ± 0.7	38.4	334.2 ± 8.1	34.8 ± 0.4
2.0MPCH	50.0 ± 0.1	62.4	366.0 ± 6.9	34.5 ± 0.5

The DLS curves of WAC hybrid adhesives exhibited a single narrow peak, indicating a monodisperse particle size distribution of the synthesized latexes (Figure 6.4). The average particle diameters and surface tensions of the WAC hybrid

adhesives were much lower than that of the neat adhesive, resulting in a good wettability and stability of the latex adhesives. The MPCH could be encapsulated by either latex particles or on the surfaces of the latex, so the average adhesive particle size was enhanced with increasing MPCH content, ranging from 281 nm to 366 nm as the MPCH contents increased from 0.5 to 2.0 wt%, respectively.

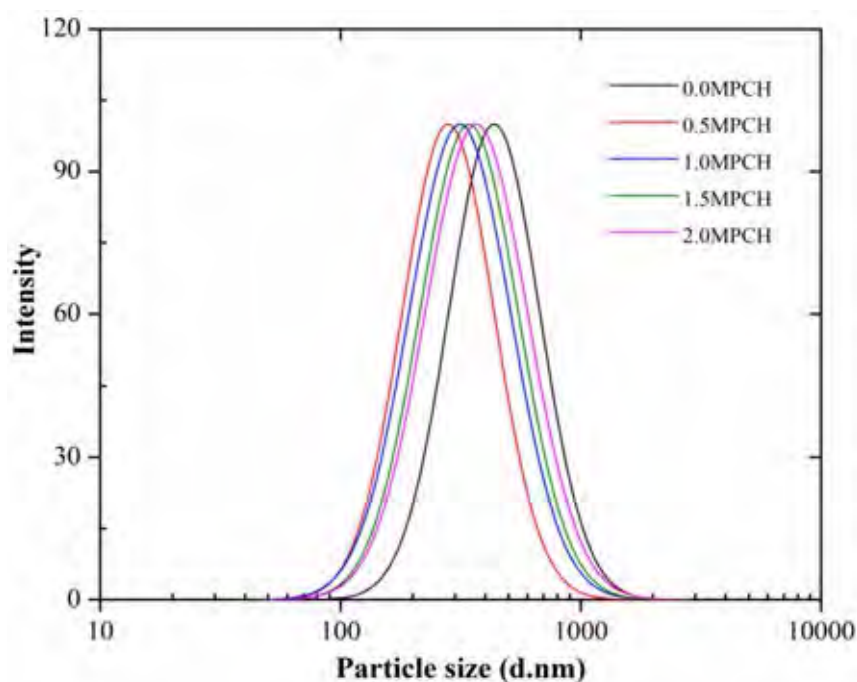


Figure 6.4 DLS curves of WAC hybrid adhesives. Curves shown are representative of those seen from five samples.

The surface morphologies of MPCH and WAC hybrid adhesives were examined by FE-SEM, with representative images as shown in Figure 6.5a-c. The MPCH exhibited a rough surface with quite small cavities due to the replacement of methacrylate-functional silanes inside or on surfaces of PCH pores. The synthesized WAC hybrid adhesive indicated a good dispersion and distribution of MPCH as compared to the neat WAC adhesive, which was due to the strong chemical bonding of vinyl groups. The quantitative elemental composition analysis in the WAC hybrid adhesives was evaluated by EDX analysis (Figure 6.5d), where the surface of 2.0

wt% MPCH was found to clearly be covered with silicon atoms (green dots) at 12.6%, which was confirmed by the point and ID method.

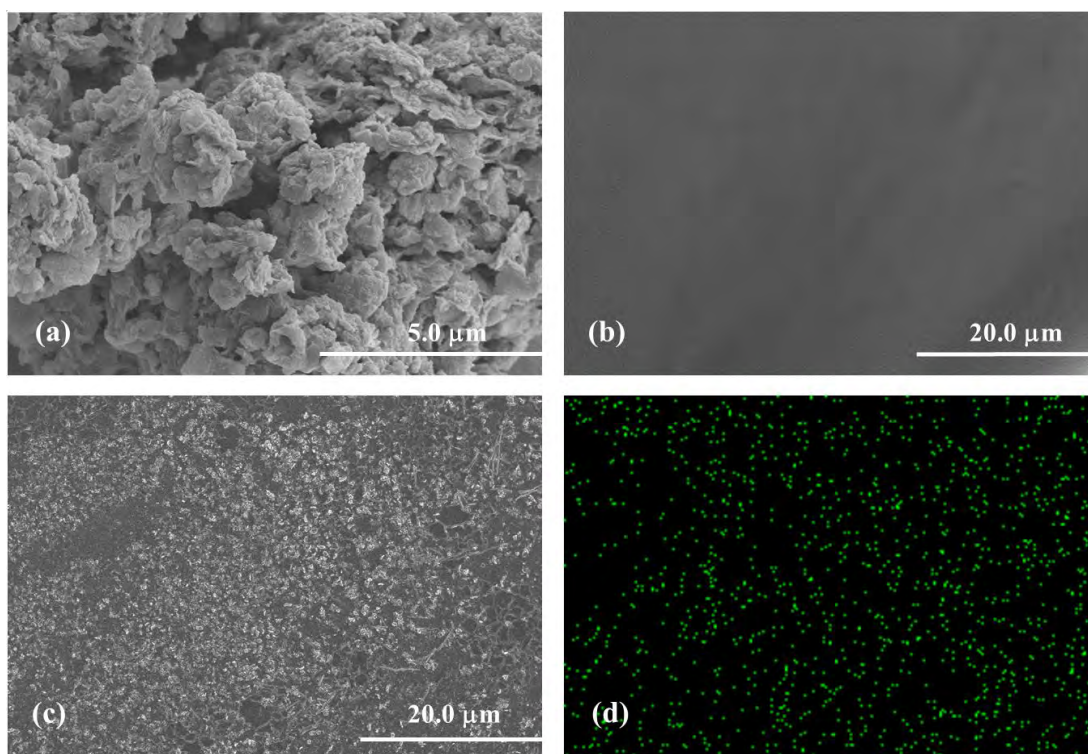


Figure 6.5 FE-SEM micrographs of (a) MPCH (10.0 kx magnification, scale bar = 5 μm), (b) 0.0MPCH, (c) 2.0MPCH (2.0 kx magnification, scale bar = 20 μm) and (d) EDX analysis showing the silicon mapping of 2.0MPCH.

The interfacial interactions of MPCH with the acrylic adhesives were examined using FTIR spectra, as indicated in Figure 6.6a. The prominent absorption bands are assigned in Table 6.2 (Feldgitscher *et al.*, 2009; Lin *et al.*, 2012; Romo-Uribe *et al.*, 2016). Neat WAC adhesive displayed a broad O-H stretching vibration (very weak) band at 3440 cm^{-1} from the residual adsorbed water. In addition, there were asymmetric and symmetric C-H stretching vibrations at $2960\text{-}2850\text{ cm}^{-1}$, and the corresponding bending vibration at 1450 cm^{-1} , C=O stretching vibration at 1730 cm^{-1} , symmetric vibration of COO at 1380 cm^{-1} and the ester C-O-C asymmetric vibration at $1240\text{-}1128\text{ cm}^{-1}$ (two bands). These absorbances showed the connectivity between MPCH and acrylic matrix due to the disappearance of C=C bonds, assuming

that entire C=C bonds from TSPM and monomers completely reacted. Meanwhile, the absorption bands of siloxane and its derivatives were observed in the presence of MPCH (see enlargement in Figure 6.6b). The FTIR spectra revealed absorbances associated with neat WAC adhesive. The asymmetric Si-O-Si stretching vibrations, symmetric Si-O-Si stretching vibration, C-H symmetric deformation of Si-CH₂, together with the Si-O-C stretching vibration located at 1095-1086, 830, 1250 and 1221 cm⁻¹, respectively, were strongly increased with increasing MPCH contents. This explicitly indicates the formation of MPCH structural units in the WAC hybrid adhesives.

Table 6.2 The most characteristic FTIR bands of the WAC hybrid adhesives

Wavenumber (cm ⁻¹)	Assignment
3440	st O-H
2960-2850	st C-H
1730	st C=O
1450	δ CH ₂
1380	st (sym) COO
1250	δ Si-CH ₂
1221	st Si-O-C
1240, 1160, 1128	st (asym) C-O-C
1095, 1086	st (asym) Si-O-Si
1030	st C-O
830	st (sym) Si-O-Si
770-700	δ O-C=O

st: stretching, δ : bending, sym: symmetric, asym: asymmetric

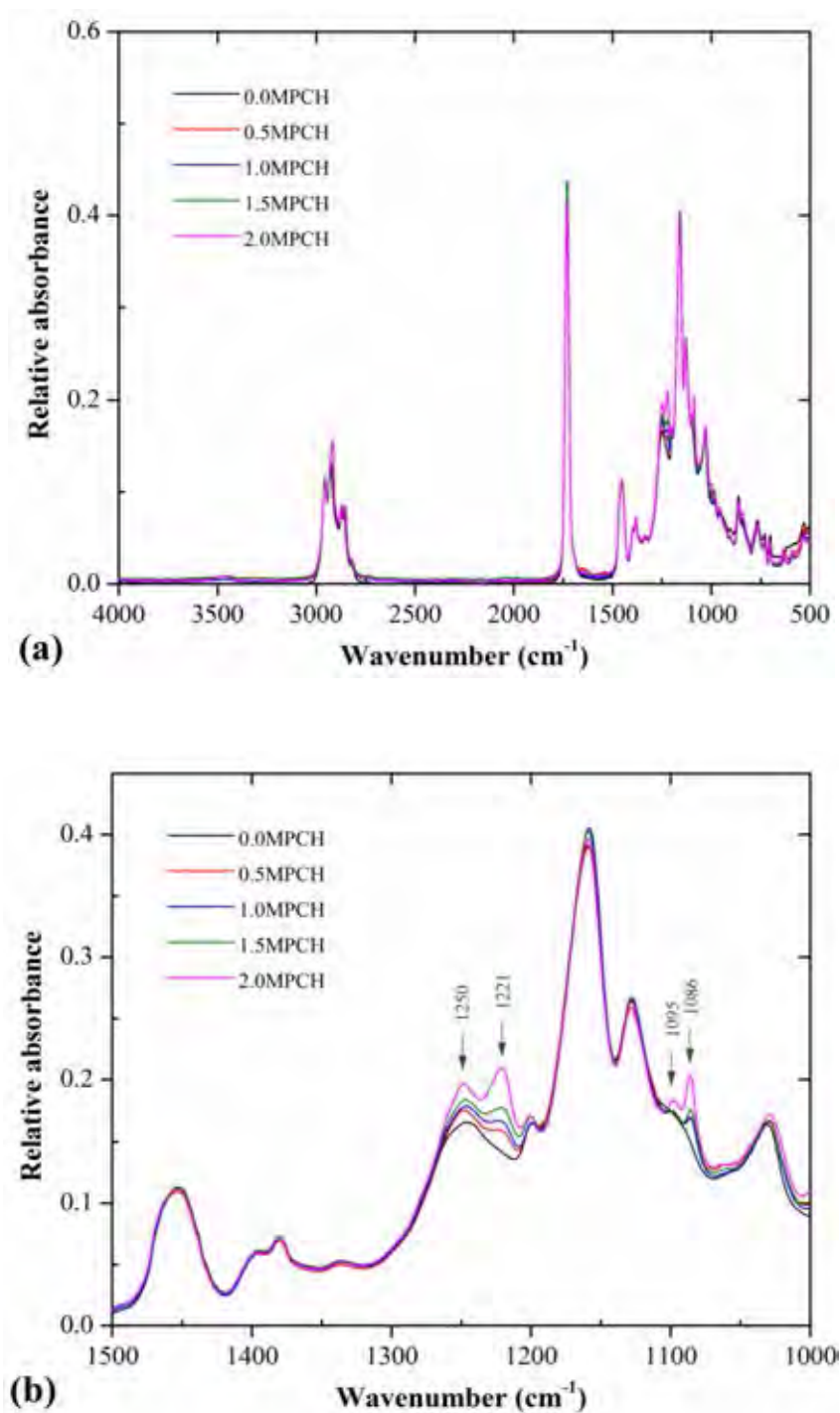


Figure 6.6 (a) full range (b) enlarged wavenumber range of 1000-1500 cm^{-1} FTIR spectra of the WAC hybrid adhesives with different MPCH contents.

The representative DSC thermograms of WAC hybrid adhesives are obviously shown in Figure 6.7. During heating, single low centered T_g was obtained,

consistent with an exothermic process. The T_g values of the WAC hybrid adhesives were affected by the MPCH content as well as its coupling agents (Mahkam and Vakhshouri, 2010). With the addition of MPCH filler, the T_g values were gradually shifted to a higher temperature range from $-49.5\text{ }^\circ\text{C}$ to $-44.0\text{ }^\circ\text{C}$ (Table 6.3). Hence, the reduction in flexibility of their phase in which the MPCH reacted to the polymer chains and its ability to inhibit polymer motion presumably via covalent attachment were achieved, resulting in the enhanced T_g .

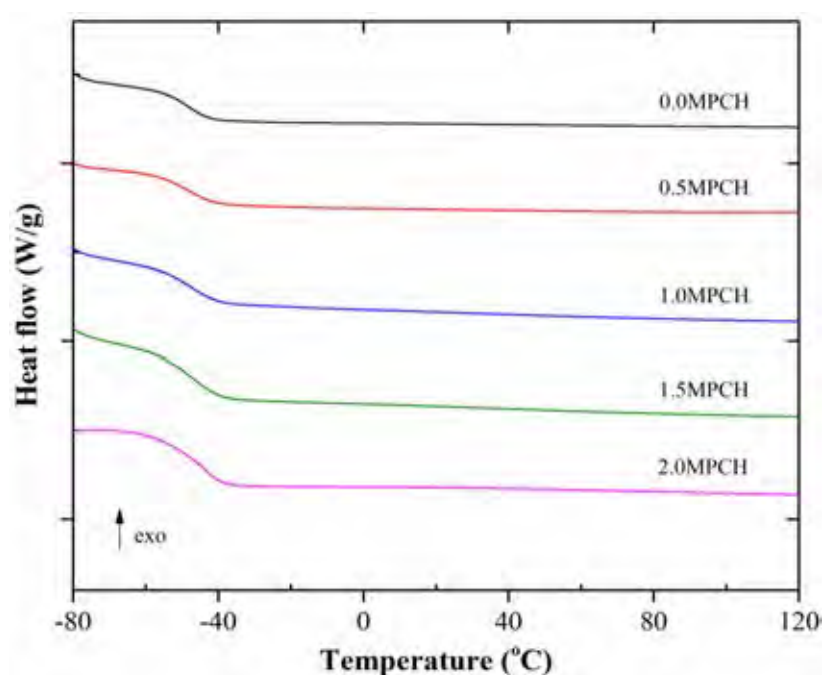


Figure 6.7 DSC thermograms of the WAC hybrid adhesives with different MPCH contents. Thermograms shown are taken from the second heating scan.

The thermal stability of WAC hybrid adhesives was then evaluated by thermogravimetric (TG) analysis, where the weight loss and weight derivative are exhibited as a function of the temperature. When increasing the temperature, one degradation stage appeared in the range of $360\text{--}430\text{ }^\circ\text{C}$ (Figure 6.8a), which was attributed to the complex procedure of depolymerization and decomposition. The neat WAC adhesive was thermally stable with a weight loss up to $360\text{ }^\circ\text{C}$, and then thermal degradation rapidly occurred at an onset temperature of $366.7\text{ }^\circ\text{C}$, which is

typical of acrylic polymers ((De la Fuente *et al.*, 2001; Campos *et al.*, 2014). The TG and derivative thermogravimetric (DTG) curves were considerably shifted to higher temperature range with increasing MPCH content up to 1.5 wt% where the maximum degradation temperature was about 52.5 °C higher than that of neat WAC adhesive (Figure 6.8b). Therefore, the WAC hybrid adhesives had a higher thermal stability and slower decomposition rate when incorporating the MPCH moiety due to the greater bonding energy of the Si-O bond compared to the C-C and C-O bonds (Sun *et al.*, 2011). Conversely, the decomposition temperature was significantly decreased when increasing the MPCH loading to 2 wt%, because the aggregation of excess MPCH particles led to phase separation between the reinforcing filler and matrix, resulting in a lower thermal stability.

Table 6.3 The glass transition temperature (T_g), decomposition temperature (T_d), activation energy (E_a) and residue of the WAC hybrid adhesives

WAC hybrid adhesives	T_g (°C)	$T_{d,onset}$ (°C)	$T_{d,max}$ (°C)	E_a (kJ/mol)	Residue (%)
0.0MPCH	-49.5	366.7	374.3	136.4	0.949
0.5MPCH	-48.8	401.5	417.9	175.0	1.766
1.0MPCH	-46.7	403.8	420.6	170.4	2.416
1.5MPCH	-46.4	416.4	426.8	195.0	5.878
2.0MPCH	-44.0	369.1	394.6	144.9	10.821

$T_{d,onset}$ is the thermal degradation onset temperature, $T_{d,max}$ is the thermal degradation maximum temperature and E_a is the apparent activation energy for each polymer.

Additionally, the activation energies (E_a) for thermal decomposition of the WAC hybrid adhesives were investigated through the modulated TGA analyses using the Hotowitz and Metzger (1963) equation, as shown in Eq. (6.4), where the activation energy was calculated from the slope (E_a/RT_{max}^2) of plot of $\ln[\ln(W_0/W_T)]$

versus θ for the main stage of the thermal degradation (assuming that the order of reaction is the unit) as depicted in Figure 6.9. The results are listed in Table 6.3.

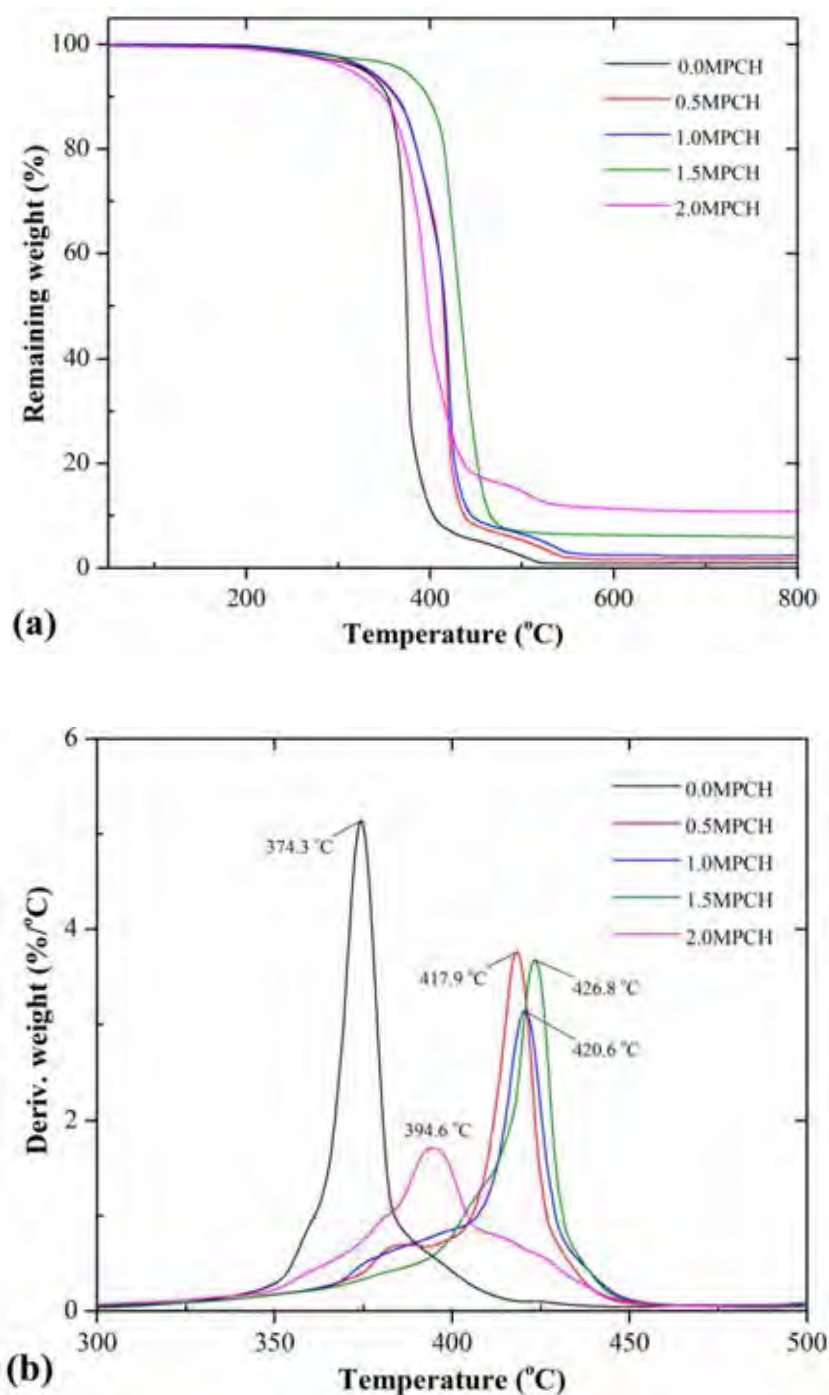


Figure 6.8 (a) TG (b) DTG thermograms of WAC hybrid adhesives with different MPCH contents.

$$\ln \left[\ln \left(\frac{W_0}{W_T} \right) \right] = \frac{E_a \theta}{RT_{max}^2} \quad (6.4)$$

where E_a is the apparent activation energy, W_0 is the initial weight of polymer, W_T is the residual weight of polymer at temperature T , θ is $T - T_{max}$ and R is the gas constant ($8.314 \text{ J mol}^{-1} \text{ K}^{-1}$).

As expected, the activation energy of the neat WAC adhesive (136.4 kJ/mol) was much lower than that of WAC hybrid adhesives. Increasing the MPCH loading levels up to 1.5 wt% increased the activation energy up to 195.0 kJ/mol. So, the hybrid adhesives required a greater maximum energy in order to destroy their chemical bonding, affirming TG and DTG result. This indicates that the introduction of MPCH into the acrylic adhesive structure gave good thermal properties.

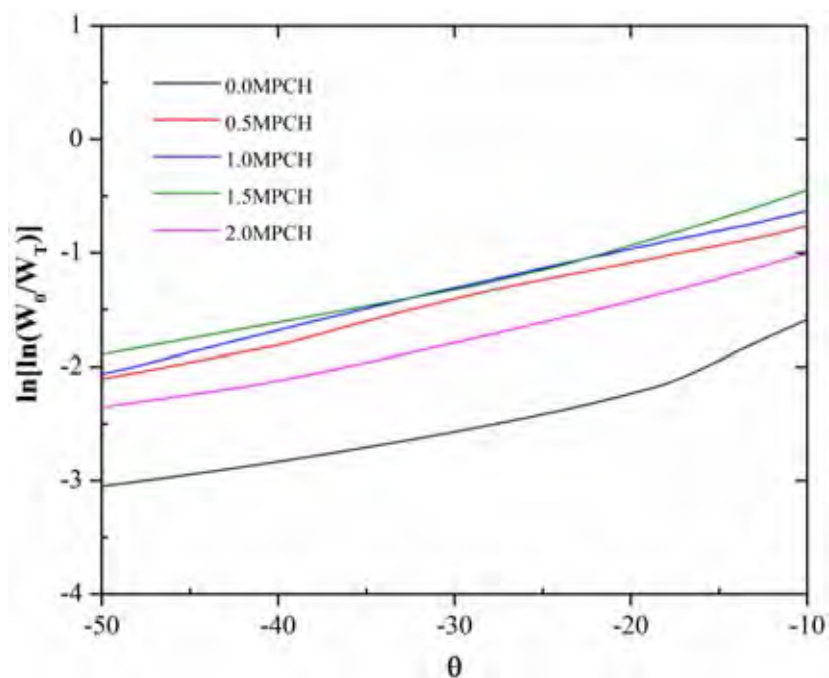


Figure 6.9 Plot of $\ln[\ln(W_0/W_T)]$ versus θ for thermal degradation of WAC hybrid adhesives under a N_2 atmosphere at a heating rate of $10 \text{ }^\circ\text{C/min}$.

6.4.3 Adhesion Properties

The 180° peel strength measurement, defined as the average load at plateau, is a reliable method for studying the adhesion property of OPP/WAC hybrid adhesives/paper joints with good reproducibility and sensitivity. The effect of the MPCH concentration on the adhesion properties of WAC hybrid adhesives is shown in Fig. 8. Unmodified WAC adhesive generally had an undesirable cohesive failure in its bulk layer due to the lack of cohesive (internal) strength. Both the cohesive and adhesive strengths could be improved by reinforcing the interfacial bond strength. With increasing MPCH contents, the 180° peel strength value was initially increased up to 140.2 N/m at 1.5 wt% MPCH, but then sharply decreased. An excess of MPCH reduced flexibility and, as a consequence, the adhesion performance (decreased peel strength). The peel strength of the commercial adhesive is 126.6 N/m, which was lower than that of the synthesized WAC hybrid adhesive.

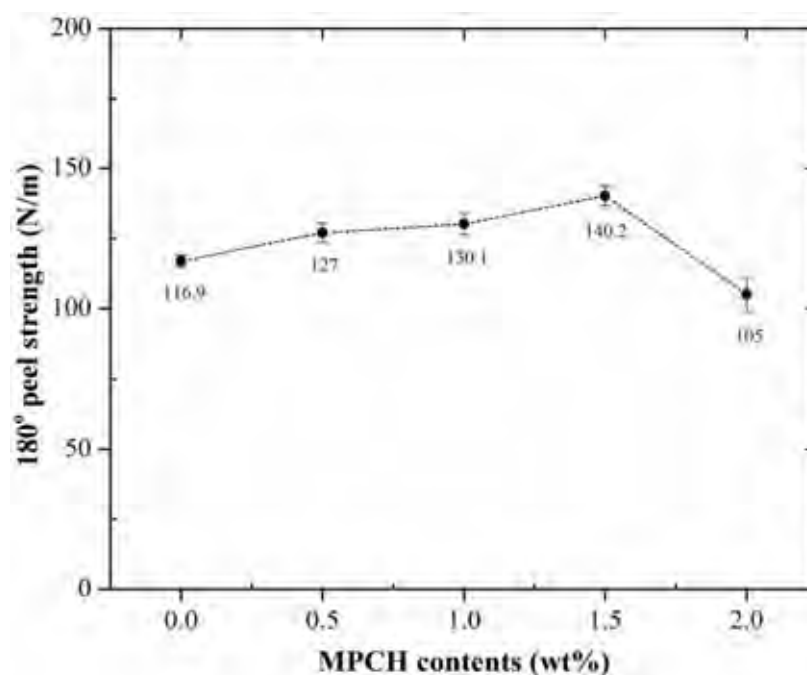


Figure 6.10 Average 180° peel strength of the WAC hybrid adhesives with different MPCH contents. Data are shown as the average derived from ten measurements.

The non-monotonic trend in adhesion and thermal properties was due to the kinetics of polymerization. The observed kinetic behavior of the emulsion polymerization process can be roughly divided into three intervals of (I) particle nucleation, (II) monomer transfer and (III) constant size and number of particles (Mirzataheri *et al.*, 2011). However, the addition of MPCH into the system has a slight retarding effect on the polymerization rate and fractional conversion. It was found that the particle morphology depended on the ability of MPCH to disperse and chemically bond throughout the polymer particles. The use of small amounts of acrylic acid as an auxiliary monomer promoted MPCH adhesion and dispersion onto the polymer surface during the batch emulsion polymerization process of the overall hydrophobic monomers. When the reactions were strictly under kinetic control, where the higher amounts of MPCH were unable to disperse during emulsion polymerization, the aggregation was observed. Thus, a reduction in the peel strength and thermal properties was exhibited at 2 wt% MPCH.

6.5 Conclusion

A series of WAC hybrid laminating adhesives were successfully synthesized using the batch emulsion polymerization based on organic/inorganic structures. This approach added in a systematic way to the knowledge skill set needed for waterborne adhesives to fully replace the presently used solventborne systems. PCHs with an extremely high specific surface area ($415.8 \text{ m}^2/\text{g}$) were modified with TSPM through a simple sol-gel process. The resultant MPCH, functionalized either in the pores or on the surfaces of the PCH, was then confirmed by the FTIR. The replacement of slit-shaped cavities of PCH host material with TSPM led to the non-porous MPCH (S_{BET} of $4.3 \text{ m}^2/\text{g}$). The WAC hybrid adhesives containing MPCH offered excellent thermal properties (low T_g values and high degradation temperature) in all samples due to the increased internal strength via the covalent attachment between acrylic matrix and MPCH. The optimal formulation was found to be with 1.5 wt.% MPCH, giving a laminated joint 180° peel strength of 140.2 N/m . This WAC hybrid based adhesive system has the possibility of replacing solventborne technology for use in the flexible packaging industry.

6.6 Acknowledgement

This research was financially supported by Research and Researchers for Industries (RRI), the Thailand Research Fund (TRF) Grant number PHD56I0019. Additionally, the authors are thankful for the utilization of the experimental facilities at College of Polymer Science and Polymer Engineering National Polymer Innovation Center, The University of Akron and the certificated proofreader, Dr. Robert Butcher, at the Publication Counseling Unit, the Department of Science, Chulalongkorn University.

6.7 References

- Araújo, P.H.H., Abad, C., de la Cal, J.C., Pinto, J.C. and Asua J.M. (1999) Emulsion polymerization in a loop reactor: effect of the operation conditions. Polymer Reaction Engineering, 7, 303-326.
- Arevalillo, A., do Amaral, M. and Asua, J.M. (2006) Rheology of concentrated polymeric dispersions. Industrial & Engineering Chemistry Research, 45, 3280.
- Barrett, E.P., Joyner, L.G. and Halenda, P.P. (1951) The determination of pore volume and area distributions in porous substances. I. computations from nitrogen isotherms. Journal of the American Chemical Society, 73(1), 373-380.
- Bonnefond, A., Mičušík, M., Paulis, M., Leiza, J.R, Teixeira, R.F.A. and Bon, S.A.F. (2013) Morphology and properties of waterborne adhesives made from hybrid polyacrylic/montmorillonite clay colloidal dispersions showing improved tack and shear resistance. Colloid and Polymer Science, 291, 167.
- Brunauer, S., Deming, L.S., Deming, W.E. and Teller, E. (1940) On a theory of the van der Waals adsorption of gases. Journal of the American Chemical Society, 62(7), 1723-1732.
- Brunauer, S., Emmett, P.H. and Teller, E. (1938) Adsorption of gases in multimolecular layers. Journal of the American Chemical Society, 60, 309-319.

- Bunnak, N., Ummartyotin, S., Laoratanakul, P., Bhalla, A.S. and Manuspiya H. (2013) Synthesis and characterization of magnetic porous clay heterostructure. Journal of Porous Materials, 21, 1-8.
- Campos, C.H., Urbano, B.F. and Rivas, B.L. (2014) Synthesis and characterization of organic-inorganic hybrid composites from poly(acrylic acid)-[3-(trimethoxysilyl)propyl methacrylate]-Al₂O₃. Composites Part B: Engineering, 57, 1-7.
- Chang, C.C., Oyang, T.Y., Chen, Y.C., Hwang, F.H. and Cheng L.P. (2014) Preparation of hydrophobic nanosilica-filled polyacrylate hard coatings on plastic substrates. Journal of Coatings Technology and Research, 11, 381-386.
- Diaconu, G., Paulis, M. and Leiza J.R. (2008) Towards the synthesis of high solids content waterborne poly(methyl methacrylate-co-butyl acrylate)/montmorillonite nanocomposites. Polymer, 49, 2444-2454.
- De la Fuente, J.L., Fernández-García, M. and Madruga E.L. (2001) Characterization and thermal properties of poly(*n*-butyl acrylate-*g*-styrene) graft copolymers. Journal of Applied Polymer Science, 80, 783-789.
- Ebnesajjad, S., editor. (2009) Adhesive technology handbook. New York: William Andrew Inc.
- Feldgitscher, C., Peterlik, H., Ivanovici, S., Puchberger, M. and Kickelbick G. (2009) Crosslinked hybrid polymer matrices with nanostructure directing abilities for lanthanum hydroxide growth. Chemical Communications, 37, 5564-5566.
- Foster, A.B., Lovell, P.A. and Rabjohns, M.A. (2009) Control of adhesive properties through structured particle design of water-borne pressure-sensitive adhesives. Polymer, 50, 1654-1670.
- Gumfekar, S.P., Kunte, K.J., Ramjee, L., Kate, K.H. and Sonawane, S.H. (2011) Synthesis of CaCO₃-P(MMA-BA) nanocomposite and its application in water based alkyd emulsion coating. Progress in Organic Coatings, 72, 632-637.
- Guo, Y., Wang, M., Zhang, H., Liu, G., Zhang, L. and Qu, X. (2008) The surface modification of nanosilica, preparation of nanosilica/acrylic core-shell

- composite latex, and its application in toughening PVC matrix. Journal of Applied Polymer Science, 107, 2671-2680.
- Hair, M.L. (1967) Infrared Spectroscopy in Surface Chemistry. New York: Marcel Dekker Inc.
- Horowitz, H.H. and Metzger G. (1963) A new analysis of thermogravimetric traces. Analytical Chemistry, 35, 1464-1468.
- Huang, S., Fan, D., Lei, Y. and Huang, H. (2004) Alkoxysilane-functionalized acrylic copolymer latexes. I. particle size, morphology, and film-forming properties. Journal of Applied Polymer Science, 94, 954-960.
- Kajtna, J., Šebenik, U. and Krajnc, M. (2014) Synthesis and dynamic mechanical analysis of nanocomposite UV crosslinkable 100% solid acrylic pressure sensitive adhesives. International Journal of Adhesion and Adhesives, 49, 18.
- Kango, S., Kalia, S., Celli, A., Njuguna, J., Habibi, Y. and Kumar R. (2013) Surface modification of inorganic nanoparticles for development of organic-inorganic nanocomposites-a review. Progress in Polymer Science, 38, 1232-1261.
- Landfester K. (2003) Polymer dispersions and their industrial applications. Macromolecular Chemistry and Physics, 204, 542.
- Lin, D.J., Don, T.M., Chen, C.C., Lin, B.Y., Lee, C.K. and Cheng L.P. (2008) Preparation of a nanosilica-modified negative-type acrylate photoresist. Journal of Applied Polymer Science, 107, 1179-1188.
- Lin, W.C., Yang, C.H., Wang, T.L., Shieh, Y.T. and Chen W.J. (2012) Hybrid thin films derived from UV-curable acrylate-modified waterborne polyurethane and monodispersed colloidal silica. Express Polymer Letter, 6, 2-13.
- Mahkam, M. and Vakhshouri L. (2010) Colon-specific drug delivery behavior of pH-responsive PMAA/perlite composite. International Journal of Molecular Sciences, 11, 1546-1556.
- Mičušík, M., Bonnefond, A., Paulis, M. and Leiza, J.R. (2012) Synthesis of waterborne acrylic/clay nanocomposites by controlled surface initiation from macroinitiator modified montmorillonite. European Polymer Journal, 48, 896-905.

- Mirzataheri, M., Mahdavian, A.R. and Atai, M. (2011) Kinetic studies of the preparation of nanocomposites based on encapsulated Cloisite 30B in poly(styrene-co-)butyl acrylate([via mini-emulsion polymerization. Polymer Intertional, 60, 613.
- Oh, J.K., Park, C.H., Lee, S.W., Park, J.W. and Kim, H.J. (2013) Adhesion performance of PSA-clay nano-composites by the in-situ polymerization and mechanical blending. International Journal of Adhesion and Adhesives, 47, 13.
- Packham, D.E. (1992) Handbook of Adhesion. Harlow: Longman Scientific & Technical.
- Romo-Urbe, A., Arcos-Casarrubias, J.A., Hernandez-Vargas, M.L., Reyes-Mayer, A., Aguilar-Franco, M. and Bagdhachi, J. (2016) Acrylate hybrid nanocomposite coatings based on SiO₂ nanoparticles by *in-situ* batch emulsion polymerization. Progress in Organic Coatings, 97, 288-300.
- Rong, M.Z., Ji, Q.L., Zhang, M.Q. and Friedrich, K. (2002) Graft polymerization of vinyl monomers onto nanosized alumina particles. European Polymer Journal, 38, 1573-1582.
- Sanchez, C., Julián, B., Belleville, P. and Popall M. (2005) Applications of hybrid organic-inorganic nanocomposites. Journal of Materials Chemistry, 15, 3559-3952.
- Sing, K.S.W., Everett, D.H., Haul, R.A.W., Moscou, L., Pierotti, R.A., Rouquérol, J. and Siemieniewska, T. (1985) Reporting physisorption data for gas/solid systems with special reference to the determination of surface area and porosity. Pure and Applied Chemistry, 57(4), 603-619.
- Solhi, L., Atai, M., Nodehi, A., Imani, M., Ghaemi, A. and Khosravi, K. (2012) Poly(acrylic acid) grafted montmorillonite as novel fillers for dental adhesives: synthesis, characterization and properties of the adhesive. Dental Materials, 28, 369-377.
- Sun, D., Miao, X., Zhang, K., Kim, H. and Yuan Y. (2011) Triazole-forming waterborne polyurethane composites fabricated with silane coupling agent functionalized nano-silica. Journal of Colloid and Interface Science, 361, 483-490.

- US Environmental Protection Agency (EPA) (2015) The 2011 National Emissions Inventory, version 2 Technical Support Document. Available at: https://www.epa.gov/sites/production/files/2015-10/documents/nei2011v2_tsd_14aug2015.pdf (accessed 20 January 2017)
- Vega-Baudrit, J., Navarro-Bañón, V., Vázquez, P. and Martín-Martínez, J.M. (2006) Addition of nanosilicas with different silanol content to thermoplastic polyurethane adhesives. International Journal of Adhesion and Adhesives, 26, 378-387.
- Wenfang, L., Zhaoxia, G. and Jian, Y. (2005) Preparation of crosslinked composite nanoparticles. Journal of Applied Polymer Science, 97, 1538-1544.
- Xiang, B. and Zhang, J. (2016) Using ultrasound-assisted dispersion and in situ emulsion polymerization to synthesize TiO₂/ASA (acrylonitrile-styrene-acrylate) nanocomposites. Composites Part B: Engineering, 99, 196-202.
- Xu, X., Jagota, A., and Hui C.Y. (2014) Effects of surface tension on the adhesive contact of a rigid sphere to a compliant substrate. Soft Matter, 10, 4625-4632.

CHAPTER VII
CORE-SHELL COPOLYACRYLATE NANOPARTICLES:
SYNTHESIS AND APPLICATIONS IN ECO-FRIENDLY
LAMINATING ADHESIVES

7.1 Abstract

Waterborne core-shell (CS) laminating adhesives were formulated by the two-stage seeded-semibatch emulsion polymerization and thereby reduced volatile organic compound emissions. In this study, the first-stage rigid core polymer was poly(styrene-co-ethylhexyl acrylate) having a glass transition temperature (T_g) of -14.9 °C, while the second-stage soft shell polymer was copolyacrylate (2-ethylhexyl acrylate (EHA), ethylene glycol methyl ether acrylate (EGMA), 2-(hydroxyethyl) methacrylate (HEMA), styrene and acrylic acid) having the T_g ranging from -18.4 °C to -32.0 °C, depending on variables. Their morphology-property relationships were studied by varying a core-to-shell ratio and EGMA concentration in the shell. An increment in soft segments within CS latex particles exhibited low T_g and good film-forming ability, whereas poor adhesion to substrates was obtained. Thus, the optimal adhesive efficiency, in terms of 180° peel strength of bonded joints, of 214.5 N/m was accomplished by core-to-shell ratio of 0.5 and 10 wt% of EGMA concentration in its shell.

Keywords: Core-shell morphology, Laminating adhesives, 180° Peel strength

7.2 Introduction

The restriction in volatile organic compounds (VOCs) emissions from the solvent-borne latexes is urgently in demand for environmental and health protection, which is a driving force to intensively develop the waterborne products (Lichman, 1990; U.S. Environmental Protection Agency, 2014). Waterborne acrylic laminating adhesives have been emerged in the flexible packaging industries with an excellent

durability, toughness, anti-oxidant, chemical resistance, oil tolerance and optical clarity (Ebnesajjad, 2009; Romo-Urbe *et al.*, 2016). However, they have faced with a catastrophic failure of bonded joints due to the inferior mechanical and adhesion properties (Schumacher, 2016). Specifically-designed core-shell (CS) copolyacrylate laminating adhesives are now evaluated to overcome these drawbacks.

The CS latex particles are a heterogeneous molecular structure consisting of at least two different polymeric domains: one locate at the center and is encapsulated by another one (Chaudhuri and Paria, 2012; Ramli *et al.*, 2013), where the monomer composition is an important factor affecting the morphologically-controlled particles. In general, the hydrophilic monomers are always in contact with the water phase, whereas the hydrophobic monomers easily penetrate into the latex particles during the emulsion polymerization process (Ma *et al.*, 2013), facilitating the formation of gradient-like (Zhang *et al.*, 2012), sandwich-like, snowman-like (hemisphere) (Hu *et al.*, 2009), raspberry-like (Chenal *et al.*, 2014; Fan *et al.*, 2015) and reverse CS particle (Chai and Tan, 2008; Bukowska *et al.*, 2017). In case of the laminating adhesive, the standard CS particles, a rigid core surrounded by a soft shell, are preferable to simultaneously achieve high cohesive strength and good adhesion to substrates. In 2010, Mishra *et al.* prepared the laminating adhesives using butyl acrylate/methyl methacrylate/glycidyl methacrylate. Thus, the adhesion properties on polyester/polyethylene joints were improved due to a crosslinking reaction of epoxy groups, resulting in T-peel strength of 162.2 N/m. Zhou *et al.* (2011) investigated the adhesiveness and heat resistance properties of vinyl acetate/acrylate CS latexes on corona-treated polyethylene films. The peel strength of 196.1 N/m and high heat resistance properties at 60 °C were obtained. However, vinyl acetate is classified as an extremely hazardous substance in the United States (USA) from Emergency Planning and Community Right-to-Know Act.

Herein, the waterborne CS laminating adhesives were designed to meet demands for eco-friendly latexes and to yield latexes without sacrificing mechanical, thermal and adhesion properties. They were synthesized by a two-stage seeded semi-batch emulsion polymerization so as to control the polymerization rate, particle size and molecular weight (Nomura *et al.*, 2005; Chern, 2008). The CS particles differing in glass transition temperature (T_g), in which the soft shell consisting of polyacrylate:

2-ethylhexyl acrylate (EHA), ethylene glycol methyl ether acrylate (EGMA), 2-(hydroxyethyl) methacrylate (HEMA), styrene and acrylic acid was polymerized in the presence of the rigid poly(styrene-co-ethylhexyl acrylate) core, were fabricated by a starved feeding mode. The high T_g core ensures the good cohesive strength, while the low T_g shell exhibits high flexibility, a good film formation, low minimum film forming temperature (MFFT) and good adhesion to laminated substrates. The morphology-property relationships were investigated and optimized by varying the core-to-shell ratio and EGMA concentration in the shell. A series of the waterborne CS laminating adhesives were characterized through gel permeation chromatography (GPC), Brookfield viscosity, dynamic light scattering (DLS), nuclear magnetic resonance (NMR), transmission electron microscopy (TEM), contact angle, DuNoüy surface tension and differential scanning calorimetry (DSC). Additionally, adhesion performance, in terms of 180° peel strength of bonded joints, was evaluated for an untreated oriented polypropylene (OPP) lamination.

7.3 Experimental

7.3.1 Materials

Monomers, including EHA, EGMA, HEMA, styrene and acrylic acid, were purchased from Sigma Aldrich, St. Louis, MO, US and purified using an inhibitor removal resin (Alfa Aesar, Tewksbury, MA, US) to remove contaminants. Sodium dodecyl sulfate (SDS) and TritonTM X-100 used as surfactants, sodium bicarbonate (NaHCO_3) used as a buffer, and ammonium persulfate (APS) used as an initiator were purchased from Sigma Aldrich, St. Louis, MO, US.

7.3.2 Laminating Adhesive Preparation

The CS laminating adhesives were synthesized using the two-stage seeded-semibatch emulsion polymerization under a nitrogen (N_2) protection, which were performed in a 1000 mL OptimaxTM 1001 working station (Mettler Toledo, Columbus, OH, US) equipped with a mechanical agitator at 300 rpm, a thermocouple for controlling a reaction temperature at 75 °C, a reflux condenser at 15 °C and two

feeding inlets for pre-emulsion and initiator solution, respectively. Peristaltic pumps were used to control an even feeding rate. The adhesives are referred to hereafter as CSxEy, where x is the core-to-shell ratio, E is the EGMA and y is the wt% of EGMA.

7.3.2.1 Preparation of Seed Latex

Poly(styrene-co-ethylhexyl acrylate) seed latex was prepared using a batchwise emulsion polymerization. The pre-emulsion including monomers (21.79 wt% of EHA and 18.21 wt% of styrene), 0.17 M SDS and 0.02 g NaHCO₃ was prepared. A mixture of 0.05 M SDS and 0.33 g NaHCO₃ was initially charged to the Optimax™ reactor, followed by a dropwise addition of the pre-emulsion and 0.1 M APS solution at a feeding rate of 0.75 and 0.22 mL/min, respectively. After complete feeding, the reaction was held for 4 h to ensure maximal conversion. The synthesized seed latex was obtained with 40 wt% solid content which is identical to the theoretical design value (according to ISO124:1997).

7.3.2.2 Preparation of Core Latex

10 wt% seed latex was initially charged to the Optimax™ reactor, followed by the dropwise addition of pre-emulsion and 0.05 M APS solution at a feeding rate of 1.0 and 0.5 mL/min, respectively. The pre-emulsion was prepared by a homogeneous dissolution of monomers (28.5 wt% of EHA and 17.5 wt% of styrene), 0.28 M SDS, 0.16 g Triton™ X-100 and 0.35 g NaHCO₃. After complete feeding, the reaction was held for 4 h to ensure maximal conversion. The core latex was then obtained with 50 wt% solid content which is identical to the theoretical design value.

7.3.2.3 Preparation of CS Latexes

The CS polymerization recipes with variables of the core-to-shell ratio and EGMA concentration in the shell were summarized in Table 7.1. The core latex was initially charged to the Optimax™ reactor, followed by the dropwise addition of a shell pre-emulsion and APS solution at a feeding rate of 0.75 and 0.2 mL/min, respectively. Each of shell pre-emulsions was prepared by dissolving surfactants, buffer and monomers (EHA, EGMA, HEMA styrene, and acrylic acid) in deionized water. After complete feeding, the reaction was held for 4 h to ensure maximal conversion. The CS laminating adhesives were obtained with 50 wt% solid

content which is identical to the theoretical design value and their conversions were approximately 99% (no residual monomer at the end of polymerization process). The pH was regulated to 7.0 using monoethanolamine.

7.3.3 Film Preparation

The adhesive films were produced by casting 20 g of latexes on a polytetrafluoroethylene (PTFE) surface and allowed the remaining trapped water to evaporate at 60 °C for 24 h under a vacuum. The obtained films (typically of 0.5 mm thickness) were then stored in a vacuum desiccator at ambient temperature prior to characterization.

7.3.4 Characterization Techniques

7.3.4.1 *Brookfield Viscosity Measurement*

The Brookfield viscometer (DV-II+ Pro) with LV-25 spindle, Brookfield engineering laboratories Inc., Middleboro, MA, US, was used at the test temperature of 25 °C and the speed of 100 rpm.

7.3.4.2 *Particle Size Analysis by DLS*

The hydrodynamic diameter (DH) of the CS latex particles was determined by DLS using a NanoBrook ZetaPALS Potential Analyzer at 90° scattering angle (Brookhaven Instruments Co., Holtsville, NY, US). The latexes were diluted to 0.05 wt% in an aqueous solution of SDS and NaHCO₃.

7.3.4.3 *Molecular Weight Analysis by GPC*

The number-average molecular weight (M_n), weight-average molecular weight (M_w) and polydispersity index (M_w/M_n) were measured using a high-performance GPC (EcoSEC HLC-8320GPC) from Tosoh Corporation, Tokyo, Japan with RI detector. Tetrahydrofuran (THF, HPLC grade) purchased from RCI Labscan Co., Ltd. was used as a solvent. The dried CS adhesive films were dissolved in THF for 24 h, and then filtered through a 0.45 μm PTFE syringe filter prior to characterization. The results were evaluated using polystyrene standard.

7.3.4.4 *DuNouy Surface Tension*

Measurement of the surface tension was performed using a DuNouy tensiometer from CSC scientific Co., Inc., Fairfax, VA, US and is reported in the CGS unit of dyne/cm.

7.3.4.5 *Contact Angle Measurement*

The contact angle (θ) of the CS latexes was measured by Krüss drop shape analysis DSA 10 Mkz model (Krüss GmbH, Matthews, NC, US), which is a quantitative measurement of wettability using a syringe to pump the latexes steadily into the sessile drop on a substrate surface.

7.3.4.6 *Latex Morphology by TEM Analysis*

Latex microstructure was observed by TEM using a Hitachi-S4800 microscope from Hitachi Asia (Thailand) Co., Ltd operated at an accelerating voltage of 100 kV. The latexes were dialyzed to remove surfactant and buffer molecules, then diluted to 0.1 wt% solid content in DIW and deposited a drop of the diluted latex on a carbon-coated grid. Preferential staining with ruthenium tetroxide (RuO_4) was used to distinguish soft and hard phases before TEM examination.

7.3.4.7 *T_g Analysis by DSC*

The T_g was characterized through DSC using a model Q2000 instrument (TA instruments, New Castle, DE, US). The inflection point of the second heating scan was measured in a temperature range between -80 °C to 120 °C at a heating rate of 20 °C/min. The temperature program was designed for a heat-cool-heat system under a N_2 purge rate of 50 mL/min to eliminate a thermal history. An approximately 5 mg of each sample was loaded in a hermetic aluminium crucible of 40 μL .

7.3.4.8 *Measurement of the 180° peel strength*

The adhesion property of the CS laminating adhesives was investigated in terms of 180° peel strength in tension testing mode according to ASTM D1876 using a Tensiometer-Instron 5567 instrument (Instron Co., Norwood, MA, US) equipped with a 100 N static load cell, a crosshead speed of 150 mm/min and a gauge length of 50 mm. Laminated test panels consisted of two rectangular-shaped adherends, paper and untreated OPP film, were properly prepared and then

bonded together in accordance with the CS laminating adhesives. Specially prepared specimens 25 mm (1 in.) wide by 305 mm (12 in.) long, but bonded only over approximately 241 mm (9 in.) of their length. The CS laminating adhesive was applied on paper using a BYK drawdown bar with an average coating thickness of 24 μm and suddenly adhered to untreated OPP. The OPP/CS laminating adhesive/paper laminated joints were post-cured at 60 °C. The 76 mm (3 in.) long unbounded ends bent apart, perpendicular to the glue line, for clamping in the grips of the testing machine. An autographic curve of peeling was calculated as the average peeling load in N/m of the specimen width required to separate the adherends.

7.4 Results and Discussion

7.4.1 Characteristics of CS Laminating Adhesives

The CS laminating adhesives were successfully formulated by the two-stage seeded semi-batch emulsion polymerization process, where the starved feeding of the second-stage monomers took place. Practically, the starved feeding condition (the majority of monomer droplets is consumed by the reaction before more adding) is used to control the particle size and molecular weight together with prevent the formation of secondary nucleation particles in the copolymer shell. The physical properties of the CS laminating adhesives with varying the core-to-shell ratio and EGMA concentration, including Brookfield viscosity, weight-average molecular weight (M_w), z-average particle diameter (D_{Pz}) and polydispersity index (PDI) are summarized in Table 7.2. As expected, the CS latex particles were found within the typical size range from several 10 nm to submicron (Ito *et al.*, 2002) obtained in emulsion polymerization. The D_{Pz} of CS latexes as determined by DLS was larger than that of the core latex (141.3 nm size), suggesting that the second-stage monomers incorporated over the core particles to form the CS structures. With varying the core-to-shell ratio and EGMA concentration, the D_{Pz} results of CS latexes have shown no statistically significant difference (~ 240 nm size with narrow PDI), confirming that the starved feeding condition was achieved. The DLS curve of the CS laminating adhesive was exhibited in Figure 7.1, where the single exponential

decay function for the monomodal particle size distribution was presented to ensure no secondary nucleation during polymerization process (Jovanović and Dubé, 2005). The slight increase of PDI revealed that the particle size distribution was relatively increased due to an interdiffusion of the soft and flexible chains from one particle to its neighbors.

Table 7.2 Physical characteristics of the CS laminating adhesives

CS laminating adhesives	Viscosity (mPa.s)	M_w (g/mol)	D_{Pz} (nm)	PDI
CS2.0E10	76.8	602,407	234.4 ± 2.3	0.07
CS1.0E10	72.0	667,122	238.1 ± 3.2	0.08
CS0.5E10	62.4	709,026	235.4 ± 3.6	0.10
CS0.5E20	61.6	557,002	239.1 ± 2.5	0.13
CS0.5E30	67.2	568,383	242.6 ± 3.9	0.15
CS0.5E40	65.6	587,407	243.8 ± 4.5	0.15
CS0.3E10	57.6	714,172	235.8 ± 2.6	0.17

M_w has a significant influence on the adhesive's mechanical and adhesion properties. The polyurethane and acrylic solventless dispersions normally have a medium M_w of 50,000 and 500,000 g/mol, respectively (Schumacher, 2016), wherein high M_w will increase the bonding strength of adhesives but decrease tack (Zhou *et al.*, 2011). According to the CS laminating adhesives, the M_w of which are very difficult to analyze in detail, as a differentiation between seed, core and shell cannot be made. The results of M_w did not show any definite trend as a function of monomer feed composition due to the starved feeding condition used to can particularly control the rate of polymerization, resulting in homogeneous D_{Pz} and M_w as well.

In fact, the D_{Pz} and M_w of the adhesive latex are viscosities increasing factors. In laminating adhesive applications, the low viscosity profile is required for better spreading and wetting of latexes on the substrates, and led to an obvious phase

separation between the core and shell morphology (Mishra *et al.*, 2010; Schumacher, 2016). The shell forms a continuous phase in the latex film, whereas the core forms a dispersed phase. With decreasing the core-to-shell ratio, the Brookfield viscosity was decreased from 76.8 to 57.6 mPa.s. Meanwhile, the increasing EGMA concentration followed an opposite trend with slightly increasing of viscosity up. It is explicitly that the large shell composition and the high EGMA concentration affect to the copolyacrylate chains, including flexibility and entanglement, as they do not facilitate the chain motion and the flow of the latex. Moreover, the coagulation of latex particles was not occurred after measuring viscosity for several months.

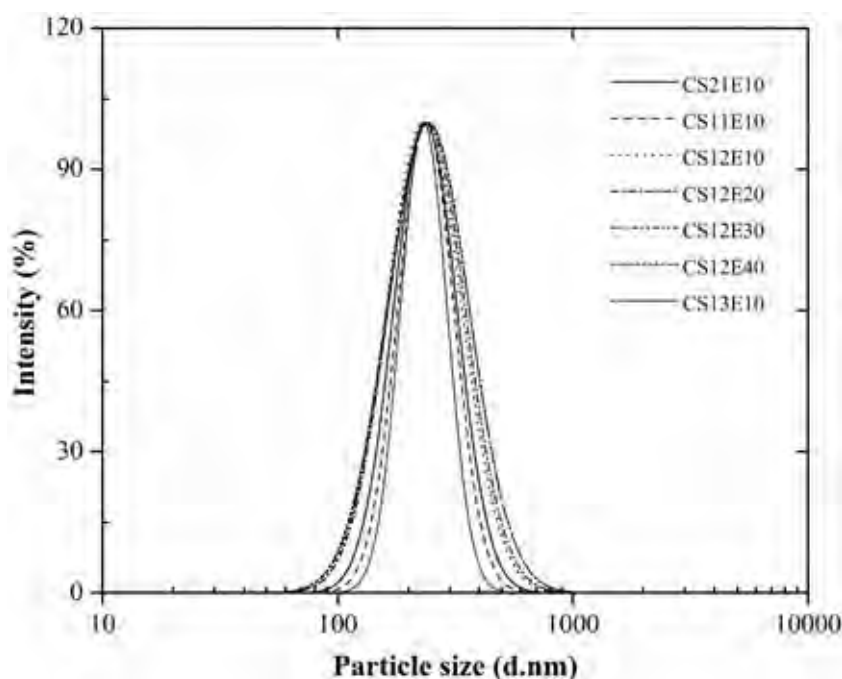


Figure 7.1 The DLS curves of the CS laminating adhesives. The curves shown are representative of those seen from five samples.

7.4.2 Wettability of CS Laminating Adhesives

The concept of the contact angle (θ) and its equilibrium is valuable because it gave a definition to the notion of wettability, which is the ability of CS laminating adhesive to form interfaces with solid surfaces, and indicated the surface parameters needing measurement. The contact angle that is formed between liquid-

solid interfaces; and the surface tension that is formed between liquid-gas interfaces were obviously investigated as indicated in Table 7.3. With decreasing the core-to-shell ratio and increasing EGMA concentration, the smaller contact angle and smaller surface tension were obtained as the tendency for the latexes to spread increases. Thus, the contact angle and surface tension are a useful inverse measure of spreadability or wettability.

Table 7.3 Contact angle and surface tension of the CS laminating adhesives

CS laminating adhesives	Contact angle (degree)	Surface tension (dyne/cm)
CS2.0E10	55.0 ± 2.8	41.1 ± 0.1
CS1.0E10	54.7 ± 2.5	41.6 ± 0.5
CS0.5E10	53.5 ± 0.7	40.4 ± 0.2
CS0.5E20	44.0 ± 2.0	36.5 ± 0.5
CS0.5E30	44.0 ± 2.0	34.0 ± 0.1
CS0.5E40	39.2 ± 0.8	32.6 ± 0.6
CS0.3E10	49.3 ± 4.04	38.8 ± 0.8

7.4.3 T_g of CS Laminating Adhesives

The T_g value is a fundamental polymer property directly corresponded to the adhesive performance. Generally, the cohesive strength increases with increasing T_g, while tackiness decreases with increasing T_g (Tan *et al.*, 2016). The representative DSC thermograms of the CS laminating adhesives with varying the core-to shell ratio and EGMA concentration are indicated in Figure 7.2. During heating, a single low centered T_g was exhibited with a narrow onset/end interval, consistent with an exothermic process. This kind of T_g could be obtained in case of a non-crosslinked core, where the core and shell copolymer compositions were quite similar. After film formation, the coalesced particles were derived a miscible CS morphology. Therefore, the difference between core and shell domains was not detected by DSC measurement. The experimental T_g values were reported in Table

7.4, as comparing with the theoretical T_g values calculated according to the *Flory-Fox equation* (Kalogeras and Brostow, 2009). The theoretical T_g values were higher than that of the experimental values because of the difference in a distribution coefficient of monomers, resulting in the difference in an alignment of polymers during the polymerization process. Additionally, the T_g values of the CS laminating adhesives with decreasing the core-to shell ratio and increasing EGMA concentration were shifted toward lower temperature. It revealed that the soft components, capable of reducing T_g values as plasticizers, were used to separate the copolymer chains, increase a free volume and then facilitate the mobility of the copolymer chains. The easier movement, the lower T_g was represented, relating to an elastic behavior (Bai *et al.*, 2016).

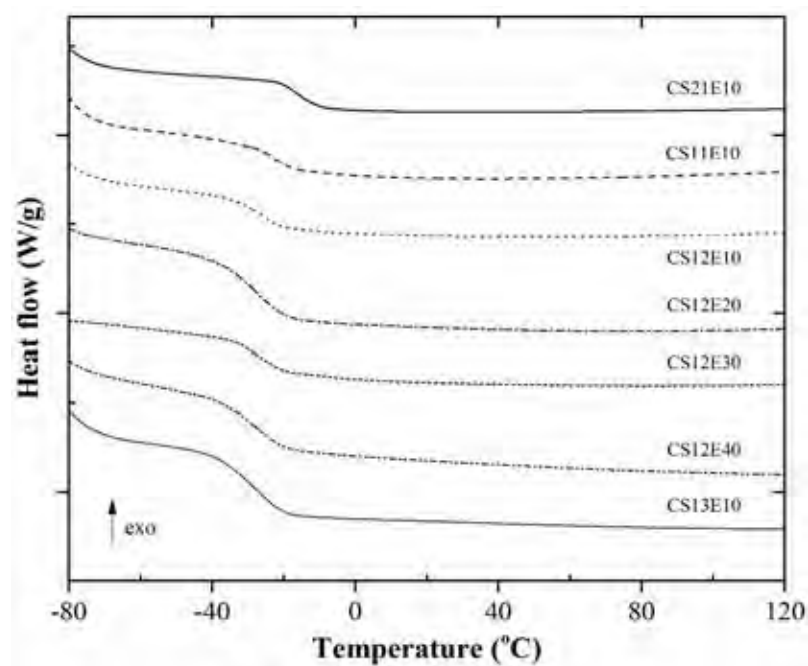


Figure 7.2 DSC thermograms of the CS laminating adhesives. Thermograms shown are taken from the second heating scan.

Table 7.4 Experimental and theoretical T_g of the CS laminating adhesives

CS laminating adhesives	T_g ($^{\circ}\text{C}$)	
	Experimental	Theoretical
Seed	-4.9	0
Core	-15.0	-10.0
CS2.0E10	-18.4	-19.4
CS1.0E10	-23.2	-19.9
CS0.5E10	-25.5	-20.0
CS0.5E20	-27.8	-21.3
CS0.5E30	-30.3	-22.9
CS0.5E40	-32.0	-24.7
CS0.3E10	-27.7	-27.6

7.4.4 Adhesion Property of CS Laminating Adhesives

The bond strength of the CS laminating adhesives on the substrates strongly depends on the cohesive strength and adhesion property, in terms of 180° peel strength measurement. In principle, peel strength is influenced by adhesive thickness, molecular weight, weight fraction of acrylic acid and T_g (Zhou *et al.*, 2011). The low molecular weight and low T_g adhesives could uniformly flow, easily wet on substrates and then exhibits high peel strength, however they suffer with a cohesive failure. Consequently, the CS laminating adhesives were fabricated to overcome this problem using the high T_g core to provide the good cohesive strength together with the low T_g shell to produce the good adhesion to substrates. The 180° peel strength measurements, defined as the average load at plateau, were evaluated for studying the adhesion property of OPP/laminating adhesive/paper joints, as shown in Figure 7.3. With decreasing the core-to-shell ratio as well as the EGMA concentration, the 180° peel strength value was initially increased up to 214.5 N/m at CS0.5E10 (core-to-shell ratio of 1:2 and 10 wt.% EGMA concentration), but then dramatically decreased. As mentioned above, an excess of the soft components could

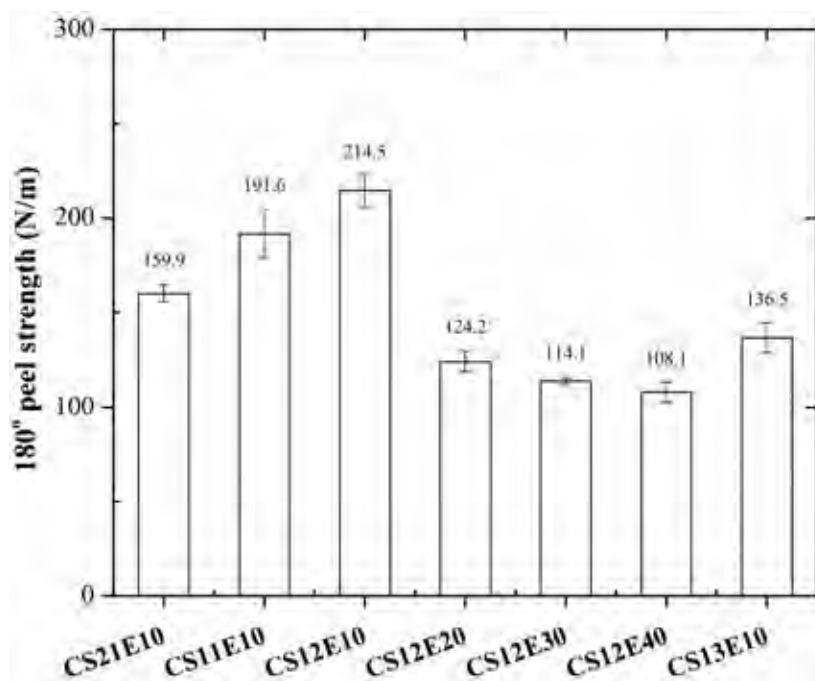


Figure 7.3 Average 180° peel strength of the CS laminating adhesives. Data are shown as average derived from ten measurements.

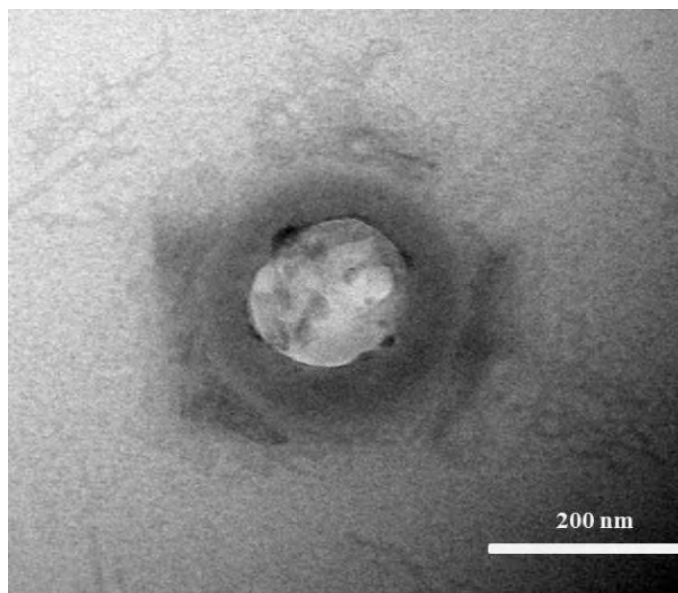


Figure 7.4 Representative TEM micrograph of CS0.5E10 (25.0 kx magnification, scale bar = 200 nm).

be generate more free volume and disorderly movement of the copolymer chains, resulting in the undesirable adhesion properties. Moreover, the 180° peel strength values of commercial adhesives imported from Taiwan and China were 126.6 and 109.6 N/m, respectively, which were much lower than that of the synthesized CS laminating adhesives (Ruanpan *et al.*, 2017). Additionally, the spherical CS0.5E10 latex morphology was analyzed using TEM in order to confirm the core-shell morphology as shown in Figure 7.4. The rigid core of poly(styrene-co-ethylhexyl acrylate) was encapsulated by the soft shell of copolyacrylate.

7.5 Conclusion

Well-establish core-shell latex nanoparticles were successfully developed with the initially polymerized poly(styrene-co-ethylhexyl acrylate) located at the center of the particle, and the later-formed copolyacrylate (2-ethylhexyl acrylate (EHA), ethylene glycol methyl ether acrylate (EGMA), 2-(hydroxyethyl) methacrylate (HEMA), styrene and acrylic acid) being incorporated into the outer shell layer. By using core-shell nanoparticles, which have hard domain (a high T_g of $-14.9\text{ }^\circ\text{C}$) and soft domain (a low T_g ranging from $-18.4\text{ }^\circ\text{C}$ to $-32.0\text{ }^\circ\text{C}$), the resulting latex is able to control its final T_g , particle structure and emulsion stability. The results reveal that CS0.5E10 has highest 180° peel strength at 214.5 N/m with $-25.5\text{ }^\circ\text{C}$ glass transition temperature and other acceptable properties.

7.6 Acknowledgement

This research was financially supported by Research and Researchers for Industries (RRI), Thailand Research Fund (TRF): Grant number PHD56I0019. Additionally, the authors gratified for the utilization of the experimental facilities at College of Polymer Science and Polymer Engineering National Polymer Innovation Center, The University of Akron and the certificated proofreader, Dr. Robert Butcher, at the Publication Counseling Unit, Science Department, Chulalongkorn University.

7.7 References

- Bai, L., Huan, S., Zhang, X., Gu, J. and Li, Z. (2016) Fabrication and evaluation of one-component core/ shell structured latex adhesives containing poly (styrene) cores and poly(acrylate) shells. International Journal of Adhesion and Adhesives, 70, 152-159.
- Bukowska, A., Bukowski, W., Hus, K., Depciuch, J. and Parlińska-Wojtan, M. (2017) Synthesis and characterization of new functionalized polymer-Fe₃O₄ nanocomposite particles. Express Polymer Letters, 11(1), 2-13.
- Chai, S.L. and Tan, H.M. (2008) Structure and property characterization of nanograde core-shell polyurethane/polyacrylate composite emulsion. Journal of Applied Polymer Science, 107, 3499-3504.
- Chaudhuri, R.G. and Paria, S. (2012) Core/shell nanoparticles: classes, properties, synthesis mechanisms, characterization, and applications. Chemical Review, 112, 2373-2433.
- Chenal, M., Rieger, J., Philippe, A. and Bouteiller, L. (2014) High yield preparation of all-organic raspberry-like particles by heterocoagulation via hydrogen bonding interaction. Polymer, 55(16), 3516-3524.
- Chern, C.S. (2008) Principles and Applications of Emulsion Polymerization. New Jersey: John Wiley & Sons, Inc.
- Ebnesajjad, S. (2009) Adhesive Technology Handbook, 2nd ed. New York: William Andrew Inc.
- Fan, X., Jia, X., Liu, Y., Zhang, B., Li, C., Liu, Y., Zhang, H. and Zhang, Q. (2015) Tunable wettability of hierarchical structured coatings derived from onestep synthesized raspberry-like poly(styrene-acrylic acid) particles. Polymer Chemistry, 6(5), 703-713
- Hu, X., Liu, H., Ge, X., Yang, S. and Ge, X. (2009) Preparation of submicron-sized snowman-like polystyrene particles via radiation-induced seeded emulsion polymerization. Chemistry Letters, 38(8), 854-855.
- Ito, F., Ma, G., Nagai, M. and Omi, S. (2002) Study of particle growth by seeded emulsion polymerization accompanied by electrostatic coagulation. Colloids and Surfaces A: Physicochemical and Engineering Aspects, 201, 131-142.

- Jovanović, R. and Dubé, M.A. (2005) Screening experiments for butyl acrylate/vinyl acetate pressure sensitive adhesives. Industrial & Engineering Chemistry Research, 44, 6668-6675.
- Kalogeras, I.M. and Brostow, W. (2009) Glass transition temperatures in binary polymer blends. Journal of Polymer Science Part B: Polymer Physics, 47, 80-95.
- Lichman, J. (1990) Water-based and solvent-based adhesives (Chapter 44). In: Skeist I, ed. Handbook of Adhesives. New York: Van Nostrand Reinhold.
- Ma, J.Z., Liu, Y.H., Bao, Y., Liu, J.L. and Zhang, J. (2013) Research advances in polymer emulsion based on “core-shell” structure particle design. Advances in Colloid and Interface Science, 197-198, 118-131.
- Mishra, S., Singh, S. and Choudhary, V. (2010) Synthesis and characterization of butyl acrylate/methyl methacrylate/glycidyl methacrylate latexes. Journal of Applied Polymer Science, 115, 549-557.
- Nomura, M., Tobita, H. and Suzuki, K. (2005) Emulsion polymerization: kinetic and mechanistic aspects. Advances in Polymer Science, 175, 1-128.
- Ramli, R.A., Laftah, W.A. and Hashim, S. (2013) Core-shell polymers: a review. RSC Advances, 3, 15543-15565.
- Romo-Uribe, A., Arcos-Casarrubias, J.A., Hernandez-Vargas, M.L., Reyes-Mayer, A., Aguilar-Franco, M. and Bagdhachi, J. (2016) Acrylate hybrid nanocomposite coatings based on SiO₂ nanoparticles by in-situ batch emulsion polymerization. Progress in Organic Coatings, 97, 288-300.
- Ruanpan, S., Soucek, M. and Manuspiya, H. (2017) Waterborne acrylic hybrid adhesives based on a methacrylate-functionalized porous clay heterostructure for potential lamination application. Journal of Materials Research, 32, 3689-3698.
- Schumacher, K.H. (2016) New water-based adhesives for flexible food packaging: chemical design, performance and toxicological safety. Journal of Applied Packaging Research, 8(1), 38-42.
- Tan, C., Tirri, T. and Wilen CE. (2016) The effect of core-shell particle morphology on adhesive properties of poly(styrene-co-butyl acrylate). International Journal of Adhesion and Adhesives, 66, 104-113.

- U.S. Environmental Protection Agency (EPA). (2014) The 2011 National Emissions Inventory Version 1.
- Zhang, X., Wei, X., Yang, W., Li, Y. and Chen, H. (2012) Characterization and properties of gradient polyacrylate latex particles by gradient emulsion polymerization. Journal of Coatings Technology and Research, 9(6), 765774.
- Zhou, C., Che, R., Zhong, L., Xu, W., Guo, D. and Lei, J. (2011) Effect of particle structure on the peel strength and heat resistance properties of vinyl acetate/acrylate latexes laminating adhesives. Journal of Applied Polymer Science, 119, 2857-2865.

CHAPTER VIII

CONCLUSIONS AND RECOMMENDATIONS

The water-based laminating adhesives were successfully synthesized by the emulsion polymerization process. Two different types of polymeric matrix, including polyurethane and polyacrylate, were used to completely disperse in deionized water as a carrier fluid with a solid content of 40 - 50% and pH value of 7 - 8. The water-based polyurethane laminating adhesives were derived by a condensation process of isophorone diisocyanate, 2,2-bis(hydroxymethyl) propionic acid and polypropylene glycol ($M_w = 2000$), while the water-based polyacrylate laminating adhesives were derived by the batchwise emulsion polymerization of 2-ethylhexyl acrylate, ethylene glycol methyl ether acrylate, styrene, 2-hydroxyethyl methacrylate and acrylic acid. Many variables, including the influence of surfactant types, initiator types, monomer compositions, natural thickeners/reinforcing fillers and wetting agent types, on the laminating adhesive performance were intensively studied. The results revealed that the water-based polyurethane incorporating with amino-functionalized porous clay heterostructure and the water-based polyacrylate incorporating with methacrylate-functionalized porous clay heterostructure were improved the laminating adhesive performance. The adhesion properties, in terms of the 180° peel strength values, were enhanced up to 126 N/m which is higher than that of commercial products. However, the adhesive failure was still occurred. The attempt to simultaneously improve the cohesive strength and adhesion to substrates was obtained. Therefore, the core-shell polyacrylate laminating adhesives were formulated by a two-stage seeded semi-batch emulsion polymerization. The rigid core of poly(styrene-co-acrylate) having a glass transition temperature (T_g) of -14.9 °C encapsulated by a soft shell of copolyacrylate having the T_g ranging of -20 °C was preferable. The cohesive strength and adhesion to substrates were presented, inducing the 180° peel strength dramatically to enhance up to 214.5 N/m with other acceptable properties. The expectation of this research is to push towards the water-based laminating adhesives to use in the laminated flexible packaging industry, especially in a smart packaging.

REFERENCES

- Ahenach, J., Cool, P. and Vansant, E.F. (2000) Enhanced bronsted acidity created on Al-grafting of porous clay heterostructure via aluminium acetylacetonate adsorption. Physical Chemistry Chemical Physics, 2, 5750-5755.
- Alexandre, M. and Dubois, P. (2000) Polymer-layered silicate nanocomposites: preparation, properties and uses of a new class of materials. Materials Science and Engineering, 28, 1-63.
- Anders, K. and Lee, G. (2015) Effect of residual solvent in polymer adhesive matrix on release and skin permeation of scopolamine. International Journal of Pharmaceutics, 491(1-2), 42-48.
- Araki, S., Doi, H., Sano, Y., Tanaka, S. and Miyake, Y. (2009) Preparation and CO₂ adsorption properties of aminopropyl-functionalized mesoporous silica microspheres. Journal of Colloid and Interface Science, 339, 382-389.
- Archer, B. (1997) Water Based Contact Adhesives - New Developments. International Journal of Adhesion and Adhesives, 18, 15-18.
- Avendaño, E., Berggren, L., Niklasson, G.A., Granqvist, C.G. and Azens, A. (2006) Electrochromic materials and devices: brief survey and new data on optical absorption in tungsten oxide and nickel oxide films. Thin Solid Films, 496, 30-36.
- Aung, M.M., Yaakob, Z., Kamarudin, S. and Abdullah, L.C. (2014) Synthesis and characterization of *Jatropha (Jatropha Curcas L.)* oil-based polyurethane wood adhesive. Industrial Crops and Products, 60, 177-185.
- Baldan, A. (2004) Adhesively-bonded joints and repairs in metallic alloys, polymers and composite materials: adhesives, adhesion theories and surface pretreatment. Journal of Materials Science, 39(1), 1-49.
- Bardzinski P.J. (2014) On the impact of intermolecular interactions between the quaternary ammonium ions on interlayer spacing of quaternized montmorillonite: a molecular mechanics and ab initio study. Applied Clay Science, 95, 323-339.

- Barrett, E.P., Joyner, L.G. and Halenda, P.P. (1951) The determination of pore volume and area distributions in porous substances. I. computations from nitrogen isotherms. Journal of the American Chemistry Society, 73(1), 373-380.
- Beyer, G. (2002) Nanocomposites: a new class of flame retardants for polymers. Plastics, Additives and Compounding, 4(10), 22-28.
- Boonruang, S., Magaraphan, R. and Manuapiya, H. (2012) Chromophores Modified Porus Clay Heterostructures for Smart Packaging Films. M.S. Thesis, The Petroleum and Petrochemical College, Chulalongkorn University, Thailand.
- Brunauer, S., Emmett, P.H. and Teller, E. (1938) Adsorption of gases in multimolecular layers. Journal of the American Chemistry Society, 60, 309-319.
- Bunnak, N., Laoratanakul, P., Bhalla, A.S. and Manuspiya, H. (2014) Surface-modified porous clay heterostructure synthesized by introduction of cationic ions: effects on dielectric behavior. Ferroelectrics, 473, 187-197.
- Cameron, A.C. and Talasila, T. (1995) Modified-atmosphere packaging of fresh fruit and vegetable. IFT Annual Meeting, Book of Abstracts, 254.
- Carter, R. (1993) Method of Laminating Multiple Layers. US5211792A.
- Chimielarz, L., Kuśtrowski, P., Dziembaj, R., Cool, P. and Vansant, E.F. (2006) Selective catalytic reduction of NO with ammonia over porous clay heterostructures modified with copper and iron species. Catalysis Today, 114, 319-332.
- Chimielarz, L., Gil, B., Kuśtrowski, P., Piwowska, Z., Dudek, B. and Michalik, M. (2009) Montmorillonite-based porous clay heterostructures (PCHs) intercalated with silica-titania pillars-synthesis and characterization. Journal of Solid State Chemistry, 182, 1094-1104.
- Corcione, C.E., Prinari, P., Cannoletta, D., Mensiteri, G. and Maffezzoli, A. (2008) Synthesis and characterization of clay-nanocomposite solvent-based polyurethane adhesives. International Journal of Adhesion and Adhesives, 28(3), 91-100.
- Corcoran, E.A. (2008) Is it time to create a centralized Thai environmental protection agency?. Thai-American Business, 4, 24-26.

- David, D.J. and Stanley, H.B. (1969) Analytical Chemistry of Polyurethanes, High Polymer Series, XVI, Part III. Wiley-Interscience: New York.
- Devanesan, J.N., Karuppiah, A. and Abirami, C.V.K. (2011) Effect of storage temperatures, O₂ concentrations and variety on respiration of mangoes. Journal of Agrobiology, 28(2), 119-128.
- Diaconu, G., Paulis, M. and Leiza, J.R. (2008) Towards the synthesis of high solids content waterborne poly(methyl methacrylate-co-butyl acrylate)/montmorillonite nanocomposites. Polymer, 49, 2444-2454.
- Ebnesajjad, S. (2009) Adhesives Technology Handbook. Amsterdam: Elsevier.
- Ebnesajjad, S. (2010) Handbook of Adhesives and Surface Preparation: Technology, Applications and Manufacturing. Amsterdam: Elsevier.
- Fennir, M.A., Landry, J.A. and Raghavan, G.S.V. (2003) Respiration rate of potatoes (*Solanum Tuberosum* L.) measured in a two-bin research scale storage facility, using heat and moisture balance and GC analysis. Canadian Biosystems Engineering, 45, 4.1-4.9.
- Galarneau, A., Barodawalla, A. and Pinnavaia, T.J. (1995) Porous clay heterostructures formed by gallery-templated synthesis. Nature, 374, 529-531.
- Galarneau, A., Barodawalla, A. and Pinnavaia, T.J. (1997) Porous clay heterostructures (PCH) as acid catalyst. Chemical communications, 17, 1661.
- Galimberti, M. (2012) Rubber Clay Nanocomposites. Advanced Elastomers-Technology, Properties and Applications. (Boczkowska, A., Ed.), Italy.
- Gopinath, S. and Sugunan, S. (2007) Enzymes immobilized on montmorillonite K10: effect of adsorption and grafting on the surface properties and the enzyme activity. Applied Clay Science, 35, 67-75.
- Gumfekar, S.P., Kunte, K.J., Ramjee, L., Kate, K.H. and Sonawane, S.H. (2011) Synthesis of CaCO₃-P(MMA-BA) nanocomposite and its application in water based alkyd emulsion coating. Progress in Organic Coating, 72, 632-637.
- Hong, S.I. and Park, W.S. (1999) Development of color indicators for kimchi packaging. Journal of Food Science, 64(2), 255-257.

- Hong, S.I. and Park, W.S. (2000) Use of color indicators as an active packaging for evaluating kimchi fermentation. Journal of Food Engineering, 46, 67-72.
- Jirapattarasakul, I., Tongta, A. and Kanlayanarat, S. (2003) Effects of heat treatment on the respiration of mango 'nam dok mai'. APEC Symposium on Postharvest Handling System, Radisson Hotel, Thailand.
- Kango, S., Kalia, S., Celli, A., Njuguna, J., Habibi, Y. and Kumar, R. (2013) Surface modification of inorganic nanoparticles for development of organic-inorganic nanocomposites-a review. Progress in Polymer Science, 38, 1232-1216.
- Kader, A. (1992) Post Harvest Biology and Technology of Agricultural Crops. Davis CA: University of California.
- Kays, S.J. (1995) Post Harvest Physiology of Perishable Plant Products. New York: Van Nostrand Reinhold
- Kim, J.H. and Shiratori, S. (2006) Fabrication of color changeable film to detect ethylene gas. Japanese Journal of Applied Physics, 45, 4274-4278.
- Kinloch, A.J. (1987) Adhesion and Adhesives: Science and Technology. London: Chapman and Hall.
- Kuan, H.C., Ma, C.C.M., Chuang, W.P. and Su, H.Y. (2005) Hydrogen bonding, mechanical properties, and surface morphology of clay/waterborne polyurethane nanocomposites. Journal of Polymer Science Part B: Polymer Physics, 43, 1-12.
- Labidi, S., Azema, N., Perrin, D. and Lopez-Cuesta, J.M. (2010) Organo-modified montmorillonite/poly(-caprolactone) nanocomposites prepared by melt intercalation in a twin-screw extruder. Polymer Degradation and Stability, 95, 382-388.
- LeBaron, P.C., Wang, Z. and Pinnavaia, T.J. (1999) Polymer-layered silicate nanocomposites: an overview. Applied Clay Science, 15, 11-29.
- Lee, L.H. (1991) Fundamentals of Adhesion. New York: Plenum Press.
- Lichman, J. (1990) Water-based and solvent-based adhesives. Handbook of Adhesives. New York: Van Nostrand Reinhold

- Lin, D.J., Don, T.M., Chen, C.C., Lin, B.Y., Lee, C.K. and Cheng, L.P. (2008) Preparation of a nanosilica-modified negative-type acrylate photoresist. Journal of Applied Polymer Science, 107, 1179-1188.
- Lovell, P.A. and El-Aasser, M.S. (1998) Emulsion Polymerization and Emulsion Polymers. Chichester: Wiley.
- Malavašič, T., Černilec, N., Mirčeva, A. and Osredkar, U. (1992) Synthesis and adhesive properties of some polyurethane dispersions. International Journal of Adhesion and Adhesives, 12, 38-42.
- Mahalik, N.P. and Nambiar, A.N. (2010) Trends in food packaging and manufacturing systems and technology. Trends in Food Science & Technology, 21, 117-128.
- Manias, E., Touny, A., Wu, L., Strawhecker, K., Lu, B. and Chung, T.C. (2001) Polypropylene/montmorillonite nanocomposites. review of the synthetic routes and materials properties. Chemistry of Materials, 13, 3516-3523.
- Mattayan, A., Magaraphan, R. and Manuapiya, H. (2009) Induced magnetic properties to surface modified mesoporous clay heterostructure for sensor application in food packaging. M.S. Thesis, the Petroleum and Petrochemical College, Chulalongkorn University, Thailand.
- Mitcham, E.J. and McDonald, R.E. (1993) Respiration rate, internal atmosphere, and ethanol and acetaldehyde accumulation in heat-treated mango fruit. Postharvest Biology and Technology, 3, 77-86.
- Mittal, V. (2009) Polymer layered silicate nanocomposites: a review. Materials, 2, 992-1057.
- Nopwinyuwong, A., Trevanich, S. and Suppakul, P. (2010) Development of a novel colorimetric indicator label for monitoring freshness of intermediate-moisture dessert spoilage. Talanta, 81, 1126-1132.
- Öztürk, N., Tabak, A., Akgöl, S. and Denizli, A. (2007) Newly synthesized bentonite-histidine (Bent-Hist) micro-composite affinity sorbents for IgG adsorption. Colloids and Surfaces A: Physicochemical and Engineering Aspects, 301, 490-497.
- Packham, D.E. (1992) Handbook of Adhesion. Harlow: Longman Scientific & Technical.

- Pacquit, A., Lau, K.T., McLaughlin, H., Frisby, J., Quilty, B. and Diamond, D. (2006) Development of a volatile amine sensor for the monitoring of fish spoilage. Talanta, 69, 515-520.
- Pacquit, A., Frisby, J., Diamond, D., Lau, K.T., Farrell, A., Quilty, B. and Diamond, D. (2007) Development of a smart packaging for the monitoring of fish spoilage. Food Chemistry, 102, 466-470.
- Patel, H.A., Somani, R.S., Bajah, H.C. and Jasra, R.V. (2007) Preparation and characterization of phosphonium montmorillonite with enhanced thermal stability. Applied Clay Science, 35, 194-200.
- Pavlidou, S. and Papispyrides, C.D. (2008) A review on polymer-layered silicate nanocomposites. Progress in Polymer Science, 33, 1119-1198.
- Petrie, E.M. (2005) Laminating Adhesives for Flexible Packaging. Omnexus Adhesives & Sealants, available on: <http://www.omnexus4Adhesives.com>.
- Ray, S.S. and Okamoto, M. (2003) Polymer/layered silicate nanocomposites: a review from preparation to processing. Progress in Polymer Science, 28, 1539-1641.
- Rowland, G.A. (1998) Adhesives and Adhesion. Chemistry in New Zealand, 71, 17-27.
- Saltveit, M.E. Measuring Respiration. Davis CA: University of California
- Seyed Mohaghegh, S.M., Barikani, M. and Entezami, A.A. (2005) Preparation and properties of aqueous polyurethane dispersions. Iranian Polymer Journal, 14(2), 163-167.
- Shen, Y.H. (2001) Preparations of organobentonite using nonionic surfactants. Chemosphere, 44, 989-995.
- Singha, K. (2012) A review on coating and lamination in textiles: processes and applications. American Journal of Polymer Science, 2(3), 39-49.
- Smolander, M., Hurme, E., Ahvenainen, R. and Siika-aho, M. (1998) Indicators for modified atmosphere packages. 24th IAPRI Symposium, Rochester.
- Society of Manufacturing Engineers (SME), (1970) Types of adhesives (Chapter1). Adhesives in Modern Manufacturing. (Bruno, E.J., ed.)

- Solomon, M.J., Almusallam, A.S., Seefeldt, K.F., Somwangthanoj, A. and Varadan, P. (2001) Rheology of polypropylene/clay hybrid materials. Macromolecules, 34, 1864-1872.
- Srithammaraj, K., Magaraphan, R. and Manuspiya, H. (2008) Surfactant-templated synthesis of modified porous clay heterostructure (PCH). Advanced Materials Research, 55-57, 317-320.
- Srithammaraj, K., Magaraphan, R. and Manuspiya, H. (2011). Modified porous clay heterostructures by organic–inorganic hybrids for nanocomposite ethylene scavenging/sensor packaging film. Packaging Technology and Science, 25, 63-72.
- Tassawat, S., Manuspiya, H., Magaraphan, R. and Nithithanakul, R. (2007) The polypropylene/organoclay nanocomposite for pH-sensitive packaging. M.S. Thesis, The Petroleum and Petrochemical College, Chulalongkorn University, Thailand.
- Twede, D. (2005) The origins of paper based packaging. conference on: Historical Analysis and Research in Marketing Proceedings, 12, 288-300.
- US Environmental Protection Agency (EPA) (2015) The 2011 National Emissions Inventory, version 2 Technical Support Document. Available at: https://www.epa.gov/sites/production/files/2015-10/documents/nei2011v2_tsd_14aug2015.pdf (accessed 20 January 2017)
- Vaia, R.A., Ishii, H. and Giannelis, E.P. (1993) Synthesis and properties of two-dimensional nanostructures by direct intercalation of polymer melts in layered silicates. Chemistry of Materials, 5, 1694-1696.
- Vaia, R.A., Price, G., Ruth, P.N., Nguyen, H.T. and Lichtenhan, J. (1999) Polymer/layered silicate nanocomposites as high performance ablative materials. Applied Clay Science, 15, 67-92.
- Voss, P.A. (2002) Water-based adhesives: solventless lamination reduces flexible packaging VOCs. FLEXO Magazine, 1-4.
- Wolf, R. (2010) A technology decision - adhesive lamination or extrusion coating/lamination. Place Conference, New Mexico, USA.

- Wu, Z., Xiang, H., Kim, T., Chun, M.S. and Lee, K. (2006) Surface properties of submicrometer silica spheres modified with aminopropyltriethoxysilane and phenyltriethoxysilane. Journal of Colloid and Interface Science, 304, 119-124.
- Yam, K.L., Takhistov, P.T. and Miltz, J. (2005) Intelligent packaging: concepts and applications. Journal of Food Science, 70(1), R1-R10.
- Zádrapa, P. and Maláč, J. (2011) The morphology and properties of selected filler/poly(ethylene-co-methacrylic acid) copolymer systems. Ph.D. Thesis, Faculty of Technology, Tomas Bata University in Zlín, Czech Republic.
- Zhang, J., Jiang, D.D. and Wilkie, C.A. (2005) Polyethylene and polypropylene nanocomposites based upon an oligomerically modified clay. Thermochimica Acta, 430, 107-113.
- Zhang, X., Ding, Y., Zhang, G., Li, L. and Yan, Y. (2011) Preparation and rheological studies on the solvent based acrylic pressure sensitive adhesives with different crosslink density. International Journal of Adhesion and Adhesives, 31(7), 760-766.

CURRICULUM VITAE

Name: Ms. Sarocha Ruanpan

Date of Birth: June 3, 1989

Nationality: Thai

University Education:

2011–2017 Doctor of Philosophy in Polymer Science, The Petroleum and Petrochemical College, Chulalongkorn University, Bangkok, Thailand

2007-2010 Bachelor Degree of Science in Chemistry, Faculty of Science, Mahidol University, Bangkok, Thailand (Second class honors degree)

Work Experience:

2016	Position:	Visiting scholar
	Company name:	Department of Polymer Engineering, The University of Akron, Akron, Ohio, USA
2015-2016	Position:	Project researcher
	Company name:	Western Digital Co.
2010	Position:	Student internship
	Company name:	SCG Chemicals Co., Ltd.

Publications:

1. Ruanpan, S. and Manuspiya, H. (2018) Synthesized Amino-Functionalized Porous Clay Heterostructure as an Effective Thickener in Waterborne Polyurethane Hybrid Adhesives for Lamination Process. International Journal of Adhesion and Adhesives, 80, 66-75.
2. Ruanpan, S., Soucek, M. and Manuspiya, H. (2017) Waterborne Acrylic Hybrid Adhesives based on a Methacrylate-Functionalized Porous Clay Heterostructure for Potential Lamination Application. Journal of Materials Research, 32, 3689-3698.

Proceedings:

1. Ruanpan, S., Magaraphan, R. and Manuspiya, H. (December 11-15, 2010) Freshness Detector Film Fabricated by Mixed-Dyes Modified Porous Clay

Heterostructure Nanocomposite. Proceedings of the 28th International Conference of the Polymer Processing Society (PPS28), Pattaya, Thailand.

Patents:

1. Ruanpan, S. and Manuspiya, H. (2017) Waterborne Polyurethane Laminating Adhesives Modified by Amino-Functionalized Porous Clay Heterostructure. Patent number 1701006105
2. Ruanpan, S. and Manuspiya, H. (2017) Waterborne Acrylic Laminating Adhesives Modified by Methacrylate-Functionalized Porous Clay Heterostructure. Patent number 1701006106

Presentations:

1. Ruanpan, S. and Manuspiya, H. (July 28, 2015) Development of Water-Based Adhesives for Oriented Polypropylene (OPP) Lamination. *Oral Presented at the 1st Research and Researcher for Industry Congress (RRi Congress I)*, Bangkok, Thailand.
2. Ruanpan, S. and Manuspiya, H. (March 12, 2015) Development of Water-Based Adhesives for Oriented Polypropylene (OPP) Lamination. *Oral Presented at RRi CU Forum 2014*, Bangkok, Thailand.
3. Ruanpan, S. and Manuspiya, H. (July 6-11, 2014) The Stabilizing Effect of Anionic Groups on Waterborne Polyurethane Adhesives for Oriented Polypropylene Lamination. *Oral Presented at The 2014 IUPAC World Polymer Congress (Macro 2014)*, Chiangmai, Thailand.
4. Ruanpan, S., Magaraphan, R. and Manuspiya, H. (May 21-23, 2013) The Colorimetric Film Fabricated by Mixed-Dyes Modified Porous Clay Heterostructure for Monitoring Fruit Freshness. *Poster Presented at The 3rd International Symposium Frontiers in Polymer Science*, Sitges, Spain.
5. Ruanpan, S., Magaraphan, R. and Manuspiya, H. (April 23, 2013) On-Package CO₂ Sensors for Fruit Freshness Detection. *Oral Presented at The 4th Research Symposium on Petrochemicals and Materials Technology and The 19th PPC Symposium on Petroleum, Petrochemicals, and Polymers*, Bangkok, Thailand.

6. Ruanpan, S., Magaraphan, R. and Manuspiya, H. (March 28, 2013) The Nanocomposite of Mixed-Dyes Modified Porous Clay Heterostructure for Freshness Detection. *Poster Presented at The 3rd Polymer Conference of Thailand (PCT3)*, Bangkok, Thailand.
7. Ruanpan, S., Magaraphan, R. and Manuspiya, H. (December 11-15, 2012) Freshness Detector Film Fabricated by Mixed-Dyes Modified Porous Clay Heterostructure Nanocomposite. *Poster Presented at The 28th International Conference of the Polymer Processing Society (PPS28)*, Pattaya, Thailand.

Awards:

1. Honourable mention awards in PTTGC Open Innovation Challenge 2016 from PTT Global Chemical Public Company Limited (May 25, 2017)
2. Award of Appreciation in “2016 Appreciation Banquet” from the Petroleum and Petrochemical College, Chulalongkorn University, Thailand (July 15, 2016)
3. Best Oral Presentation Award in Chemistry and Material Science section from the 1st Research and Researcher for Industry Congress (RRi Congress I), Thailand. (July 28, 2015)